Scuola Internazionale Superiore di Studi Avanzati - SISSA

Trieste, Italy

PRION PROTEIN INVOLVEMENT IN REELIN/DAB1 SIGNALLING: PHYSIOLOGICAL AND PATHOLOGICAL ASPECTS

Thesis submitted for the degree of "*Philosophiae Doctor*"

CANDIDATE
Irene Giulia Rolle

SUPERVISOR
Prof. Giuseppe Legname, Ph.D.

Academic year 2015/2016

DECLARATION

The work described in this thesis has been carried out at Scuola Internazionale Superiore di Studi Avanzati (SISSA), Trieste, Italy, from November 2012 to October 2016.

During my Ph.D. course I contributed to the following research article:

- Ladan Amin, Xuan T. A. Nguyen, Irene Giulia Rolle, Elisa D'Este, Gabriele Giachin, Thanh Hoa Tran, Vladka Čurin Šerbec, Dan Cojoc, Giuseppe Legname (2016). "Characterization of Prion Protein Function by Focal Neurite Stimulation", Journal of Cell Science. 2016 Sep 2. pii: jcs.183137.

INDEX

LIST OF ABBREVIATIONS 1

ABSTRACT 5

INTRODUCTION 9

NEURODEGENERATIVE DISEASES 9

PRION DISEASES 10

HUMAN PRION DISEASES 14

THE CELLULAR PRION PROTEIN 16

PrP^C EXPRESSION AND SUBCELLULAR ENVIRONMENT 18

PHYSIOLOGICAL FUNCTION OF CELLULAR PRION PROTEIN 22

INSIGHTS FROM KNOCKOUT MODELS 22

PrP^C SIGNALLING 26

SEARCH FOR PRION PROTEIN INTERACTORS 26

PrP^C AND THE SRC FAMILY KINASES (SFK) 28

PrP^C AND THE PI3K/AKT PATHWAY 30

OTHER PrP^C SIGNALLING EFFECTORS 31

REELIN/DAB1 SIGNALLING CASCADE 33

REELIN STRUCTURE AND PROCESSING 33

REELIN SIGNAL TRANSDUCTION 35

MOUSE MODELS OF REELIN-SIGNALLING DISRUPTION 38

REELIN EXPRESSION AND BIOLOGICAL FUNCTIONS 41

ROLE IN DISEASES 42

REELIN/DAB1 SIGNALLING IN ALZHEIMER'S DISEASE 42

REELIN/DAB1 SIGNALLING IN PRION DISEASES 43

AIM OF THE PROJECT 45

MATERIALS AND METHODS 47

HUMAN SAMPLES 47

ANIMALS 47

INTRACEREBRAL INOCULATION OF PRIONS 48

PRIMARY NEURONAL CULTURES PREPARATION 49

PRODUCTION OF REELIN-CONDITIONED SUPERNATANT 49

PRODUCTION OF RECOMBINANT MOUSE FULL-LENGTH PrP (recMoPrP) 50

PRODUCTION OF RECOMBINANT MOUSE PrP-hFc FUSION PROTEIN (moPrP-hFc) 50
PRIMARY NEURONAL CULTURES STIMULATION WITH REELIN, recMoPrP AND PrP-hFc 51
PRIMARY NEURONS LYSATES PREPARATION 51
TISSUE HOMOGENIZATION FOR PROTEIN EXTRACTION 52
BIOCHEMICAL ANALYSIS OF BRAIN HOMOGENATES AND NEURONAL LYSATES 52
IMMUNOPRECIPITATION OF DAB1 FROM BRAIN HOMOGENATES 53
CO-IMMUNOPRECIPITATION EXPERIMENTS 54
ANTIBODIES 56
RNA EXTRACTION FROM BRAIN SAMPLES AND REAL-TIME PCR 57
STATISTICAL ANALYSIS 59
RESULTS 61
ANALYSIS OF REELIN/DAB1 SIGNALLING PATHWAY ACTIVATION STATE IN *Prnp*$^{+/+}$ AND *Prnp*$^{0/0}$ MOUSE BRAIN DURING EARLY POSTNATAL DAYS 61
DAB1 EXPRESSION ANALYSIS 61
REELIN-SIGNALLING PATHWAY EXPRESSION ANALYSIS 64
ANALYSIS OF REELIN/DAB1 SIGNALLING PATHWAY ACTIVATION STATE IN *Prnp*$^{+/+}$ AND *Prnp*$^{0/0}$ PRIMARY NEURONAL CULTURES 69
STIMULATION WITH REELIN-CONDITIONED MEDIUM 69
STIMULATION WITH recMoPrP (23-231) AND moPrP-hFc 73
ANALYSIS OF PrP^{C} EXPRESSION IN DIFFERENT MOUSE MODELS OF REELIN-SIGNALLING DISRUPTION 78
ANALYSIS OF REELIN/DAB1 SIGNALLING PATHWAY IN PRION-INFECTED MICE 84
DAB1 GENE EXPRESSION ANALYSIS IN CREUTZFELDT-JAKOB DISEASE PATIENTS 91
DISCUSSION 93
CONCLUSIONS AND PERSPECTIVES 103
ACKNOWLEDGEMENTS 105
BIBLIOGRAPHY 107

LIST OF ABBREVIATIONS

Actb: β-Actin

AD: Alzheimer's disease

ApoE: apolipoprotein E

ApoER2: apolipoprotein E receptor 2

APP: amyloid precursor protein

BCA: bicinchoninic acid

BSE: bovine spongiform encephalopathy

CC: charged cluster

CDK5: Cyclin-dependent kinase 5

CID: collision induced dissociation

CNS: central nervous system

CJD: Creutzfeldt-Jakob disease

CREB: cyclic AMP response element binding protein

CRKL: Crk-like protein

CTF: C-terminal fragment

Cul5: Cullin 5

Dab1: Disabled-1

DIV: days *in vitro*

dpi: days post inoculation

Dpl: Doppel

DSP: dithiobis(succinimidyl propionate)

E: embryonic day

EGF: epidermal growth factor

ER: endoplasmic reticulum

FBS: fetal bovine serum

fCJD: familial Creutzfeldt-Jakob disease

FFI: fatal familial insomnia

GAPDH: glyceraldehyde 3-phosphate dehydrogenase

GPI: glycophosphatidylinositol

GSK3β: glycogen synthase kinase 3β

GSS: Gerstmann-Sträussler-Scheinker syndrome

HC: hydrophobic core

hFc: human Fc of immunoglobulin G_1

HRP: horseradish peroxidase

iCJD: iatrogenic Creutzfeldt-Jakob disease

KO: knockout

LIS1: lissencephaly protein 1

LTP: long term potentiation

LRP8: low-density lipoprotein receptor-related protein 8

moPrP-hFc: mouse prion protein fused to human Fc of immunoglobulin G_1

NCAM: neural cell adhesion molecule

neo: neomycin

NMDA: Nmethyl-d-aspartate

NMDAR: Nmethyl-d-aspartate receptor

OR: octapeptide repeats

ORF: open reading frame

P: postnatal day

PBS: phosphate-buffered saline

PBST: phosphate-buffered saline plus Tween-20

PFHM: protein-free hybridoma medium

PI3K: phosphatidylinositol 3-kinase

PK: proteinase K

PKA: protein kinase A

PKC: protein kinase C

PrP^{C}: cellular prion protein

PrP^{Sc}: scrapie prion protein

PSD95: postsynaptic density protein 95

recMoPrP: recombinant mouse prion protein

RML: Rocky Mountain Laboratory

RPTPα: receptor protein tyrosine phosphatase α

RR: Reelin repeats

RT: room temperature

sCJD: sporadic Creutzfeldt-Jakob disease

SFK: Src family kinases

STI1: stress-inducible protein 1

TACE: TNFα-converting enzyme

TALEN: transcription activator-like effector nuclease

TBS: Tris-Buffered Saline

TBST: Tris-Buffered Saline plus Tween-20

tcTPC: time-controlled transcardiac perfusion cross-linking

tPA: tissue plasminogen activator

TSE: transmissible spongiform encephalopathies

Tubb3: βIII-tubulin

UTR: untranslated region

vCJD: variant Creutzfeldt-Jakob disease

VLDLR: very-low-density lipoprotein receptor

WB: Western blotting

WT: wild-type

YP: Tyrosine-phosphorylated

ABSTRACT

Cellular prion protein (PrP^{C}) has been widely investigated since its misfolded isoform, scrapie prion protein (PrP^{Sc}), which form aggregates that accumulate in the brain, causes prion diseases. The pathogenesis of prion diseases is currently under debate as they could be gain of toxic function consequences of the formation of PrP^{Sc}, or could be due to the loss of the normal physiological function of PrP^{C}. For this reason, a better definition of the exact physiological function of PrP^{C} represents a critical challenge since *Prnp* knockout mice lack striking phenotype.

PrP^{C} is highly abundant in the nervous system where it plays an important role in modulating cell signalling, acting as a dynamic scaffold for the assembly of many different signalling molecules at the neuronal surface. Importantly for the present study, it has been reported that PrP^{C} is able to modulate Fyn, PI3K, AKT/PKB and GSK3β activity. All these intracellular kinases could be also regulated by yet another protein, Reelin, an extracellular matrix glycoprotein that activates a linear downstream signalling pathway. Interestingly, it has been reported that Reelin-signalling pathway is involved in both Alzheimer's and prion diseases. Indeed, the intracellular adaptor protein Dab1 is able to affect APP processing and intracellular trafficking and to influence amyloid beta deposition in sporadic Creutzfeldt–Jakob disease.

In the present study, taking advantage of different mouse models, we analysed the functional interaction between the prion protein and Dab1 signalling cascade from physiological and pathological point of view.

In the first part of the project, using a *Prnp* knockout mouse model, we addressed the question whether PrP^{C} could modulate the Reelin-signalling cascade. If this is the case, we could expect impairments in Reelin downstream signalling when PrP^{C} expression is ablated. Indeed, the expression level and the activation state of Dab1 were evaluated in wild-type ($Prnp^{+/+}$) and PrP^{C}-null ($Prnp^{0/0}$) mice brain and primary neuronal cultures. Reelin-conditioned medium, obtained from stably transfected HEK293T cells, was used to stimulate Dab1 activation *in vitro* and analyse a putative differential activation

between the two genotypes. Moreover, recombinant PrP and fusion PrP-hFc proteins were applied in the same system to evaluate the ability of PrP^C to stimulate directly the signalling cascade. Dab1 protein resulted upregulated in *Prnp*$^{0/0}$ brain in comparison to wild-type animals, with no changes in mdab1 gene transcription levels. Moreover, *Prnp*$^{0/0}$ neurons appeared less responsive to Reelin stimulation than controls, leading to reduced phosphorylation of Dab1. Unfortunately, in our conditions, neither recombinant PrP nor PrP-hFc fusion protein were able to induce Dab1 phosphorylation, suggesting a modulating role, instead of a direct effect, of PrP^C on the pathway. Expression analysis of different component of the pathway revealed no statistical differences between the two genotypes, with the exception of Fyn kinase, which resulted less phosphorylated in *Prnp*$^{0/0}$ mice compared to wild-type controls. Immunoprecipitation experiments failed to unravel an interaction between PrP^C and Reelin or its receptor ApoER2, suggesting that impairments in Dab1 expression and phosphorylation are not due to a direct coupling between these proteins at the cell surface. Interestingly, in *Prnp*$^{0/0}$ neurons, reduced levels of NCAM protein, a known PrP^C interactor, were detected.

In the second part of the project, taking advantage of different mouse models of Reelin pathway disruption, we addressed the opposite question to understand whether alteration of the Reelin-signalling pathway could affect the expression of PrP^C. However, PrP^C expression levels did not resulted significantly different in comparison to their respective controls in none of the genotypes analysed. These results suggest that, while PrP^C is able to modulate Reelin-signalling cascade and in particular Dab1 activation state, alterations of this pathway do not affect PrP^C expression.

Finally, terminally sick mice intracerebrally inoculated with RML prion strain were used as prion pathology model. Interestingly, in terminal stages of prion infection, Dab1 and Reelin receptors signals are no longer detectable. NCAM expression level seems not affected by prion infection, while Fyn kinase and AKT levels are reduced by 30% and 50% respectively. Total Reelin amount is not modified by prion infection, while full-length protein is reduced by almost 50% in RML-infected samples compared to controls with a concomitant 2-fold increase of both cleavage products.

Taken together, these findings suggest the existence of a functional interplay between prion protein and Dab1 signalling. Results obtained using PrP^{C}-null mice as model of loss-of-function indicate a role for PrP^{C} in promoting Dab1 signalling. However, as Reelin and its receptors are not affected by *Prnp* ablation, more likely PrP^{C} indirectly modulate Dab1 signalling through NCAM and Fyn pathway. Interestingly, Dab1 signalling resulted completely abolished in RML-inoculated terminally sick mice, used as prion disease model, together with strong alteration in Reelin processing, already reported in Alzheimer's disease patients. Further experiments are in progress in order to clarify the mechanisms by which PrP^{C} and PrP^{Sc} modulates Dab1 signalling pathway.

INTRODUCTION

NEURODEGENERATIVE DISEASES

Neurodegenerative disorders are characterized by progressive dysfunction and loss of neurons in specific areas of the nervous system, which determines the clinical manifestation of the disease. Pathogenic mechanisms shared by neurodegenerative disorders are protein misfolding and accumulation (Table 1), increased oxidative stress, impaired cellular metabolism, mitochondrial dysfunction and DNA damage, dysfunction of neurotrophins, neuroinflammation and induction of cell death [1].

DISEASE	PROTEIN	PATHOLOGICAL FINDING
Prion diseases	PrP^{Sc}	PrP amyloid plaques
Alzheimer's disease	Aβ	Aβ amyloid plaques
	Tau	Paired helical filaments in neurofibrillary tangles
Parkinson's disease	α-Synuclein	Lewy bodies
Frontotemporal dementia	Tau	Straight filaments and paired helical filaments
Pick's disease	Tau	Pick bodies
Progressive supranuclear palsy	Tau	Straight filaments in neurofibrillary tangles
Amyotrophic lateral sclerosis	Neurofilament	Neuronal aggregates
Huntington's disease	Huntingtin	Nuclear inclusions
Spinocerebellar ataxia		
Type 1	Ataxin 1	Nuclear inclusions
Type 2	Ataxin 2	Cytoplasmic inclusions
Machado–Joseph disease	Ataxin 3	Nuclear inclusions

Table 1. Protein deposition in neurodegenerative diseases. Misfolding and accumulation of proteins in the nervous system represent a pathogenic mechanism shared by most neurodegenerative disorders [2].

PRION DISEASES

Prion diseases, also defined as transmissible spongiform encephalopathies (TSEs), are a group of fatal neurodegenerative disorders that may be characterized by infectious, genetic or sporadic aetiology [2]. These diseases may affect both animals and human, as shown in Table 2 [3].

Spectrum of prion diseases of humans and animals

Prion disease	Natural host species	Etiology
sCJD	Humans	Unknown (somatic *PRNP* mutation?)
Familial Creutzfeldt-Jakob disease (fCJD)	Humans	Familial (germ line *PRNP* mutation)
Iatrogenic Creutzfeldt-Jakob disease (iCJD)	Humans	Surgical procedures (infection)
vCJD	Humans	Ingestion of BSE-contaminated food; transfusion medicine (infection)
Kuru	Humans	Ingestion, ritualistic cannibalism (infection)
Fatal Familial Insomnia (FFI)	Humans	Familial (germ line *PRNP* mutation)
Gerstmann-Sträussler-Scheinker Syndrome	Humans	Familial (germ line *PRNP* mutation)
Scrapie	Sheep, goats	Infection, natural; mode of transmission unclear
Chronic Wasting Disease (CWD)	Deer, Elk	Infection; mode of transmission unclear
BSE	Cattle	Ingestion of BSE-contaminated feed (infection)
Transmissible mink encephalopathy	Mink	Ingestion (infection); Origin unclear
Feline spongiform encephalopathy	Cats	Ingestion of BSE-contaminated feed (infection)
Spongiform encephalopathy of zoo animals	Zoologic bovids, primates	Ingestion of BSE-contaminated feed (infection)

Table 2. Prion diseases of humans and animals. Prion disorders may affect both animals and humans, and may be characterized by infectious, genetic or sporadic aetiology [3].

TSEs may present a heterogeneous spectrum of clinical symptoms, including dementia, insomnia, ataxia and many others. Indeed, different prion diseases may be characterized by different clinical features, that, besides clinical manifestation, include aetiology, incidence, affected brain regions and time course of the disease [2]. However, although the clinical presentation may differ among TSEs, these disorders are characterized by shared neuropathological hallmarks, as misfolded scrapie prion protein (PrP^{Sc}) aggregation, synaptic and neuronal loss, spongiform vacuolation and brain inflammation (Figure 1) [4].

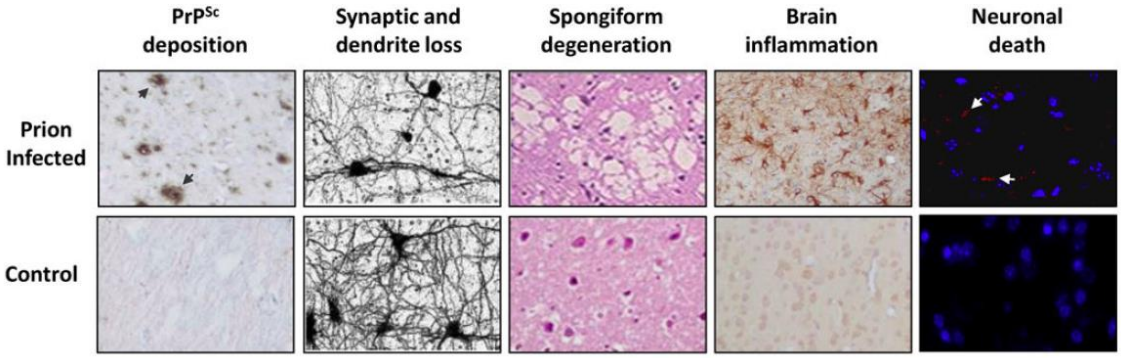

Figure 1. Neuropathological features of prion diseases. PrP^{Sc} deposits, synaptic damage and neuronal death, spongiform degeneration and brain inflammation are hallmarks of prion disorders [4].

The pathogenic agent at the basis of TSEs is named prion, a term introduced by Stanley B. Prusiner in 1982 to indicate a "proteinaceous infectious particle" with the unique capacity to self-replicate without requiring nucleic acids [5]. Indeed, the scrapie agent is resistant to inactivation by most procedures used to destroy nucleic acids [6]. Enzymatic digestion of brain extracts from prion-infected animals followed by size-exclusion chromatographic analysis allowed the isolation of PrP^{27-30}, a protein with a molecular weight of 27-30 kDa, which represents the resistant core of PrP^{Sc} [7]. Following sequencing of the PrP^{27-30} N-terminal domain, oligonucleotide probes were synthesized and used to screen cDNA libraries derived from healthy and scrapie-infected hamster brains through Southern Blot, allowing the identification of the gene (*Prnp*) that encodes for an endogenous protein named cellular prion protein (PrP^{C}) [8]. The fact that both PrP^{C} and PrP^{Sc} are encoded by the same cellular gene suggested that the different properties of these two proteins are determined by post-translational modifications [9]. Indeed, according to the "protein-only" hypothesis, PrP^{Sc} results from the conformational change of the host-encoded PrP^{C}, that is progressively converted into prions during the course of the disease [10].

PrP^{C} and its pathological isoform PrP^{Sc} show different biochemical properties, due to post-translational modifications by which the α-helical enriched structure of PrP^{C} (40% α-helix, 3% β-sheet) is converted into a prominent β-sheet folding (30% α-helix, 45% β-sheet). As a result of these structural changes, PrP^{Sc} is insoluble, prone to aggregation and partially resistant to proteases (Figure 2) [11, 12].

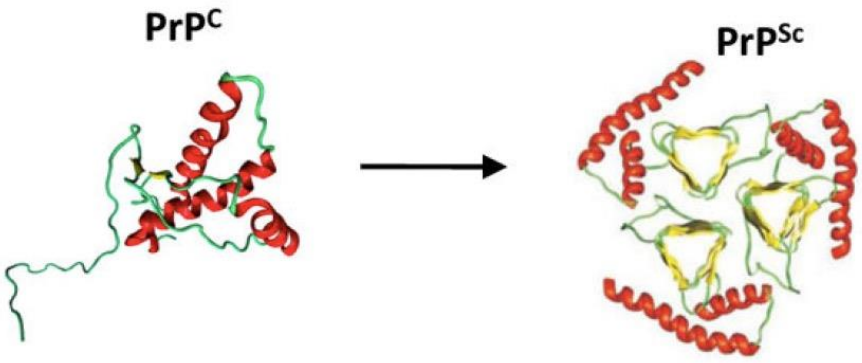

Figure 2. The conversion of the natively folded PrP^{C} into PrP^{Sc} triggers disease. The structure of PrP^{C} corresponds to the experimentally determined tridimensional conformation of the protein by nuclear magnetic resonance, while the structure of PrP^{Sc} corresponds to a model based on low resolution techniques [4].

Two mechanisms of prion conversion have been proposed (Figure 3). The "refolding" or template-assistance model hypothesizes an interaction between exogenously introduced PrP^{Sc} and endogenous PrP^{C}, which is forced to convert itself into further PrP^{Sc}. A high-energy barrier prevents spontaneous conversion of PrP^{C} into PrP^{Sc}. The "seeding" or nucleation-polymerization model proposes that PrP^{C} and PrP^{Sc} are in a reversible thermodynamic equilibrium, and only if several monomeric PrP^{Sc} molecules are mounted into a highly ordered seed further monomeric PrP^{Sc} can be recruited and eventually aggregate to amyloid. Fragmentation of these aggregates results in the increase of seeding nuclei, which can recruit further PrP^{Sc} [13].

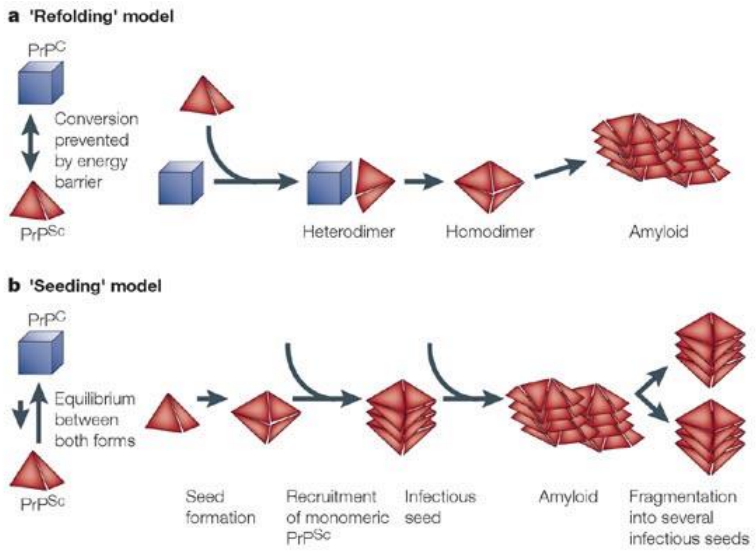

Figure 3. Proposed mechanisms of prion conversion. Two models of the conversion of PrP^{C} into the misfolded PrP^{Sc} have been proposed. A) The refolding model proposes that there is an interaction between externally introduced PrP^{Sc} and cellular PrP^{C}, which is forced to convert itself into further PrP^{Sc}. B) The seeding model proposes that PrP^{C} and PrP^{Sc} are in a reversible equilibrium, and only if several monomeric PrP^{Sc} molecules are mounted into a highly ordered seed further monomeric PrP^{Sc} can be recruited and eventually aggregate to amyloid [13].

Although the formation and the progressive accumulation of PrP^{Sc} in the brain is thought to represent the pathogenic event leading to neurodegeneration, the underlying mechanisms are still under debate [4]. Many evidences point to a gain-of-function mechanism, meaning that the misfolded protein is able to induce direct neurotoxicity. Indeed, purified PrP^{Sc} from the brain of infected animals triggers apoptosis of treated N2a neuroblastoma cells [14], while prion protein oligomers resulted to be neurotoxic both *in vitro* and *in vivo* [15]. However, resistance of *Prnp* knockout mice to prion infection [16] underlines that PrP^{Sc} is not sufficient to develop the disease. Moreover, high levels of accumulated PrP^{Sc} within PrP^{C}-expressing tissue grafted into the brains of PrP^{C}-null mice do not propagate the infectivity in the host tissue [17]. Finally, progressive propagation of PrP^{Sc} in glial cells is not able to induce death of surrounding neurons depleted of PrP^{C} [18], also arguing against a direct neurotoxic effect of misfolded PrP^{Sc}. Indeed, the loss of a critical physiological function of PrP^{C} may represent a possible mechanism by which PrP^{Sc} formation leads to neurodegeneration. On the other hand, the lack of striking phenotypes and the absence of neurodegeneration in the brain of *Prnp* knockout mice argue against the

loss-of-function hypothesis [19, 20]. Consequently, it is still under debate whether prion toxicity is mediated by gain-of-function of misfolded protein or loss-of-function of normal prion protein, or, more likely, by a combination of the two. Indeed, multiple mechanisms may contribute to the pathology of prion diseases, leading to progressive neurodegeneration.

HUMAN PRION DISEASES

Prion diseases may occur as sporadic, genetic and infectious disease in humans [2]. The first cases of human prion disease, Creutzfeldt-Jakob disease (CJD), were reported in 1920s. The number of human TSEs has increased and now includes Gerstmann-Sträussler-Scheinker syndrome (GSS), fatal familial insomnia (FFI) and Kuru (Table 2) [21].

Creutzfeldt-Jakob disease was originally described as a sporadic disease with no known cause (sporadic CJD, sCJD). CJD affects about 1 person over one million per year, and it is characterized by rapid cognitive decline, causing dementia, and cerebellar symptoms as ataxia [21]. It has been hypothesized that sCJD could be caused by somatic mutations in the *PRNP* gene, or by unrecognized infections or by the propensity of PrP^{C} to self-assemble into PrP^{Sc} aggregates, thus initiating prion replication. However, none of these hypotheses have been proven, thus the cause of sCJD remains unknown [21, 22]. It has been proposed that the clinicopathological phenotypes of sCJD patients can be determined by the type of PrP^{Sc} (named types 1 and 2) that accumulates in the affected brains and by the genotype at codon 129 of the *PRNP* gene, the site of a methionine/valine polymorphism [23]. Type 1 and type 2 PrP^{Sc} differ by the size of their proteinase K (PK) resistant core (21 and 19 kDa, respectively), that depends on the PK cleavage site (residues 82 and 97, respectively) [24].

Variant CJD (vCJD) resulted from transmission of prions from cattle infected with bovine spongiform encephalopathy (BSE) to humans through the consumption of contaminated beef products [22]. Another infectious form of CJD is the iatrogenic CJD (iCJD), which is accidentally transmitted by medical or surgical procedures, such for example corneal transplantation, *dura mater* grafts, treatment with human growth hormone and gonadotrophin [21]. Moreover, some cases of iCJD were caused by the

use of inefficiently sterilized implanted electrodes and instruments during neurosurgical procedures [22]. Besides, infectious forms of prion diseases include Kuru, an endemic disease among some tribes of New Guinea, which is transmitted by ritual cannibalism of dead relatives [21, 22].

Several mutations in the *PRNP* gene have been identified in families with genetic forms of prion diseases, such as familial CJD (fCJD), Gerstmann-Sträussler-Scheinker syndrome (GSS) and fatal familial insomnia (FFI). fCJD may be caused by point mutations affecting the region between the second and third helix of the C-terminus or by insertions in the octarepeat region at the N-terminus. fCJD is an autosomal dominant inherited disease, characterized by different clinicopathological phenotypes depending on mutation type, codon 129 polymorphism and many other factors [21]. Interestingly, the point mutation D178N can cause either fCJD or FFI, depending on the polymorphism present at codon 129. D178N coupled with 129MV (heterozygosity methionine-valine) causes fCJD, with dementia and widespread deposition of PrP^{Sc}, while in presence of 129MM (homozygosity for methionine) it associates with FFI, with thalamic deposition of prions [22]. Indeed, FFI is a genetic prion disease characterized by disruption of normal sleep-wake cycle, sympathetic over activity, endocrine abnormalities and impaired attention [21]. Besides, GSS, another autosomal dominant form of prion disease, is characterized by earlier age at onset, longer disease duration and more prominent cerebellar ataxia than fCJD [21]. The most common mutation causing GSS is the point mutation P102L of the *PRNP* gene [25].

THE CELLULAR PRION PROTEIN

The cellular prion protein is encoded by *Prnp* gene (on mouse chromosome 2, *PRNP* on human chromosome 20), and is highly conserved across species. The *Prnp* gene is a single-copy gene that contains either three (mouse, rat, bovine, sheep) or two exons (humans, hamster). However, the entire open reading frame (ORF) of PrP^C is contained into a single exon in all the known *Prnp* genes (Figure 4) [26-29].

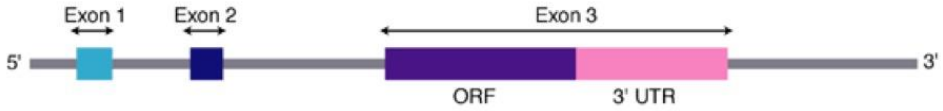

Figure 4. The murine PrP gene (*Prnp*). The murine PrP gene possesses three exons; exon 3 contains the entire open reading frame (ORF) and a 3' untranslated region (3' UTR) [30].

PrP^C is a ubiquitously expressed endogenous glycoprotein, which is mainly exposed to the outer layer of the cell surface as an N-glycosylated glycophosphatidylinositol (GPI)-anchored protein (Figure 5) [31, 32].

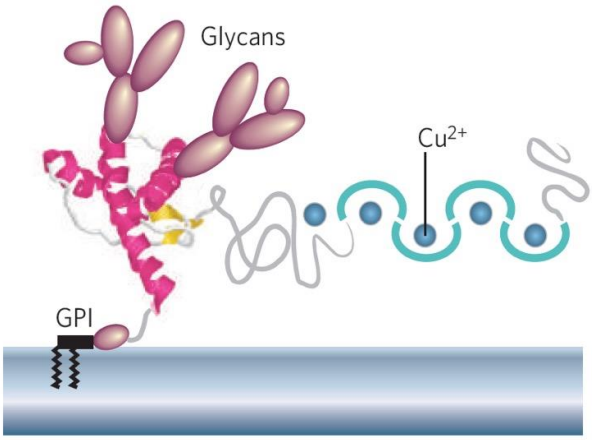

Figure 5. Mature form of the cellular prion protein, PrP^C. PrP^C is a GPI-anchored protein, with a flexible, random coil N-terminal domain and a globular C-terminal domain. The N-terminal domain of PrP^C contains octapeptide repeats (in light blue), which can bind divalent cations such as copper ions. The C-terminal domain of PrP^C contains three α-helices (in pink) and an antiparallel β-pleated sheet formed by two β-strands (in yellow). Depending on the glycosylation status of two Asn residues, PrP^C can be found as un-, mono- or di-glycosylated protein [33].

PrP^C precursor protein presents two signal peptides. At the N-terminal region, a signal peptide of 22 amino acids targets the protein to the secretory pathway, where it undergoes a glycosylation process, while at the C-terminal region a second signal sequence of 23 amino acids is needed for the attachment of the GPI moiety at the C-terminus of PrP^C (Figure 6). After proteolytic cleavage and post-translational modification in the endoplasmic reticulum (ER) and in the Golgi, PrP^C is exported to the cell surface as a mature protein of 208-209 amino acids.

The mature form of PrP^C structurally consists of two domains, as determined by nuclear magnetic resonance [34]: an N-terminal flexible unfolded domain and a C-terminal folded globular domain. The N-terminal domain consists of a random coil sequence of about 100 amino acids, that contains the octapeptide repeats (OR), that confer to the protein the ability to bind copper ions [35], and two positively charged clusters, CC_1 and CC_2. The globular domain presents three α-helices and two β-strands organized in an antiparallel β-pleated sheet. A single disulphide bond links cysteine residues 178 and 213 (mouse numbering). Two glycosylation sites are presents in the C-terminus of PrP^C (Asn180 and Asn196). The glycosylation status of these two residues determines whether PrP^C is expressed as un-, mono- or di-glycosylated protein [36]. N- and C-terminal domains are linked by the hydrophobic core (HC), a sequence of hydrophobic amino acids (Figure 6) [34].

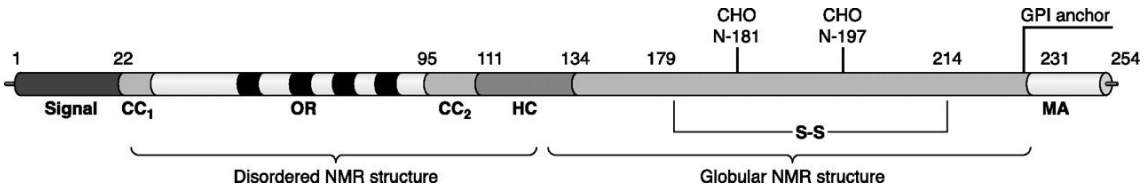

Figure 6. Outline of the primary structure of the cellular prion protein including post-translational modifications. A secretory signal peptide is located at the extreme NH_2 terminus. CC_1 and CC_2 indicate the charged clusters. OR indicates the four octapeptide repeats. HC defines the hydrophobic core. MA denotes the membrane anchor region. S-S indicates the single disulphide bridge, and the glycosylation sites are designated as CHO. The numbers describe the position of the respective amino acids [37].

PrP^C EXPRESSION AND SUBCELLULAR ENVIRONMENT

PrP^C is highly expressed in the developing and mature nervous system, although differences in its content are observed among brain regions, cell types and neurons with distinct neurochemical phenotypes [38]. However, many non-neuronal tissues also express PrP^C, such as blood lymphocytes, gastro-epithelial cells, heart, kidney and muscles [39, 40]. Despite the special relevance of PrP^C in the nervous system, its expression pattern suggests a role for PrP^C not limited to this tissue.

PrP^C expression in the nervous system starts from the embryogenesis and is developmentally regulated, generally increasing during brain development [41-45]. Indeed, PrP^C expression increases markedly during brain development, starting from the embryogenesis and reaching a peak at the end of the synaptogenesis [44]. Regional differences in PrP^C expression were observed, with the highest PrP^C expression in structures characterized by plasticity during adulthood, such as the hippocampus and the olfactory bulb, and lower expression in thalamus and cortex (Figure 7) [44].

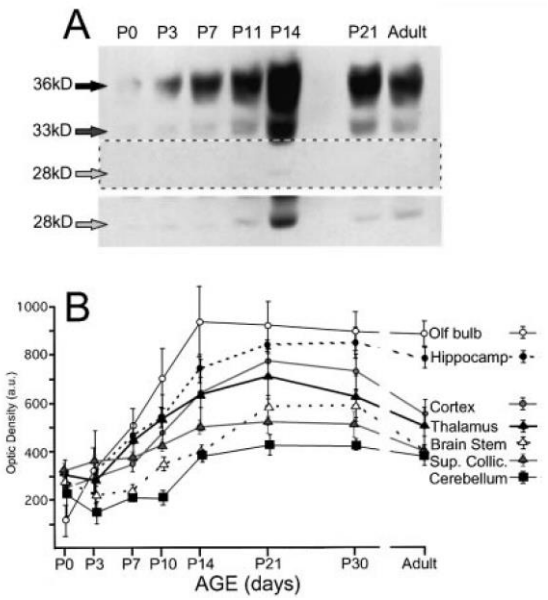

Figure 7. PrP^C protein expression in the developing and adult hamster brain. A) PrP^C expression increases markedly during brain development, from postnatal day 0 (P0) to P14, slightly decreasing during adulthood. B) Regional differences in PrP^C expression were observed, with the highest PrP^C expression in the hippocampus and the olfactory bulb, and lower expression in thalamus and cortex [44].

Spatiotemporal analysis of PrP^C expression during mouse central nervous system (CNS) development revealed that the hippocampus, the thalamus and the hypothalamus are the regions with the earliest and the highest PrP^C expression. During brain early postnatal development, PrP^C is highly expressed in the hippocampus, and in particular the *stratum lacunosum-molecolare*, a synapse-rich region, revealed the highest PrP^C expression. Moreover, high PrP^C expression was also observed in some specific white matter structures, such as the hippocampal fimbria, the *stria terminalis* and the fasciculus retroflexus (Figure 8) [45].

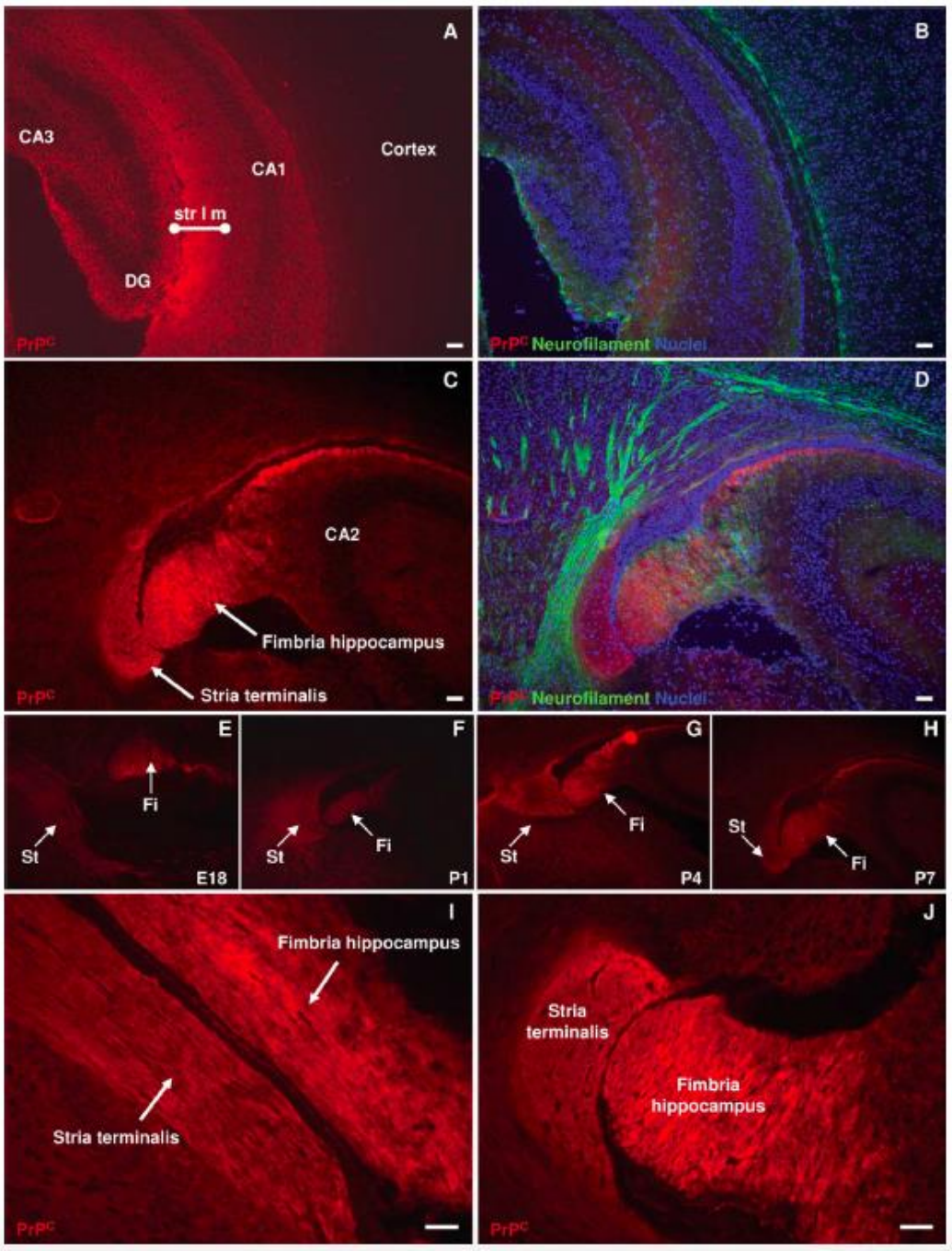

Figure 8. PrP^C expression in the hippocampus during development. A, B) At P7 PrP^C (in red; A) is detected throughout the hippocampus, and in particular at high levels in the *stratum lacunosum-molecolare* (str l m), a synapse-dense region. No signal for PrP^C is detected in the cortex. A merged image is shown in B (PrP^C, in red; neurofilament, in green; nuclei signals in blue). C–H) PrP^C is specifically and highly expressed by the fimbria of the hippocampus and the *stria terminalis* at P7 (C, D). The fimbria of the hippocampus (Fi) and the *stria terminalis* (St) express high level of PrP^C also at embryonic stages (E18.5), and progressively increase the level of expression during postnatal development: P1 (F), P4 (G), and P7 (H). I, J) Higher magnification of longitudinal (I) and coronal (J) section of the fimbria of the hippocampus and the *stria terminalis*, highlighting the net boundaries of PrP^C expression between other brain regions and these structures. Scale bars ¼ 50 lm [45].

Concerning subcellular localization, PrP^C is mainly located at the synapses, both presynaptically and postsynaptically [40, 46-49]. During its normal life cycle, PrP^C is bound to the cell membrane via a GPI-anchor and it is mainly found in specialized membrane regions, named lipid rafts, that are detergent-insoluble membrane microdomains enriched in cholesterol and sphingolipids [38]. PrP^C is recycled between the cell surface and the endocytic compartment via two mechanisms. In neurons, PrP^C is internalized through clathrin-coated vescicles, while in other cell types, such as in glial cells, PrP^C is endocyted through a caveolin-mediated mechanism [38, 50, 51].

PHYSIOLOGICAL FUNCTION OF CELLULAR PRION PROTEIN

During the last few decades, many efforts have been carried out to investigate the physiological function of PrP^C. All these attempts were focused using multiple approaches, such as the identification of interaction partners, genetic studies of human PRNP locus, overexpression of ectopic PrP^C in several cell types and organisms, and PrP^C expression ablation in mice, cows and goats (Figure 8). Despite these studies have provided many hints on PrP^C function, a conclusive view is still missing [52].

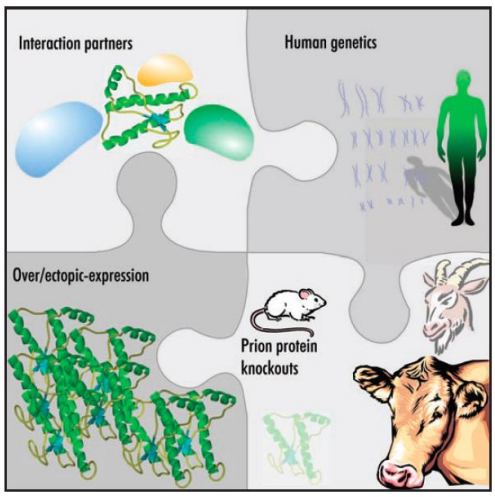

Figure 9. Different approaches to study the physiological function of PrP^C. Many approaches to study the normal function of PrP^C have been used, none of which have conclusively shown PrP^C function. Interacting partners of PrP^C have yielded many interesting candidates, while human genetic studies have found associations of PrP^C with diseases beyond prion disease and even to learning and memory. Over- and ectopic-expression studies constitute another approach to determine the function of PrP^C, together with prion protein knockouts, that provided some interesting clues to the physiology of PrP^C [52].

INSIGHTS FROM KNOCKOUT MODELS

The high conservation of PrP^C among mammalian species suggests that this protein may play some critical physiological roles during evolution [22]. Indeed, great expectations were placed on the generation of PrP^C-deficient mouse models and several groups independently generated several knockout mice, taking advantage of

homologous recombination, to investigate the physiological functions of PrP^C (Figure 10a).

The first *Prnp* knockout mouse strains, Zurich I and Edinburgh, were generated by inserting neomycin resistance (neo) cassette into exon 3 of the *Prnp* gene. These mice, in which the genetic modification is restricted to *Prnp* ORF, develop and reproduce normally, do not show gross behavioural and learning impairments and failed to show any striking phenotype [19, 53]. However, genetic compensation and developmental plasticity may mask the effects of PrP^C ablation [52]. Indeed, more recent studies pointed out that these mice present subtle phenotypes, such as demyelinating pathology in peripheral nervous system in aging [54], alteration of circadian rhythms [55], impaired long term potentiation (LTP) [56], enhanced susceptibility to oxidative stress [57, 58] and excitotoxicity [59].

In contrast, another set of knockout models, Nagasaki, Rcm0 and Zurich II, develop normally but undergo severe ataxia during aging, due to cerebellar atrophy and loss of Purkinje cells [60]. These mice were generated by a knockout procedure that disrupted not only the *Prnp* ORF, but affected also its flanking regions, leading to the formation of a chimeric transcript between *Prnp* and a paralog gene, *Prnd*, located 16 kb downstream (Figure 10b,c) [61]. *Prnd* encodes for an N-glycosylated GPI-anchored protein named Doppel (Dpl), normally expressed in many tissues but not in the adult brain, which physiological function is still unknown [62]. As a consequence of the deletion strategy used to generate these models, *Prnd* is placed under the control of *Prnp* promoter, leading to ectopic expression of Dpl protein. Levels of Dpl expression in the brain were inversely correlated to the onset of the phenotype [63]. Reintroduction of *Prnp* in these mice rescued the phenotype, thus PrP^C counteracts Dpl neurotoxicity through a still unknown mechanism [64]. Indeed, ectopic expression of Dpl in the absence of PrP^C, rather than absence of PrP^C itself, causes the strong phenotype observed in these knockout models.

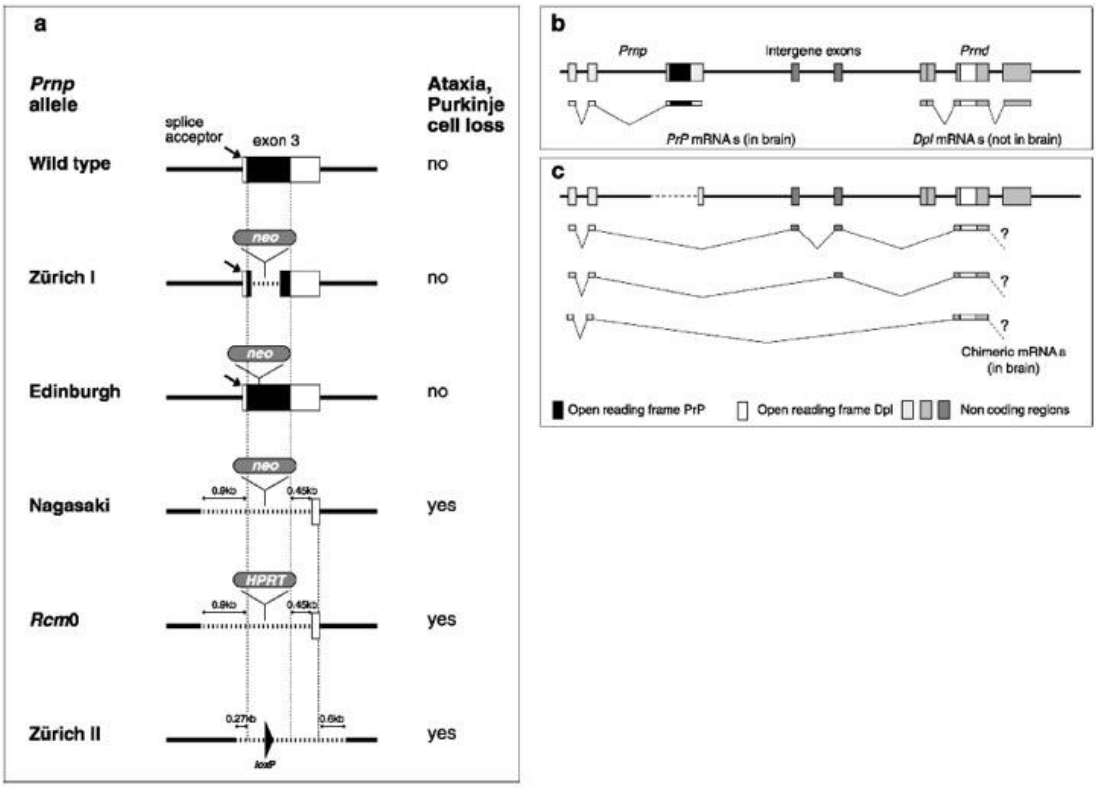

Figure 10. *Prnp* knockout strategies and their consequences. A) Various strategies used to target *Prnp* by homologous recombination. The black boxes represent PrP ORFs; white boxes, non-coding *Prnp* regions; grey boxes, inserted sequences; dotted line, deleted regions; neo, neomycin phosphotransferase; HPRT, hypoxanthine phosphoribosyltransferase; loxP (black arrowhead), a 34-bp recombination site from phage P1. B) Coding and non-coding exons of *Prnp*, *Prnd* and intergenic exons of unknown function. C) Exon skipping leads to expression of Doppel under the control of the *Prnp* promoter. Deletion of the splice receptor site upstream of the third *Prnp* exon entails the formation of several chimeric mRNAs comprising the first two exons of *Prnp* [65].

All *Prnp* knockout mice presented above were generated by means of homologous recombination in embryonic stem cells obtained from the 129 strain of mouse, and then backcrossed to non-129 strains. This results in the presence of systematic genetic confounders at the *Prnp* locus. More recently, in order to overcome these limitations, a new co-isogenic line of *Prnp* knockout mice (Zurich-3, ZH3) was generated using transcription activator-like effector nuclease (TALEN)-based genome editing on a pure C57BL/6J genetic background [66].

Unfortunately, due to the lack of striking phenotypes, data from knockout models failed to conclusively define any important role for PrP^C in the physiology of the nervous system. However, upon deeper examination many subtle phenotypes emerged, thus several PrP^C physiological functions have been proposed. PrP^C modulates sleep-wake cycles, hippocampal-dependent spatial learning and memory formation [21, 33, 38]. At the cellular level, PrP^C plays an anti-apoptotic role and protects against oxidative stress [21]. Indeed, a recent work from our group reported that PrP^C exerts its neuroprotective role modulating NMDA receptor activity [67]. Moreover, many studies reported a role for PrP^C in modulating synaptic activity, neuronal excitability and neurite outgrowth. In the peripheral nervous system, PrP^C is involved in myelin maintenance. Besides these functions strictly related to the nervous system, PrP^C also seems to play immunomodulatory functions and to affect hematopoietic and neural stem cell biology [21, 33, 52].

Figure 11 summarizes some of the cellular processes in which PrP^C is involved in the nervous system.

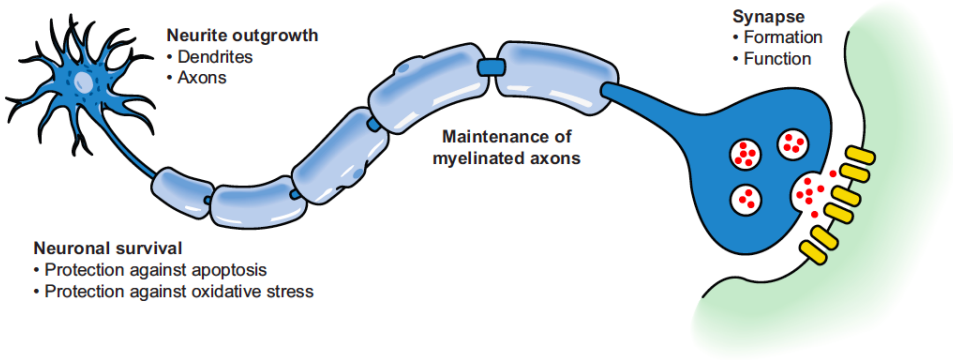

Figure 11. Physiological processes involving PrP^C. Neurite outgrowth, including growth of axons and dendrites, was observed to be reduced in neurons lacking PrP^C. PrP^C has been reported to promote neuronal survival, in particular following apoptotic or oxidative stress. Cerebellar granule cell apoptosis was observed in mice expressing toxic N-terminal deletion mutants of PrP. In addition, the latter transgenic mice show an impaired maintenance of myelinated axons in the white matter. Another site of PrP^C action might be the synapse, which is often affected in the first stage of prion diseases and whose formation was found to be reduced in neuronal cultures devoid of PrP^C. Furthermore, electrophysiological studies indicate a role of PrP^C in synapse function, especially in neurotransmitter release [21].

PrP^C SIGNALLING

Several lines of evidence suggest that PrP^C can act as a cell-signalling molecule, playing a role in signal transduction in response to interactions with multiple binding partners. Thus, PrP^C can link stimuli between the extracellular environment and the cell, being able to participate in multiple neuronal processes, ranging from survival to synaptic plasticity [68, 69]. In line with the topic and the aim of this thesis, the particular role of PrP^C in cell signalling will be described in detail in the following paragraphs.

SEARCH FOR PRION PROTEIN INTERACTORS

The subcellular localization of PrP^C in lipid rafts may indicate a possible involvement in signal transduction. Indeed, many signalling molecules are located in these particular regions of the plasma membrane, which are considered "hot spots" for signal transduction [70]. As the identification of cellular partners of PrP^C may help to unravel its physiological functions, many studies were aimed to disclose PrP^C interactome at the cell membrane. Indeed, signal transduction requires the interaction between a ligand and its receptor, that is usually a transmembrane protein with a cytosolic domain that transfers the signal from the extracellular environment to the intracellular compartment [71]. PrP^C is a GPI-anchored protein bound to the outer leaflet of the cell membrane, thus it lacks the cytosolic domain required for the signal transduction. Indeed, a lot of efforts were done to identify possible interactors of PrP^C that could act as co-receptors.

Among them, neural cell adhesion molecule (NCAM) was identified as binding partner of PrP^C applying a mild in situ crosslinking method that maintains the microenvironment of PrP^C on the membrane of mouse neuroblastoma cells (N2a) [72]. More recently, NMR structural studies revealed that the regions involved in this functional interaction are the N-terminal region of the human PrP^C and the second module of NCAM Fibronectin type-3 domain [73]. The physiological relevance of this interaction in modulating neurite outgrowth was proven [74, 75] and will be discussed below.

Other well characterized interactors of PrP^C are laminin receptor precursor and laminin receptor [76, 77], the extracellular matrix glycoprotein laminin [78] and the co-chaperone stress-inducible protein 1 (STI1) [79].

More than 20 proteins residing in the proximity of PrP^C were identified using a time-controlled transcardiac perfusion cross-linking (tcTPC) strategy. This novel technique was used for the study of protein interactions in complex tissues, and in particular to study the cellular microenvironment of PrP^C in the brain. Many of the identified proteins are involved in cell adhesion and neurite outgrowth (Table 3) [80]. Interestingly, using this technique, amyloid precursor protein (APP) appeared to form a complex with PrP^C. More recently, PrP^C was identified as a functional receptor for Aβ-oligomers [81], the molecular species that triggers toxicity in Alzheimer's disease (AD). However, the exact role of PrP^C in the pathogenesis of AD is still under debate [82-84].

Identified proteins	Accession no. (NCBI)	MW (kDa)	Subcellular location[a]	CID[b] spectra	Domains[c]
Prion protein (PrP)	AAH06703	28	GPI anchor	12	
Apolipoprotein E (ApoE)	P08226	36	Secreted	11	
Neural cell adhesion molecule 1 (N-CAM1)	P13595	119	GPI anchor/type I TM	17	FNIII, C2
Dipeptidyl aminopeptidase-like protein 6 (DPPX)	AAC97366	91	Type II TM (probable)	13	
Myelin-associated glycoprotein (MAG)	NP_034888	68	Type I TM	8	C2
Dynamin-1	P39053	97	Microtubule associated	10	
Neural adhesion molecule F3 (contactin1)	NP_031753	113	GPI anchor	10	FNIII, C2
Neural cell adhesion molecule 2 (N-CAM2)	O35136	93	GPI anchor/type I TM	9	FNIII, C2
Amyloid precursor protein (APP)	NP_031497	79	Type I TM	7	
Limbic system–associated membrane protein (LSAMP)	XP_156147	25	GPI anchor	5	C2
Myelin/oligodendrocyte glycoprotein (MOG)	AAA03180	25	Type I TM	2	Ig
Immunoglobulin superfamily receptor (PGRL)	AAL02217	65	Type I TM	5	Ig
Nectin-like 1	NP_444429	43	Type I TM	4	C2
Clusterin precursor	Q06890	52	Secreted	3	
Opioid binding protein (OBCAM)	XP_284477	37	GPI anchor	2	C2
Neurotrimin	AAK00276	38	GPI anchor	2	C2
Cell adhesion molecule L1 (L1cam)	XP_109546	141	Type 1 TM	6	FNIII, C2
Extracellular matrix protein 2 (SPARC like-1)	NP_034227	72	Secreted	3	
Protein disulfide isomerase (PDI)	P09103	57	ER lumen	2	
A disintegrin and metalloprotease domain 23 (ADAM23)	NP_035910	91	Type I TM (probable)	3	
Chaperone BiP	CAA05361	72	ER lumen	2	
Amyloid precursor protein-binding family B member 1 (Fe65)	Q9QXJ1	77	Binds to C-terminus of APP	2	
Amyloid beta (A4) precursor-like protein 2 (APLP2)	XP_134705	87	Type I TM	2	
Calsyntenin 1	NP_075538	109	Type I TM	2	
Plasma membrane 2, ATPase Ca^{2+} transporting, wriggle	NP_033853	133	Type III TM	2	

Table 3. The molecular microenvironment of PrP in the living brain consists predominantly of membrane proteins that harbor immunoglobulin C2 and/or FNIII-like domains. tcTPC of outbred mice followed by high stringency immunoaffinity purification and mass spectrometry enabled identification of more than 20 protein components of PrP containing crosslinking complexes. All proteins listed were identified with high confidence based on strong and unique collision induced dissociation (CID) spectra from at least two peptides. Proteins are listed in order, with the position of a given protein in the table reflecting the percentage of primary structure corresponding to the combined unique CID spectra. Note the predominance of GPI-anchored proteins and that all entries are either integral membrane proteins or are known to reside in spatial proximity to the cell membrane [80].

Recently, a more physiological approach was used to characterize the interactome of a fully functional Myc-tagged PrP^C, taking advantage of co-immunoprecipitation strategy under native conditions. Several proteins interacting with PrP^C were identified by mass spectrometry and many of them resulted to be involved in myelin maintenance [85].
The interactions between PrP^C and its binding partners have been functionally validated and resulted involved in many cellular processes, such as neuroprotection, cell death and neurite outgrowth.

PrP^C AND THE SRC FAMILY KINASES (SFK)

Src family kinases are non-receptor tyrosine kinases that are generally associated with the inner face of the cell membrane, that integrate several signals transduced by the cell surface receptors in response to a large number of extracellular stimuli. Src kinases play a role in many cellular events, such as cell growth and proliferation, cell adhesion and migration, differentiation, survival and death. This family of kinases is composed by nine members: Src, Yes, Fyn, Fgr, Lyn, Hck, Lck and Blk [86, 87].
The first demonstration of PrP^C involvement in cell signalling was achieved using antibodies against the prion protein in order to mimic a putative physiological ligand. Indeed, antibody cross-linking of PrP^C at the cell membrane of 1C11 cells, a murine line that can differentiate in serotonergic and noradrenergic neurons, led to phosphorylation of p59fyn kinase [88]. Moreover, the Fyn kinase inhibitor PP2 completely abolished the downstream activation of ERK kinase in the same system [89]. As Fyn was shown to mediate NCAM-induced neurite outgrowth [90], and as PrP^C is known to directly interact with NCAM at the neuronal surface [72], more recently the role of PrP^C in NCAM-mediated signalling was unravelled. Indeed, the interaction with PrP^C promotes NCAM recruitment to lipid rafts and regulates Fyn kinase activity through the receptor protein tyrosine phosphatase α (RPTPα) and stimulate neurite outgrowth [74]. Moreover, PrP^C is not only able to regulate neurite outgrowth by interaction with NCAM *in cis*, but also *in trans* interactions between NCAM and recombinant PrP added to the culture medium are able to provide the same result, thus supporting previously reported data [91]. More recently, we confirmed the role of recombinant full-length PrP (recPrP) in promoting neurite outgrowth. Notably, PrP^C

knockout neurons were insensitive to recPrP stimulation, thus suggesting that recPrP functions as a signaling molecule and its homophilic interaction with membrane-anchored PrP^C may promote neurite outgrowth. Interestingly, pre-treatment of the neurons with a selective Src family kinases inhibitor or with a monoclonal antibody against NCAM strongly impairs the response to recPrP, thus supporting the role of NCAM and SFKs in the PrP^C signalling complex [75]. Finally, in PrP-null brains, increased total levels, but lower activation, of Fyn have been reported [74].

The functional interaction between prion protein, NCAM and Fyn kinase was also examined in prion diseases, in order to evaluate the possible involvement of the NCAM-mediated Fyn signalling in prion propagation. *In vivo* experiments on knockout animals failed to show differences in incubation time and PrP^{Sc} deposition in $NCAM^{-/-}$ and in $Fyn^{-/-}$ mice compared to wild-type (WT) animals [72, 92]. However, increased levels of phosphorylated Fyn were detected both in chronically prion-infected cell lines and in animal models of prion disease [93, 94].

Interestingly, it was recently shown that the detrimental effects on synaptic function mediated by interaction between PrP^C and Aβ-oligomers also depend on Fyn activation, which triggers the phosphorylation of the NR2B subunit of NMDA receptors and their loss from the post-synaptic membrane [65].

More recently, it was reported that PrP^C has the ability to recruit another member of the Src family kinases, the Lyn kinase [95], which was previously found to be present in the microenvironment of PrP^C at the plasma membrane of primary cerebellar neurons [96]. In this work, GSK3β, a kinase whose inhibition is neuroprotective, was also reported to be a downstream target of PrP^C. Indeed, the PrP^C-dependent GSK3β inactivation resulted to be mediated by a caveolin-Lyn complex located on neuronal cell bodies. Moreover, *in vivo* data highlighted increased GSK3β activity in PrP-null mouse brain [95].

PrP^C AND THE PI3K/AKT PATHWAY

The phosphatidylinositol 3-kinase/AKT (PI3K/AKT) pathway plays a role in the regulation of cellular processes, such as neuronal survival and apoptosis [97], and in cancer progression [98].

The first demonstration of a functional interaction between PrP^C and the PI3K/AKT pathway was provided by the use of the PI3K inhibitor wortmannin, that was able to block axon elongation induced by PrP-Fc fusion protein in mouse cerebellar granules [99]. Later on, significantly higher PI3K activity levels were found in both mouse neuroblastoma N2a cells and immortalized hippocampal HpL cells transfected with wild-type PrP^C in comparison to their controls. Moreover, PI3K activity was found to be reduced in PrP-null mouse brain compared to WT animals [100]. PI3K is known to be sensitive to superoxide and hydrogen peroxide [101], and to be activated by copper(II) ions [102]. Indeed, it was shown that the recruitment of PI3K by PrP^C promotes cell survival in response to oxidative stress and serum deprivation, and that this PrP^C-mediated effect is dependent on copper binding to the octapeptide region of the prion protein [100].

These findings suggest that PrP^C may exert a neuroprotective function, and its absence may increase susceptibility to neuronal injuries. Indeed, it was shown that both transient and permanent ischemia result in increased infarct volumes in *Prnp* knockout mice compared to WT controls. Moreover, in PrP^C-null mice reduced phosphorylation of AKT and increased activation of caspase-3 were observed [103]. Interestingly, PrP^C overexpression is able to reduce the infarct volume after ischemic injury, but does not affect AKT phosphorylation [104].

Recently, it has been shown that protein synthesis in neurons is enhanced by PrP^C-STI1 interaction by the PI3K-mTOR signalling pathway, and that this effect is responsible for neuroprotection and neuritogenesis. Interestingly, protein synthesis stimulation mediated by PrP^C-STI1 is impaired in neuronal cell lines chronically infected with prions, as well as in primary cultured hippocampal neurons acutely exposed to PrP^{Sc}. Indeed, these findings indicate that the impairment of this process during prion infection may contribute to neurodegeneration [105].

OTHER PrP^C SIGNALLING EFFECTORS

Other reported intracellular effectors of PrP^C signalling include the protein kinase A (PKA) [106-108] and protein kinase C (PKC) [91, 109], the MAP kinases ERK1/2 [89, 106, 107, 110], the enzyme NADPH oxidase [89] and the metalloprotease TNFα-converting enzyme (TACE) [111]. Moreover, functional interaction with several transcription factors, such as CREB, Egr-1 and c-fos [112], as well as with calcium signalling [113-116] have been reported.

A summary of PrP^C signalling effectors is reported in Table 4.

Targets	Cell type/tissue	Physiological response
Src kinases		
Fyn	1C11-derived bioaminergic neuronal cells	
	Primary hippocampal neurons	Neurite outgrowth
	PC12 neuronal cells	Neurite outgrowth
Lyn	1C11-derived serotonergic neuronal cells	Potentiation of neurotransmitter release
	Raphe	Potentiation of neurotransmitter release
PI3K/Akt	N2a neuroblastoma cells	Cell survival
	Primary hippocampal neurons	Protein synthesis
	1C11-derived serotonergic neuronal cells	Potentiation of neurotransmitter release
PKA	Rat retina	Neuroprotection
	Primary hippocampal neurons	Neuroprotection
	Hippocampal slices	Synaptic plasticity
NADPH oxidase	1C11-derived bioaminergic neuronal cells	
ERK1/2	Rat retina	Neuroprotection
	SN56 cells	
	Primary hippocampal neurons	Neurite outgrowth
	1C11-derived bioaminergic neuronal cells	
	Primary hippocampal neurons	Neurite outgrowth
GSK3β	1C11-derived serotonergic neuronal cells	Potentiation of neurotransmitter release
	Raphe	Potentiation of neurotransmitter release
TACE	1C11-derived bioaminergic neuronal cells	Neurotransmitter catabolism
mTOR	Primary hippocampal neurons	Protein synthesis
CREB	1C11-derived bioaminergic neuronal cells	Transcription of IEG
SMase	Hippocampal cell lines, mouse brain	
Ca2+	Hippocampal neurons	
	Primary hippocampal neurons	Neuroprotection, neuronal survival
	Primary hippocampal neurons	Neurite outgrowth
	Dorsal root ganglia neurons	Axonal growth

Table 4. Downstream targets of PrP^C-mediated signalling in a neuronal context. The diverse array of PrP^C signalling effectors is reported, together with the observed physiological response [69].

The data obtained in the presented literature suggest that PrP^C may act as a dynamic scaffolding protein on the cell surface with the ability to assemble with multiple sets of interactors to trigger different signalling cascades, according to the cell type and physiological state [38, 68].

REELIN/DAB1 SIGNALLING CASCADE

As previously discussed, of relevance for the present study, it has been reported that PrP^C directly interacts with NCAM at neuronal surface, thus regulating Fyn kinase activity [74], and could affect PI3K [100], Akt/PKB [103] and GSK3β [95] activity. All these intracellular kinases could be also regulated by yet another protein, Reelin, an extracellular matrix glycoprotein that activates a linear downstream signalling pathway [117]. Besides signal transduction, Reelin is also able to exert its biological functions via proteolytic activity as a serine protease of the extracellular matrix, having an important role in the modulation of cell adhesion [118]. Interestingly, it has been reported that PrP^C inhibits Reelin-mediated shedding of contactin-associated protein Caspr from the cell surface, thus increasing its surface levels and potentiating the inhibitory effect of this protein on neurite outgrowth [119].

REELIN STRUCTURE AND PROCESSING

The human RELN gene, located on the long arm of chromosome 7, was mapped and sequenced in 1997. This gene encodes for a large extracellular glycoprotein that consists of 3461 amino acids and has a predicted molecular weight of 388 kDa. Human Reelin is 94.2% identical to the mouse protein at the aminoacidic level, suggesting a strong functional conservation of the protein among species [120].

Reelin protein has a modular structure, composed by several domains (Figure 12) [121]. At the N-terminal region, a cleavable signal peptide of 27 amino acids is required for targeting the protein to the secretory pathway. The signal peptide is followed by a region of similarity with F-spondin, a protein secreted by floor plate cells that controls cell migration and neurite outgrowth. The N-terminal region of Reelin is prone to aggregation and presents a CR-50 epitope that can be recognized by CR-50 antibody, and is fundamental for Reelin-Reelin homophilic interactions. Indeed, it was shown that Reelin protein binds to each other to form a large protein complex, both *in vitro* and *in vivo*, and that this assembly formation is inhibited by CR-50 antibody [122]. Moreover, when the CR-50 region of Reelin is mutated, the protein fails to efficiently

activate downstream signalling cascade, meaning that Reelin exerts its physiological function by multimerization through this region [123]. The most striking feature of Reelin is the presence of eight internal repeats, so-called Reelin repeats (RR) that are composed of about 350 amino acids. Each repeat contains two related subdomains, A and B, and a central EGF-module enriched in cysteine residues [124]. At the C-terminal region of the protein is located a basic stretch of 33 amino acids, enriched in positively charged arginine residues, highly conserved among mammalian species and necessary for efficient activation of downstream signalling cascade [124, 125].

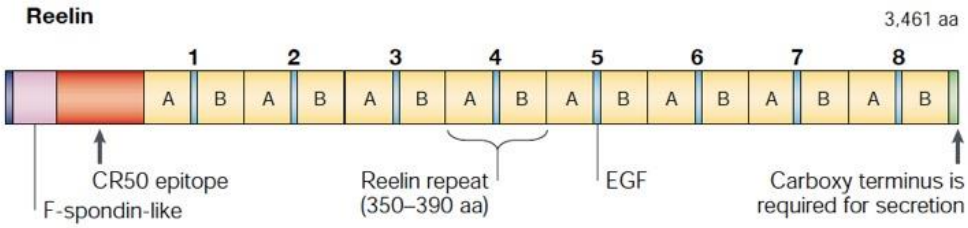

Figure 12. Domain structure of Reelin. Reelin contains a cleavable signal peptide at the amino terminus, followed by a region of similarity to F-spondin. The most striking feature of Reelin is the presence of a series of eight internal repeats comprising 350–390 amino acids (aa). These so-called Reelin repeats contain two related subdomains, A and B, separated by a stretch of 30 amino acids harbouring an epidermal growth factor (EGF)-like motif. A region rich in arginine residues at the carboxy terminus is required for secretion [121].

In vivo, Reelin is processed by cleavage in two sites located, respectively, between repeats 2 and 3 and between repeats 6 and 7. This processing does not occur in $Reln^{rl\text{-}Orl}$ mutant mice, in which Reelin is not secreted, suggesting that the cleavage takes place after secretion. Moreover, the cleavage is inhibited by zinc chelators, suggesting that one or more metalloproteases are involved [126]. Indeed, more recently, three enzymes involved in Reelin processing have been identified: the serine protease tissue plasminogen activator (tPA) cleaves Reelin at its C-terminal site, the extracellular matrix metalloproteinase ADAMTS-4 and the disintegrin and metalloproteinase ADAMTS-5 are able to cleave Reelin at both N-terminal and C-terminal sites [127]. As a result of the processing, Reelin is cleaved in five fragments that could be discriminated on molecular weight basis. Commonly used N-terminal antibodies allow detection of full-length Reelin and two smaller fragments, named N-

R6 (about 300 kDa) and N-R2 (about 180 kDa) (Figure 13). Even though the physiological function of this processing is not fully understood, it has been reported that the central fragment of Reelin is necessary and sufficient to activate the downstream signalling cascade [128]. However, a more recent work shown that the N-terminal cleavage of Reelin strongly impairs its signalling ability in comparison to the full-length protein [129].

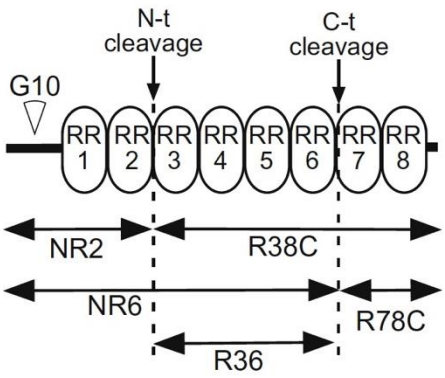

Figure 13. Schematic representation of Reelin protein. The epitope of G10 antibody is shown (N-terminal region of Reelin). The N-t and C-t cleavage sites are located after RR2 and RR6, respectively. RR; Reelin repeat [129].

REELIN SIGNAL TRANSDUCTION

Reelin-signalling pathway is triggered by binding of Reelin to two transmembrane lipoprotein receptors, named apolipoprotein E receptor 2 (ApoER2), also known as low-density lipoprotein receptor-related protein 8 (LRP8), and very-low-density lipoprotein receptor (VLDLR) [130]. Reelin binds to its receptors in form of oligomers, promoting the clustering of receptors on the plasma membrane. Upon clustering, the intracellular adaptor protein Disabled-1 (Dab1) could be recruited by binding to NPxY motifs in the receptor tails and could be phosphorylated by Src family kinases, such as Src and Fyn, on five tyrosine residues (Tyr185, Tyr198, Tyr200, Tyr220, Tyr232) [131-134]. Upon tyrosine phosphorylation, Dab1 is activated and can transduce the downstream signals. Among them, activated Dab1 could activate PI3K, leading to the activation of AKT, which in turn inhibits GSK3β, the major kinase involved in the

phosphorylation of microtubule-associated protein Tau [131, 135-137]. Indeed, Tau hyperphosphorylation is observed in mice in which Reelin pathway is disrupted [131].

Other downstream interactors of Dab1 are Crk-like protein (CRKL), which controls actin cytoskeleton rearrangements [138], and lissencephaly protein 1 (LIS1), which is involved in the regulation of neuronal migration and cortical lamination [139].

Finally, it has been shown that ApoER2 receptor could form a complex with postsynaptic density protein 95 (PSD95) and that this interaction is fundamental for the coupling between Reelin-signalling and NMDA receptors, and consequently for Reelin-mediated synaptic modulation [140, 141].

Reelin-signalling cascade is schematized in Figure 14 [117].

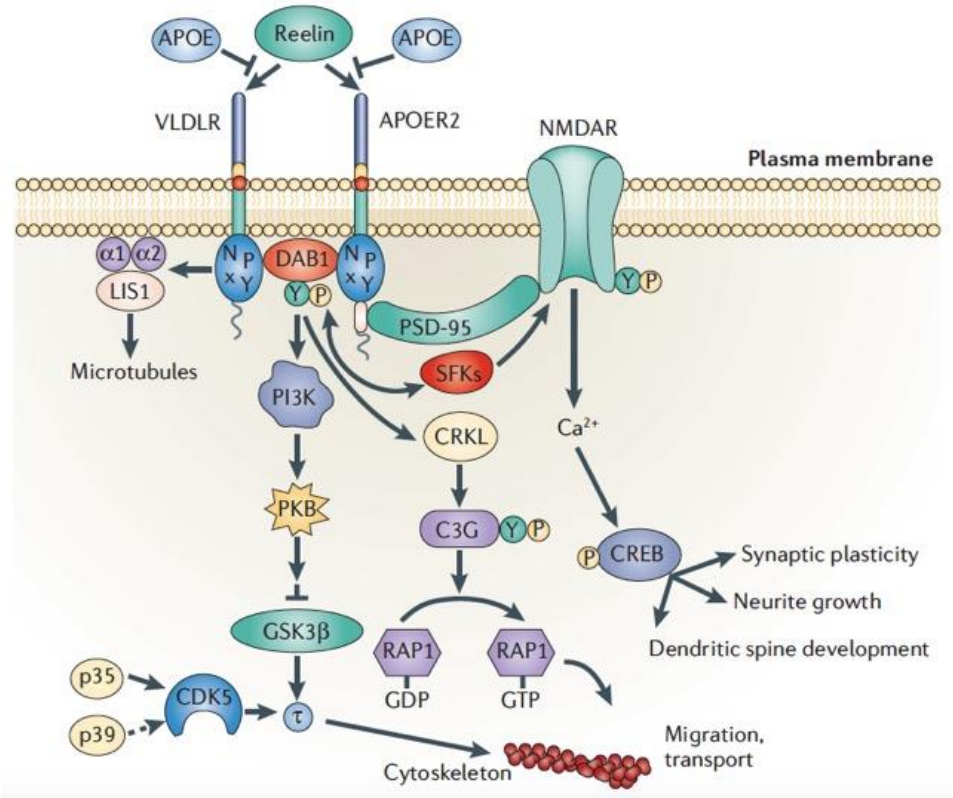

Figure 14. Reelin-initiated signalling events in neurons. Reelin binds to lipoprotein receptors, VLDLR and ApoER2, with high affinity at the cell surface. Binding of Reelin to the receptors induces feed-forward activation of Dab1, an adaptor protein that interacts with NPxY motifs in both receptor tails. The clustering of Dab1 activates Src family tyrosine kinases (SFKs), which potentiates tyrosine phosphorylation of DAB1. Phosphorylated Dab1 further activates phosphatidylinositol-3-kinase (PI3K) and subsequently protein kinase B (PKB). PKB activation inhibits the activity of glycogen synthase kinase 3β (GSK3β). As a result, phosphorylation of tau protein (τ) is reduced, promoting microtubule stability. Tyrosine-phosphorylated (YP) Dab1 also recruits CRK-like (CRKL), which induces phosphorylation of a guanine nucleotide exchange factor, C3G122. Activated C3G promotes the formation of RAP1-GTP, which controls actin cytoskeleton rearrangement. Lissencephaly 1 (LIS1) is another binding partner of tyrosine-phosphorylated Dab1. It associates with α-subunits to form a Pafah1b complex, which regulates microtubule dynamics. Cyclin-dependent kinase 5 (CDK5) acts in parallel with Reelin on numerous substrates, including microtubules. p35 and p39 are activating subunits of CDK5. ApoER2 associates with postsynaptic density protein 95 (PSD-95), an abundant scaffolding protein in the PSD, through an alternatively spliced exon. This interaction is crucial for the coupling of the Reelin-signalling complex to the NMDA (Nmethyl-d-aspartate) receptor (NMDAR). Reelin-activated SFKs tyrosine phosphorylate the NMDAR on NR2 subunits, resulting in the potentiation of NMDAR-mediated Ca^{2+} influx. Elevated intracellular Ca^{2+} can activate the transcription factor cyclic AMP response element binding protein (CREB), thereby potentially initiating the expression of genes that are important for synaptic plasticity, neurite growth and dendritic spine development [117].

The majority of the signalling pathways present desensitization mechanisms that allow the cell to switch off the signal and to be ready to respond again to a repeated stimulation. Many evidences reported that Reelin-signalling pathway also displays a negative feedback mechanism. Indeed, disruption of the Reelin-signalling cascade (by genetic ablation of Reelin, VLDLR, ApoER2, or Fyn and Src) leads to the accumulation of Dab1 protein *in vivo*, while Dab1 mRNA expression is unchanged, suggesting the existence of a regulatory mechanism mediated by Dab1 downregulation [132, 133, 142-145]. Dab1 downregulation is mediated by poly-ubiquitination and targeting to the proteasome, and this mechanism is dependent on Reelin-mediated tyrosine phosphorylation of Dab1 [146, 147]. Recently, Cullin 5 (Cul5) has been identified as the E3 ubiquitin ligase responsible for Dab1 poly-ubiquitination and degradation [148].

MOUSE MODELS OF REELIN-SIGNALLING DISRUPTION

Developmental defects in neuronal migration are commonly found in neurological disorders. Currently, several mouse models of developmental brain disorders are available, and allowed the identification of genes involved in neural positioning and the study of the effects of their disruption [149].

Among them, the spontaneously arising mutant *reeler* mouse, in which Reelin expression is completely abolished, presents behavioural abnormalities, such as ataxia, tremors and reeling gaits [150]. The study of this mutant allowed the identification of the mouse Reelin protein [151]. Moreover, the study of the morphology of the mutant brain revealed cerebellar malformation, with severe hypoplasia, and disrupted laminar organization of cortical layers (Figure 15) [152]. Therefore, *reeler* mutation affects the positioning of neurons within specific layers, leading to abnormal migration of neurons, thus allowing to understand the fundamental role of Reelin in the correct organization of neurons in layered structures [152].

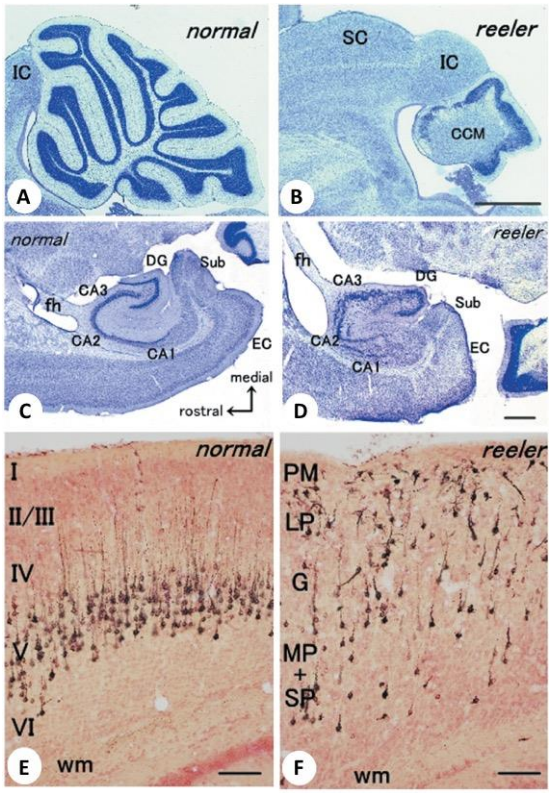

Figure 15. Comparison of cerebellar, hippocampal and cortical morphology between normal (A, C, E) and *reeler* (B, D, F) mouse. A, B) Cerebellar morphology. Sagittal sections of the cerebellum of the normal (A) and reeler (B) mice are stained with cresyl violet. The size of the cerebellum of the reeler (A) is much reduced compared with the normal counterpart (B). A thin quasi-normal cerebellar cortex occupies the surface of the reeler cerebellum. Many malpositioned Purkinje cells are aggregated in the center of the reeler cerebellum, forming a central cellular mass (CCM). IC, inferior colliculus; SC, superior colliculus. Scale bar 1 mm. C, D) Hippocampal morphology. Horizontal sections of the hippocampus of the normal (C) and reeler (D) mice stained with cresyl violet. The distinct laminar structure of the hippocampus proper (i.e. Ammon's horn) and dentate gyrus (DG) of the normal mouse (C) is disrupted in those of the reeler mouse (D). CA1–CA3, sectors 1–3 of Ammon's horn; EC, entorhinal cortex; fh, hippocampal fimbria; Sub, subiculum. Scale bar 0.5 mm. E, F) Retrogradely labeled corticospinal tract (CST) neurons in the motor cortex of postnatal day 9 normal (E) and reeler (F) mice. CST neurons in the motor cortex are retrogradely labeled by injection of horseradish peroxidase (HRP) in the spinal cord 2 days before death. HRP-labeled neurons are accumulated in layer V of the normal cortex (E), whereas they are scattered throughout the radial axis of the reeler cortex (F). Neutral red counterstaining. G, granular cell layer; I–VI, cortical layers of I–VI; LP, large pyramidal cell layer; MP + SP, medium and small pyramidal cell layer; PM, polymorphic cell layer; wm, white matter. Scale bar 100 μm [152].

As models of Reelin pathway disruption, ApoER2 and VLDLR knockout mice were generated by inserting a neomycin resistance cassette into the open reading frame of the two genes. Both ApoER2$^{-/-}$ and VLDLR$^{-/-}$ mice were born at the expected genetic ratio, appeared neurologically normal, with no signs of ataxia or other *reeler* phenotypes. On the contrary, double knockout mice (ApoER2$^{-/-}$;VLDLR$^{-/-}$) lacking the combination of these two receptors presented a typical *reeler* neurological phenotype characterized by progressive ataxia, reeling gaits and tremors. Histological analysis of mutant brains revealed strong disorganization of neurons in the hippocampus and in the cerebellum, that appeared in a rudimentary form, completely lacking its foliation (Figure 16). Indeed, both receptors can compensate for each other to a certain extent, since only the lack of both receptors causes the *reeler* phenotype, while the loss of ApoER2 or VLDLR alone causes only subtle but distinguishable phenotypes [144].

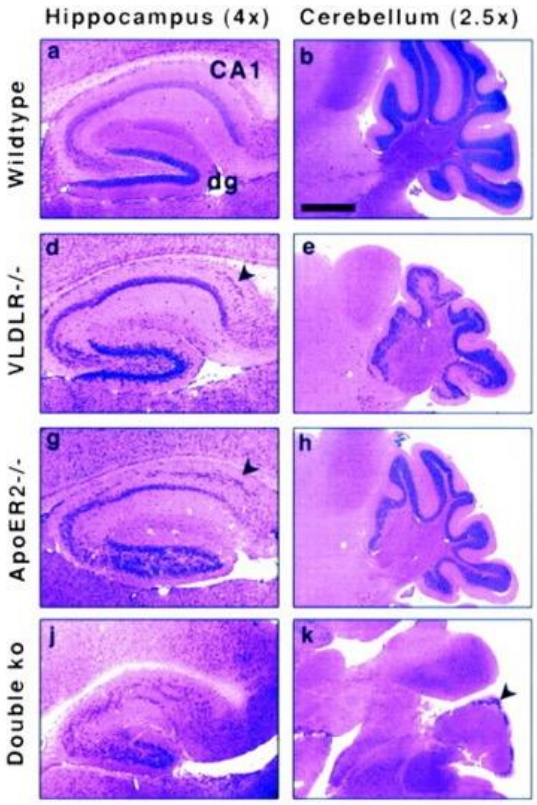

Figure 16. Histologic analysis of hippocampus and cerebellum of wild-type and VLDLR$^{-/-}$, ApoER2$^{-/-}$ and double mutant mice. Hematoxylin/eosin-stained sagittal sections of hippocampus at 43 (a, d, g, and j) and cerebellum at 2.53 (b, e, h, and k) relative magnification of P20 wild type (a, b), VLDLR$^{-/-}$ (d, e), ApoER2$^{-/-}$ (g, h), and double knockout (j, k) are shown. Arrows in (d) and (g) point at the split in the CA1 region, which is also a characteristic feature in reeler and mDab1-deficient mice. The arrow in (k) points to the small rim of dysplastic granule cells in the double knockout [144].

Scrambler mouse is a spontaneously arising mutant that appeared in 1991 and exhibited a phenotype identical to *reeler* mouse [153]. Moreover, the scrambler mutation resulted in a loss of lamination in the cortex, hippocampus and cerebellum that is indistinguishable from that observed in the *reeler* mouse [154, 155]. Another mouse mutant, the *yotari* mouse, was also described as phenotypically indistinguishable from the *reeler* mouse [156]. Both scrambler and yotari mutants arise from mutations in mdab1 gene and express little or no Dab1 protein [142]. The *reeler* phenotype and the impairment in cortical, hippocampal and cerebellar layering is also observed in mdab1 knockout animals [157]. Indeed, the similar phenotypes of *reeler*, *scrambler*, *yotari* and mdab1 null mice suggest that Reelin and Dab1 function as signalling molecules that play a fundamental role in neuronal positioning [142].
Finally, disruption of both Src and Fyn kinases resulted in a phenocopy of the reeler phenotype, with impaired layering organization of neurons [145].

REELIN EXPRESSION AND BIOLOGICAL FUNCTIONS

During embryogenesis, Reelin is highly expressed by Cajal-Retzius neurons, located at the marginal zone of the developing neocortex. Already in the prenatal period, Reelin gene expression could be detected in the olfactory bulb, *striatum*, ventral telencephalon, hypothalamus, thalamus and *pretectum* [158]. Even though Cajal-Retzius neurons disappear after birth, Reelin expression is maintained also in adulthood. In particular, Reelin is strongly expressed by cortical GABAergic interneurons, with the highest levels in layers I and V. In the hippocampus, Reelin is expressed by interneurons present in the *stratum oriens* and *stratum radiatum*. Moreover, Reelin expression could also be detected in the cerebellar granule cells, mitral cells of the olfactory bulb and in some areas of the hypothalamus, *striatum* and *superior colliculus* [117].

Prenatally, Reelin is expressed by the Cajal-Retzius neurons of the developing neocortex. These neurons migrate a short distance toward the marginal zone, where they form the pial surface of the cortex [159]. Later born neurons migrate from the

ventricular zone towards the pial surface and, as they reach the marginal zone, they receive a stop signal from Reelin [160]. Through this inside-out mechanism, the formation of organized cortical layers take place [161]. Reelin is fundamental for the correct organization of neurons in layered structures, such as cortex, hippocampus and cerebellum. Indeed, the absence of Reelin expression in the *reeler* mouse leads to impaired cortical and cerebellar lamination, as the neurons fail to acquire their proper layer position [151, 152].

Reelin expression is maintained during adulthood; therefore this protein should play a physiological role also postnatally. Indeed, a direct influence on synapses have been reported, being able to modulate synaptic plasticity, hippocampal-dependent learning and memory processes [117].

ROLE IN DISEASES

Altered Reelin pathway plays a role in the pathogenesis of neurodevelopmental and neuropsychiatric disorders, such as schizophrenia, autism and bipolar disorder. Indeed, Reelin expression is reduced by hypermethylation of the RELN gene in schizophrenia and autism. Moreover, a link between Reelin pathway and epilepsy and pain sensitivity has been observed [117]. Finally, disruption of the RELN gene in humans is responsible of lissencephaly (reduction in the number of brain convolutions) with cerebellar hypoplasia, severe ataxia, epilepsy and cognitive delay [162].

REELIN/DAB1 SIGNALLING IN ALZHEIMER'S DISEASE

Many evidences point to an involvement of Reelin pathway in Alzheimer's disease pathogenesis and progression. Indeed, tau protein resulted hyperphosphorylated in mouse models in which Reelin pathway is disrupted [131, 163, 164]. Moreover, a reduced expression level of Reelin accelerates Aβ deposition [164]. Viceversa, *in vitro* treatment with Aβ impairs Reelin signalling [165]. Finally, Reelin is able to interact with APP and, *in vitro*, with Aβ, while APP also interacts with ApoER2 and Dab1 [166-171]. These findings reveal that Reelin and the components of its signalling cascade may

influence APP processing and, viceversa, APP may influence Reelin-signalling [172]. Indeed, it has also been shown that APP cytosolic domain may bind Dab1, retaining it in the cytoplasm and thus impairing Reelin signalling [173]. Besides, Reelin receptors may bind apolipoprotein E (ApoE) that could impair Reelin signalling by competing with Reelin for the binding [130, 131]. Finally, it has been shown that apolipoprotein J, also known as clusterin, is a ligand for Reelin receptors which is able to trigger the same signalling cascade [174]. Interestingly, many evidences reported an important role of clusterin in both AD and prion diseases [175-178].

The progression of AD may influence Reelin-signalling and, viceversa, alterations in Reelin pathway and its components may contribute to neuronal dysfunction and disease progression [172].

Despite many efforts were done, still no consensus on Reelin expression levels during AD has been reached [172]. However, Reelin processing is thought to play an important role in the disease, as dysfunction of Reelin proteolysis in post-mortem AD tissues has been reported [179]. Indeed, increased levels of N-R2 fragment have been observed in AD and frontotemporal dementia patients [180, 181].

Interestingly, Dab1 is able to interact with APP altering its processing and intracellular trafficking. Indeed, it has been shown that Dab1 increases cell surface expression of APP, increases its α-cleavage and decreases Aβ production [182]. Recently, it has been shown that this effect of Dab1 is mediated by Fyn kinase, which promotes the localization of both APP and Dab1 in the lipid rafts [183, 184].

REELIN/DAB1 SIGNALLING IN PRION DISEASES

Interestingly for the present work, despite the role of Dab1 in prion diseases has not been deeply investigated, it has been reported that APP processing and β-amyloid deposition in sporadic Creutzfeldt-Jakob patients are dependent on Dab1. In particular, a direct correlation between Dab1 phosphorylation, Aβ deposition and PrP^{Sc} type in human sCJD has been shown. In PrP^{Sc} type 1 patients increased Dab1 phosphorylation and lower β C-terminal fragment (CTF) production, with absence of Aβ deposition, were observed, while PrP^{Sc} type 2 patients were charactherized by lower levels of Dab1 phosphorylation, βCTF production and relevant Aβ deposition [185].

AIM OF THE PROJECT

Prion diseases are a group of rare, fatal and progressive neurodegenerative disorders affecting both humans and animals. Among neurodegenerative diseases, prion disorders are of prominent biological and pathological interest since they may present with genetic, sporadic and infectious origin. The cellular form of the prion protein (PrP^{C}), which is endogenously encoded by the *Prnp* gene, has been widely investigated since its misfolded isoform (scrapie prion protein, PrP^{Sc}), enriched in β-sheets and prone to aggregation, is the causative agent of prion diseases [2, 37]. The pathogenesis of prion diseases, and the nature of the neurotoxicity observed in these disorders, is currently under debate, as they could be gain of toxic function consequences of the formation of PrP^{Sc}, or could be due to the loss of the normal physiological function of PrP^{C} [4]. According to the gain of toxic function hypothesis, the misfolded protein acquires novel toxic functions and, therefore, is able to trigger direct neurotoxicity [14, 15, 38]. However, PrP^{Sc} alone is not sufficient to induce prion disease [16-18]. Therefore, it has been proposed that the loss of a critical physiological function of PrP^{C} may cause neurodegeneration [38]. However, genetic ablation of *Prnp* expression causes subtle phenotypic effects and does not induce neurodegeneration by itself [19, 20], thus arguing against the loss-of-function hypothesis. Indeed, multiple mechanisms may contribute to the pathology of prion diseases, leading to progressive neurodegeneration.

For this reason, a better definition of the exact physiological function of PrP^{C} represents a critical challenge of the prion field, that may help to better understand pathogenetic mechanisms underlying neurodegeration, as well as to propose new therapeutic strategies. Despite many efforts have been done in the past years, PrP^{C} physiological function has not been completely defined. However, it has been suggested that PrP^{C}, which is mostly abundant in the nervous system, plays a role in neurite outgrowth, neuronal survival, synapse formation and function, and in the maintenance of myelinated axons [21]. Importantly for the present work, it has been reported that PrP^{C} also plays a fundamental role in modulating cell signalling, acting as

a dynamic scaffold for the assembly of many different signalling molecules at the neuronal surface [38, 68, 69]. Indeed, PrP^C directly interacts with NCAM at neuronal surface, thus regulating Fyn kinase activity [74]. Moreover, PrP^C could affect PI3K and Akt/PKB activity [100, 103]. Finally, more recently, it has also been shown that PrP^C induces GSK3β inactivation in a caveolin/Lyn-dependent fashion [95]. All these intracellular kinases could be also regulated by yet another protein, Reelin, an extracellular matrix glycoprotein that activates a linear downstream signalling pathway [117].

Interestingly, it has been reported that Reelin-signalling pathway is involved in both Alzheimer's and prion diseases. Indeed, the intracellular adaptor protein Dab1 is able to affect APP processing and intracellular trafficking, increasing cell surface expression of APP and its α-cleavage and decreasing Aβ production [182]. Moreover, Dab1 has been shown to influence amyloid beta deposition in sporadic Creutzfeldt–Jakob disease [185].

In light of these considerations, this thesis is aimed to investigate the functional interaction between the prion protein and the Reelin/Dab1 signalling cascade from a physiological and a pathological point of view.

Taking advantage of *Prnp* knockout mice ($Prnp^{0/0}$) and wild-type ($Prnp^{+/+}$) littermates, expression and activation state of different components of the Reelin/Dab1 signalling pathway were evaluated in mouse brains during early postnatal days (postnatal day 4 (P4)). To better investigate the effects of PrP^C absence on Dab1 activation in response to Reelin, an *ex vivo* model based on primary cortical neurons obtained from $Prnp^{0/0}$ and $Prnp^{+/+}$ embryos was used.

Viceversa, we took advantage of different mouse models of Reelin-signalling disruption to investigate the effects of signalling ablation on PrP^C. Indeed, PrP^C expression was evaluated in mouse brains of different genotypes at postnatal day 4.

Moreover, prion-infected mice were used as prion pathology model and the expression of different components of the Reelin/Dab1 signalling pathway was evaluated in brains obtained from terminally sick animals.

Finally, Dab1 gene expression was evaluated in human samples obtained from sporadic Creutzfeldt–Jakob disease patients.

MATERIALS AND METHODS

HUMAN SAMPLES

Postmortem human brain samples were derived from four sCJD type 1 patients, four sCJD type 2 patients and four healthy controls. Frontal cortex of each subject was collected and immediately frozen in liquid nitrogen. In parallel, whole blood from two symptomatic sCJD patients and two healthy controls were collected in PAXgene Blood RNA tubes. Samples were then processed for RNA extraction and gene expression analysis as described below.

ANIMALS

Inbred FVB/N *Prnp*$^{+/+}$ and littermates FVB *Prnp*$^{0/0}$ mice were used as a model for PrP^{C} depletion. The FVB *Prnp*$^{0/0}$ were obtained by backcrossing the original Zurich I *Prnp*$^{0/0}$ mice [19] to FVB/N inbred mice for more than 20 generations [186]. Genotypes were confirmed by PCR analysis as described [187]. The day of birth was considered as postnatal day (P) 0. Sex-matched P4 animals were sacrificed by decapitation, brains were extracted, immediately frozen in liquid nitrogen and stored at -80°C for further applications.

For neuronal primary cultures, FVB *Prnp*$^{+/0}$ pregnant mice were used. The day of vaginal plug detection was considered as embryonic day (E) 0. At E16, the pregnant females were sacrificed with CO_2 and the embryos were extracted by caesarean cut and further processed for cultures preparation. Genotypes were confirmed by PCR analysis as described [187].

Reeler mutant mice, ApoER2$^{-/-}$, VLDLR$^{-/-}$, ApoER2$^{-/-}$/VLDLR$^{-/-}$ and Dab1$^{-/-}$ mice were used as model for Reelin pathway disruption. Littermates wild-type were used as controls. For what concern ApoER2$^{-/-}$/VLDLR$^{-/-}$ double knockout mice, VLDLR$^{-/-}$ littermates were used as controls. The animals were on a C57BL/6JxSv129Ev mixed background. Genotypes were confirmed by PCR analysis. P4 animals were sacrificed by

decapitation, brains were extracted and dissected to obtain 4 samples from each animal: brain hemisphere, cortex, hippocampus and cerebellum. Samples were immediately frozen in liquid nitrogen and stored at -80°C.

Age and sex-matched CD1 mice (Crl:CD1(ICR) strain code 022, charles river) were used for prion infection experiments. Adult animals were sacrificed with CO_2, brains were extracted, immediately frozen in liquid nitrogen and stored at -80°C.

All experiments were performed in accordance with European regulations [European community Council Directive, November 24, 1986 (86/609/EEC)] and were approved by the local authority veterinary service. All efforts were made to minimize animal suffering and to reduce the number of animals used.

INTRACEREBRAL INOCULATION OF PRIONS

Rocky Mountain Laboratory (RML) prion infected brain homogenate was prepared at a 10% w/v in phosphate-buffered saline (PBS).

For the first set of experiments, 20 µL of 10% brain homogenate was stereotactically injected in the striatum of 2-months old outbred CD1 mice (n = 5). Not inoculated age- and sex-matched CD1 mice were used as control (n = 5). Inoculated mice were monitored daily for clinical signs of prion disease. All the animals were sacrificed at the terminal stage of prion infection.

For the second set of experiments, 2.5 µL of 10% brain homogenate was stereotactically injected in the hippocampus of 2-months old outbred CD1 mice (n = 16). Not inoculated age- and sex-matched CD1 mice were used as control (n = 16). Pre-symptomatic animals (n = 8) were sacrificed 97 days post inoculation (d.p.i.). Terminal stage animals (n = 8) were monitored daily for clinical signs of prion disease and were sacrificed at the end stage of clinical prion disease.

PRIMARY NEURONAL CULTURES PREPARATION

Mouse embryonic cortical neurons were isolated and cultured as previously described [188], with some modifications. E16 embryos were collected from FVB *Prnp*$^{+/0}$ pregnant females. Cerebral hemispheres were dissected under sterile conditions. Briefly, the cortices were separated from the midbrain and the meninges were stripped off. Cortices from each embryo were incubated in 2 mL of 0.05% Trypsin-EDTA (Gibco) supplemented with 10mM $MgCl_2$ and 0.05 mg/mL DNaseI (Roche), for 10 min at 37°C and 10 min at RT. The tissue was then homogenized by pipetting in 1 mL of neuron growth media [Neurobasal Medium (Gibco) containing 10% B27 supplement (Gibco), 1% Penicillin-Streptomycin (Gibco), 1% Glutamax (Gibco)] supplemented with 0.1 mg/mL DNaseI. Following centrifugation at 100 g for 5 min, pellets were resuspended in 1 mL of neuron growth media and neurons were plated on dishes pre-coated overnight a 37°C with poly-L-ornithine 0.05 mg/mL (Sigma-Aldrich). The neurons were allowed to differentiate for 5 days *in vitro* (DIV) and were then treated as described below. After stimulation, cells were lysed and processed for Western Blot (WB) analysis. To detect Reelin secreted by neurons under basal conditions, neuron growth media was collected after 5 DIV, filtered using 0.22 μm filters (Millipore) and stored at -80°C. Total protein content was measured using bicinchoninic acid (BCA) assay (Sigma-Aldrich). Reelin content was then evaluated through WB analysis loading onto a 4-12% precast gradient gel (NuPAGE™ Novex™ 4-12% Bis-Tris Midi Protein Gels, Invitrogen) the same total protein amount for each sample.

PRODUCTION OF REELIN-CONDITIONED SUPERNATANT

Reelin-containing supernatants and control supernatants were prepared as previously described [189]. Brefly, HEK-293T cells stably transfected with the expression plasmid pCrl encoding full-length mouse Reelin [122] and control cells transfected with an empty vector (mock) were grown in DMEM (Gibco) supplemented with 10% fetal bovine serum (FBS, Gibco), 1% Penicillin-Streptomycin and 0.9 g/L G418 (Geneticin, Gibco) for 2 days to subconfluency. Cells were switched to serum-free DMEM + 1%

Penicillin-Streptomycin and grown for 2 days at 37°C in 5% CO_2. Conditioned medium was then collected and concentrated 10-fold using 100 kDa cut-off centrifugal filters (Millipore), sterile-filtered (0.22 μm filters, Millipore), aliquoted and stored at −80°C until used. Reelin content was analysed by WB using anti-Reelin G10 monoclonal antibody (see Table 5).

PRODUCTION OF RECOMBINANT MOUSE FULL-LENGTH PrP (recMoPrP)

Full-length MoPrP(23-231) was cloned, expressed and purified according to our previous protocols [190, 191]. The purified protein was prepared in sterile phosphate-buffered saline (PBS) for neuronal cultures treatment at a concentration of 0.25 mg/mL, equivalent to 10 μM concentration. The quality of the protein was confirmed by SDS/PAGE analysis followed by WB using an anti-PrP primary antibody (see Table 5).

PRODUCTION OF RECOMBINANT MOUSE PrP-hFc FUSION PROTEIN (moPrP-hFc)

For mouse PrP-hFc fusion protein production, the sequence encoding the extracellular portion of mouse PrP was amplified by PCR using the forward primer 5'-ATAGAATTCAATGAAAAAGCGGCCAAAGCCTG-3' and the reverse primer 5'-ATAGAATTCACGCTGGATCTTCTCCCGTCGTAA-3' (including EcoRI restriction site). This fragment was cloned into the expression vector pFUSE containing the Fc portion of human IgG_1. The mouse PrP-hFc fusion protein was produced by transient transfection in HEK293T cells. The supernatant containing PrP-hFc protein was purified using AKTA-prime and prepacked protein A Sepharose column. The quality of the protein was confirmed by SDS/PAGE analysis followed by Coomassie staining or by WB using an anti-PrP primary antibody (see Table 5).

PRIMARY NEURONAL CULTURES STIMULATION WITH REELIN, recMoPrP AND PrP-hFc

Reelin stimulation of neuronal cultures was performed as previously described [133], with some modifications. After 5 DIV, cortical neurons were stimulated with mock- or Reelin-conditioned medium diluted 10-fold in the neuron growth media for 15 min at 37°C in 5% CO_2.

Stimulation of primary cultures with recombinant full-length MoPrP(23-231) was performed as described in literature [91], adjusting the published protocol to our experimental setup. After 5 DIV, cortical neurons were stimulated with 1 μM or 2 μM of recMoPrP diluted in the neuron growth media for 20 min at 37°C in 5% CO_2. PBS treatment (vehicle only), under the same conditions, was used as negative control.

Stimulation of primary cultures with purified PrP-hFc protein has been performed adapting a published protocol to our setup [74]. After 5 DIV, cortical neurons were stimulated with 2 μg/mL of protein diluted in the neuron growth media for 20 min at 37°C in 5% CO_2. Control neurons were treated with purified human Fc (hFc) or with a purified unrelated fusion protein (RAE-1γ-hFc) under the same conditions.

PRIMARY NEURONS LYSATES PREPARATION

After treatment, cells were washed in PBS and lysed in CHAPS buffer (50mM Tris-HCl, pH 7.5, 150mM NaCl, 1mM EDTA, 0.5% CHAPS, 10% glycerol) supplemented with protease inhibitor cocktail (complete mini EDTA-free protease inhibitor cocktail, Roche) and phosphatase inhibitors [5mM Na_3VO_4, 0.5mM NaF, phosphatase inhibitor cocktail 2 and 3 (Sigma-Aldrich)]. Samples were cleared by centrifugation at 10000rpm for 10min at 4°C, supernatants were collected and total protein concentration was measured using BCA assay. Samples were then stored at -20°C before being processed for WB analysis.

TISSUE HOMOGENIZATION FOR PROTEIN EXTRACTION

Brains from *Prnp*$^{0/0}$ and *Prnp*$^{+/+}$ mice were homogenized in CHAPS buffer supplemented with protease inhibitor cocktail (complete mini EDTA-free protease inhibitor cocktail, Roche) and phosphatase inhibitors [5mM Na_3VO_4, 0.5mM NaF, phosphatase inhibitor cocktail 2 and 3 (Sigma-Aldrich)]. Brains from prion-inoculated mice were homogenized in PBS supplemented with protease inhibitor cocktail. After homogenization, samples were left on a rotating wheel at 4°C for 30 minutes to allow the complete lysis, sonicated for 30 seconds using a probe-type sonicator and cleared by centrifugation (10000rpm, 10min, 4°C). Supernatants were collected and total protein concentration was measured using BCA assay. Samples were stored at -20°C for further applications.

BIOCHEMICAL ANALYSIS OF BRAIN HOMOGENATES AND NEURONAL LYSATES

Protein expression was analysed using WB technique. The same total amount of protein (15-30 μg) for each sample was loaded onto a Tris-Glycine SDS-PAGE gel for protein separation, after denaturation at 95°C for 5 min in 2X loading buffer (0.1 M TrisHCl pH 6.8, 4% SDS, 20% glycerol, 8 M Urea, 0.2 M DTT, 0.004% bromophenol blue). Different acrylamide percentage gels were used depending on the molecular weight of analysed proteins. Proteins were then transferred onto a nitrocellulose membrane (GE Healthcare). The membranes were blocked with 5% non-fat milk in TBST (Tris-Buffered Saline, 0.1% Tween-20) or with 5% bovine serum albumin (BSA) in PBST (Phosphate-Buffered Saline, 0.1% Tween-20) for 1 hour at RT. Overnight incubation at 4°C with primary antibodies followed (see Table 5). After the incubation for 1 hour at room temperature (RT) with secondary antibody horseradish peroxidase(HRP)-conjugated diluted in blocking solution, the signal was detected using enhanced chemiluminescent system (ECL, Amersham Biosciences) and recorded with the digital imaging system Alliance 4.7 (UVITEC, Cambridge, UK). Densitometric

analysis was performed using Uviband Analysis Software 15.0 (UVITEC, Cambridge, UK).

For non-phosphorylated proteins, the signals were normalized against β-Actin or β-III-Tubulin. For phosphorylated proteins, the membranes were developed twice in order to detect on the same immunoblot both the phosphorylated and, subsequently, the total protein (non-phosphorylated plus phosphorylated). After the detection of the phospho-protein, the membrane was incubated with 0.01% sodium azide in 5% non-fat milk in TBST for 3 hours at RT. Following several washes, the membrane was then incubated overnight at 4°C with the primary antibody against the total protein, and developed as described above. The signal of the phosphorylated protein was then normalized on the signal of the total protein.

IMMUNOPRECIPITATION OF DAB1 FROM BRAIN HOMOGENATES

Immunoprecipitations experiments were carried out using the PureProteome Protein A Magnetic Bead System (Millipore). Three hundred micrograms of total protein extracts were incubated with 2 µg of anti-Dab1 antibody (H-103, Santa Cruz Biotechnologies), or with 2 µg of normal rabbit IgG (12-370, Millipore) as control, for 2 hours at 4°C on a rotating wheel. Fifty microliters of the beads suspension were used for each sample. The pre-formed antibody-antigen complex was added to the beads and then incubated for 2 hours at 4°C on a rotating wheel. The beads were then extensively washed with PBS + 0.1% Tween 20 and resuspended in 40 µL of 2X loading buffer. After 5 min boiling at 95° C, samples were subjected to standard immunoblotting procedures, as described above. On the same membrane used to detect immunoprecipitated protein, 30 µg of starting material (input) were loaded. The signal of the phosphorylated protein was detected using anti-phosphotyrosine 4G10 antibody (Millipore), while anti-Dab1 antibody (Abcam) was used to detect the signal of the total protein (see Table 5).

Dab1 expression was measured performing the ratio between immunoprecipitated Dab1 and the starting amount of protein present in the input material. The amount of

phosphorylated Dab1 was normalized on total Dab1 signal. Data are expressed as ratio between *Prnp*$^{0/0}$ and *Prnp*$^{+/+}$ mice ± standard error.

CO-IMMUNOPRECIPITATION EXPERIMENTS

Co-immunoprecipitation experiments were carried out applying four different protocols (described here following the presenting order of the results).

In the first approach (see Figure 19a), 30 µl of Protein A/G-Sepharose (GE Healthcare) were incubated with 1 ml of anti-PrP W226 hybridoma cell supernatant overnight at 4°C on a rotating wheel. As negative controls, 14F2 anti-DISC1 antibody and protein-free hybridoma medium (PFHM, Gibco) were used. After removing the supernatant, two washes in TBS (Tris-Buffered Saline) + 0.3% Sarcosyl were performed. *Prnp*$^{+/+}$ brain sample was processed in CHAPS buffer, as described above (without sonication step), to obtain a 10% w/v brain homogenate, that is then diluted to 1% w/v in TBS + 0.3% Sarcosyl. 1 ml of 1% brain homogenate was incubated with the preformed antobody-bead complex overnight at 4°C on a rotating wheel. The day after, the resin was firstly washed in ice-cold IP1 buffer (50 mM Tris-HCl pH=7.5, 150 mM NaCl, 1% NP-40, 0.5% DOC), then in ice-cold IP2 buffer (50 mM Tris-HCl pH=7.5, 0.5 M NaCl, 0.1% NP-40, 0.05% DOC) and finally in ice-cold IP3 buffer (50 mM Tris-HCl pH=7.5, 0.1% NP-40, 0.05% DOC). The beads were then resuspended in 30 µL of 2X loading buffer. After 5 min boiling at 95° C, samples were subjected to standard immunoblotting procedures, as described above. On the same membrane used to detect immunoprecipitated proteins, 20 µL of starting material (input) were loaded. To perform the reverse experiment, immunoprecipitation of Reelin or ApoER2 were performed following the same protocol using 3 µg of anti-Reelin or anti-ApoER2 antibody, respectively. In these cases, normal mouse IgG (12-371, Millipore) or normal rabbit IgG (12-370, Millipore), respectively, were used as negative control.

The second approach used is based on a published protocol [74] with some modifications (see Figure 19b). *Prnp*$^{+/+}$ brain homogenates were prepared in 50 mM Tris-HCl buffer (pH 7.5), containing 0.32 M sucrose, 1 mM $CaCl_2$, 1 mM $MgCl_2$, and 1 mM $NaHCO_3$. Samples containing 1 mg of protein were then lysed for 30 min in 50 mM

Tris-HCl buffer (pH 7.5), containing 150 mM NaCl, 0.5% Triton X-100, 1% β-octyl-d-glucopyranoside, 1 mM sodium fluoride, 2 mM $NaVO_4$, 0.1 mM PMSF, and EDTA-free protease inhibitor cocktail (Roche). Samples were then centrifuged for 15 min at 20,000 g and 4°C. Supernatants were incubated with 3 µg of anti-Reelin or anti-ApoER2 antibody, or with normal mouse IgG or normal rabbit IgG, respectively, as negative control, overnight at 4°C on a rotating wheel. Precipitation with 30 µL of Protein A/G-Sepharose beads for 3 h at 4°C followed. The beads were then washed three times with RIPA buffer (150 mM NaCl, 1.0% NP-40, 0.5% DOC, 0.1% SDS, 50 mM Tris-HCl pH=8.0) and once with PBS. The beads were then resuspended in 30 µL of 2X loading buffer. After 5 min boiling at 95° C, samples were subjected to standard immunoblotting procedures, as described above. On the same membrane used to detect immunoprecipitated proteins, 20 µL of starting material (input) were loaded.

In the third protocol (see Figure 19c), 1 ml of 1% w/v *Prnp*$^{+/+}$ brain homogenate prepared in CHAPS buffer, as described above (without sonication step) was incubated overnight at 4°C with 3 µg of anti-Reelin or anti-ApoER2 antibody, or with normal mouse IgG or normal rabbit IgG, respectively, as negative control. Precipitation with 30 µL of Protein A/G-Sepharose beads for 3 h at 4°C followed. The beads were then washed three times with CHAPS buffer and resuspended in in 30 µL of 2X loading buffer. After 5 min boiling at 95° C, samples were subjected to standard immunoblotting procedures, as described above. On the same membrane used to detect immunoprecipitated proteins, 20 µL of starting material (input) were loaded.

Finally, protein crosslinking was applied to brain samples, following manifacturer's instruction, before proceding with immunoprecipitation (see Figure 20). Briefly, *Prnp*$^{+/+}$ brain sample was homogenized in PBS supplemented with 1 mM $MgCl_2$ and 0.1 mM $CaCl_2$, lysed for 40 minutes at 4°C on a rotating wheel and cleared by centrifugation (16000rcf, 10 min, 4°C). 1 ml of supernatant was then incubated with 30 µL of 20 mM DSP (dithiobis[succinimidyl propionate], ThermoScientific) for 30 minutes at RT on a rotating wheel (protected from light). 50 µL of 1M Tris pH=7.5 were added and the sample was then incubated 15 minutes at RT on a rotating wheel. Following centrifugation (21000rcf, 20min, 4°C), the pellet was resuspended in 800 µL of CHAPS buffer supplemented with protease and phosphatase inhibitors. After adding 50 µL of

SDS 1%, the sample was subjected to a brief sonication. Finally, immunoprecipitation was performed following the third protocol described above.

ANTIBODIES

Primary and secondary antibodies against non-phosphorylated proteins were diluted in 5% non-fat milk in TBST, while antibodies against phosphorylated proteins were used in 5% BSA in PBST. All the primary antibodies used in the present work are reported in Table 5. Secondary antibodies, goat anti-mouse and goat anti-rabbit HRP-conjugated, were from DAKO and were diluted 1:2000 in blocking solution. Secondary antibody goat anti-human HRP-conjugated (ThermoScientific) was diluted 1:5000 in blocking solution. To avoid immunoglobulin detection, Mouse TrueBlot® ULTRA (diluted 1:30000) and Rabbit TrueBlot® (diluted 1:10000) secondary antibodies (Rockland Laboratories) were used to visualize Fyn and Dab1 signal, respectively, in mouse brains in standard WB (for Fyn kinase) or after immunoprecipitation (for Dab1).

TARGET	ANTIBODY	COMPANY/REFERENCE	DILUTION
Reelin	Mouse monoclonal G10	Millipore	1:1000
Reelin	Mouse monoclonal 20E12	Prof. Korth's laboratory	IP
DISC1	Mouse monoclonal 14F2	Prof. Korth's laboratory	IP
ApoER2	Rabbit monoclonal [EPR3326]	Abcam	1:1000
VLDLR	Mouse monoclonal 6A6	Millipore	1:1000
Dab1	Rabbit monoclonal [EP2248Y]	Abcam	1:1000
Dab1	Rabbit polyclonal H-103	Santa Cruz Biotechnology	1:500
Phospho-Tyrosine	Mouse monoclonal 4G10	Millipore	1:1000
Fyn	Rabbit monoclonal 04-343	Millipore	1:2000
Fyn	Mouse monoclonal (FYN-59)	Santa Cruz Biotechnology	1:1000
Phospho-Src family (Tyr416)	Rabbit polyclonal 2101S	Cell Signalling Technologies	1:1000
NCAM	Rabbit polyclonal AB5032	Chemicon International	1:1000
AKT	Rabbit polyclonal 9272	Cell Signalling Technologies	1:1000
Prion protein	Humanized D18 antibody fragment (Fab)	[192]	1:1000
Prion protein	Mouse monoclonal W226	[193]	1:1000

Table 5. List of the primary antibodies used for immunoblotting.

RNA EXTRACTION FROM BRAIN SAMPLES AND REAL-TIME PCR

In order to evaluate the expression of Dab1 gene, total RNA was extracted from brain samples of sex-matched P4 mice. Two independent sets of samples were analized: four *Prnp*$^{0/0}$ and four *Prnp*$^{+/+}$ females, and four *Prnp*$^{0/0}$ and four *Prnp*$^{+/+}$ males.

For prion-infected samples, RNA was extracted from brains of four animals for each group: WT controls of 5 months of age, WT controls of 7 months of age, RML-infected mice 3 months post-inoculation and RML-infected mice at the terminal stage of infection.

One brain hemisphere for each sample was homogenized in TRIzol reagent (Invitrogen) and total RNA was extracted following manufacturer's instructions. Samples were treated with RNase-free DNase set (Qiagen) to reduce DNA contamination, and then purified with RNeasy mini kit (Qiagen). RNA quantification was performed using NanoDrop 2000 spectrophotometer (Thermo Scientific) and RNA quality was evaluated through agarose gel electrophoresis. Besides, integrity of the 18S and 28S ribosomal bands was assessed by capillary electrophoresis using the 2100 Bioanalyzer (Agilent Technologies).

Retrotranscription of 4 μg of RNA was performed using SuperScriptIII RT (Invitrogen) and oligo-dT primer (5'-GCT GTC AAC GAT ACG CTA CGT AAC GGC ATG ACA GTG$(T)_{24}$-3'). In parallel, for each sample a non-retrotranscribed negative control (-RT) was prepared by omitting the enzyme in the reactions in order to evaluate genomic DNA contamination.

Expression analysis of targets of interest by quantitative reverse transcription real-time PCR (RT-qPCR) was performed using gene-specific primer pairs. All primers used for RT-qPCR are listed in Table 6. The specificity of each couple of primers for the intended target gene was verified through non-quantitative PCR followed by agarose gel electrophoresis. RT-qPCR was carried out using 2X iQ™ SYBR® Green Supermix (Bio-Rad Laboratories, Inc.) and 400 nM of forward and reverse primers (Sigma-Aldrich) on an iQ5 Multicolor Real-Time PCR Detection System (Bio-Rad Laboratories, Inc.). A starting amount equivalent to 1 ng of RNA was used for each reaction. After initial denaturation for 3 min at 95°C, 40 cycles were performed at 95°C for 15 seconds and

60°C for 1 min. -RT controls were included in the plates for each primer pair and sample. The expression of the target genes was normalized on the expression of two housekeeping genes: β-Actin and β-III-Tubulin. The relative expression of each gene of interest *versus* the housekeeping gene chosen as reference was calculated using the $\Delta\Delta C_T$ method [194]. Significance was calculated with unpaired student t-test (p-value < 0.05).

For what concern mdab1 gene transcription, three murine Dab1 mRNA isoforms encoding proteins of 555, 217, and 271 residues have been described. Dab217 mRNA differs from the Dab555 mRNA by a consensus splice donor sequence, encodes a further 18 residues before a stop codon, and terminates with a 3'-UTR that is different from Dab555. Dab271 mRNA contains an additional exon that encodes 30 residues before a stop codon [147]. Indeed, to quantify Dab1 mRNA expression we used two couples of primers published in literature: primer pair 1 (Dab1) bridges exons 2 and 3 of the Dab1 gene, which are shared by Dab555, Dab271 and Dab217, while primer pair 2 (Dab555), which bridges exons 9 and 10, was designed to detect the Dab555 mRNA only (that encodes for the 80 kDa Dab1 protein) [147].

For what concern human Dab1 gene, its relative expression was normalized on the expression of three housekeeping genes: β-Actin, GAPDH and RpL19. As for murine samples, the relative expression of Dab1 gene *versus* the housekeeping gene chosen as reference was calculated using the $\Delta\Delta C_T$ method [194]. Significance was calculated with unpaired student t-test (p-value < 0.05).

TARGET	PRIMER NAME	SEQUENCE (5'-3')	AMPLICON SIZE (bp)	ACCESSION NUMBER	REFERENCE
Mouse Dab1	MoDab1_fw	GCCAAGAAAGACTCCAGGAAGA	79	NM_177259.4 NM_010014.3	[147]
	MoDab1_rev	GGACCCCTTCGCCTTTAAAC			
Mouse Dab1	MoDab555_fw	TTATGATGTGCCAAAAAGTCAACCT	51	NM_177259.4	[147]
	MoDab555_rev	AGTTCTAGTTGGGTCACAGCACTTAC			
Mouse β-Actin	MoActb_fw	CACACCCGCCACCAGTTC	164	NM_007393.5	[195]
	MoActb_rev	CCCATTCCCACCATCACACC			
Mouse βIII-Tubulin	MoTubb3_fw	CGCCTTTGGACACCTATTC	240	NM_023279.2	[196]
	MoTubb3_rev	TACTCCTCACGCACCTTG			
Human Dab1	HuDab1_fw	CACCGGGCCTTTGGATATGT	88	NM_021080.3	Designed
	HuDab1_rev	GAATAACAGGTTCAGCCGCC			
Human β-Actin	HuActb_fw	AGAGCTACGAGCTGCCTGAC	184	NM_001101.3	[197]
	HuActb_rev	AGCACTGTGTTGGCGTACAG			
Human GAPDH	HuGAPDH_fw	CCTGCACCACCAACTGCTTA	108	NM_001289746.1	Modified from [198]
	HuGAPDH_rev	TCTTCTGGGTGGCAGTGATG			
Human RpL19	HuRpL19_fw	CTAGTGTCCTCCGCTGTGG	169	NM_000981.3	[199]
	HuRpL19_rev	AAGGTGTTTTTCCGGCATC			

Table 6. Primer list for qRT-PCR experiments. (bp = base pairs)

STATISTICAL ANALYSIS

All the results concerning Western Blot analysis of protein expression in mouse brain were compared between *Prnp*$^{+/+}$ and *Prnp*$^{0/0}$ samples performing the Student's t-Test setting two-tailed distribution and two-sample unequal variance. For what concern Fyn kinase activation in brain samples, the amount of the phosphorylated protein was normalized on the total protein signal and the ratios obtained were compared between *Prnp*$^{+/+}$ and *Prnp*$^{0/0}$ samples performing the Student's t-Test setting two-tailed distribution and two-sample unequal variance. The same statistical test was applied to *reeler* mutant mice, ApoER2$^{-/-}$, VLDLR$^{-/-}$, ApoER2$^{-/-}$/VLDLR$^{-/-}$ and Dab1$^{-/-}$ samples, comparing each genotype with the respective wild-type control, and to prion-infected samples compared to non-infected controls.

Immunoprecipitation experiments (Dab1 protein expression and phosphorylation) were analysed as follows. Dab1 expression was measured performing the ratio

between immunoprecipitated Dab1 and the starting amount of protein present in the input material. The amount of phosphorylated Dab1 was normalized on total Dab1 signal. The results of all the experimental replicates were compared between *Prnp*$^{+/+}$ and *Prnp*$^{0/0}$ samples performing the paired Student's t-Test setting two-tailed distribution.

For primary cultures experiments, in each WB were analysed two technical replicates of each treatment, and the average between them was calculated. In order to measure Dab1 and Fyn activation after each treatment, the amount of the phosphorylated protein was normalized on the total protein signal, and the ratio between Reelin-, recMoPrP- or PrP-hFc-treated samples, and mock-, PBS- or hFc- and Rae-1γ-hFc-treated controls respectively was performed. The calculated ratios were then compared between *Prnp*$^{+/+}$ and *Prnp*$^{0/0}$ samples performing the Student's t-Test setting two-tailed distribution and two-sample unequal variance. Statistical analysis of untreated samples was performed comparing *Prnp*$^{+/+}$ and *Prnp*$^{0/0}$ cultures performing the Student's t-Test setting two-tailed distribution and two-sample unequal variance.

Each experiment was performed in triplicate, unless differently specified.

Statistical significance: $p < 0.05$.

RESULTS

ANALYSIS OF REELIN/DAB1 SIGNALLING PATHWAY ACTIVATION STATE IN *Prnp*$^{+/+}$ AND *Prnp*$^{0/0}$ MOUSE BRAIN DURING EARLY POSTNATAL DAYS

As shown in Figure 14, Reelin signalling pathway is triggered by binding of Reelin to its transmembrane lipoprotein receptors, ApoER2 and VLDLR, leading to Fyn-mediated Dab1 phosphorylation for further downstream signalling transduction [117].

Taking advantage of a *Prnp* knockout mouse model, we addressed the question whether PrP^{C} could modulate the Reelin-signalling cascade, and if this is the case, we could expect impairments in Reelin downstream signalling when PrP^{C} expression is ablated.

Dab1 is the intracellular adaptor protein that is phosphorylated on tyrosine residues upon Reelin binding to its receptors, being the key regulator of Reelin-signalling [131]. Indeed, the expression level and the activation state of Dab1 were evaluated in wild-type (*Prnp*$^{+/+}$) and PrP^{C}-null (*Prnp*$^{0/0}$) mouse brains.

DAB1 EXPRESSION ANALYSIS

In order to evaluate the existence of a functional interaction between PrP^{C} expression and the Reelin pathway, we measured Dab1 expression levels in *Prnp*$^{+/+}$ and *Prnp*$^{0/0}$ mouse brain during early postnatal days. Immunoprecipitated Dab1 was normalized on input material. Data are shown as ratio between *Prnp*$^{0/0}$ and *Prnp*$^{+/+}$. In PrP^{C}-null mice, Dab1 protein expression is increased of about 40% compared to WT animals, in both males and females (Figure 17a). Conversely, transcriptional analysis of mdab1 gene in the same samples reveals that Dab1 mRNA expression is not modified by the absence of *Prnp* (Figure 17b).

Reelin pathway displays a negative feedback mechanism by which the signal is switched off, based on Dab1 poly-ubiquitination and targeting to the proteasome [148]. Interestingly, disruption of the Reelin-signalling cascade leads to the accumulation of Dab1 protein *in vivo*, while Dab1 mRNA expression remains unchanged [132, 133, 142-145]. As Dab1 degradation is dependent on its phosphorylation, the protein tends to accumulate when its phosphorylation is impaired [146, 147]. Indeed, having observed Dab1 protein accumulation in our $Prnp^{0/0}$ brains, we next sought to analyse Dab1 phosphorylation status in the same samples. Taking advantage of immunoprecipitation experiments, we measured the phosphorylation status of Dab1 in age- and sex-matched $Prnp^{+/+}$ and $Prnp^{0/0}$ mice during early postnatal days. Phosphorylated Dab1 protein is normalized on total Dab1 content in each sample. Data are shown as ratio between $Prnp^{0/0}$ and $Prnp^{+/+}$. Due to altered expression level of Dab1 in PrP^{C}-null mice and high variability among independent experiments, we were not able to obtain convincing results regarding Dab1 phosphorylation status in brain samples. Therefore, we decided to take advantage of an *ex vivo* model (see below) (Figure 17c).

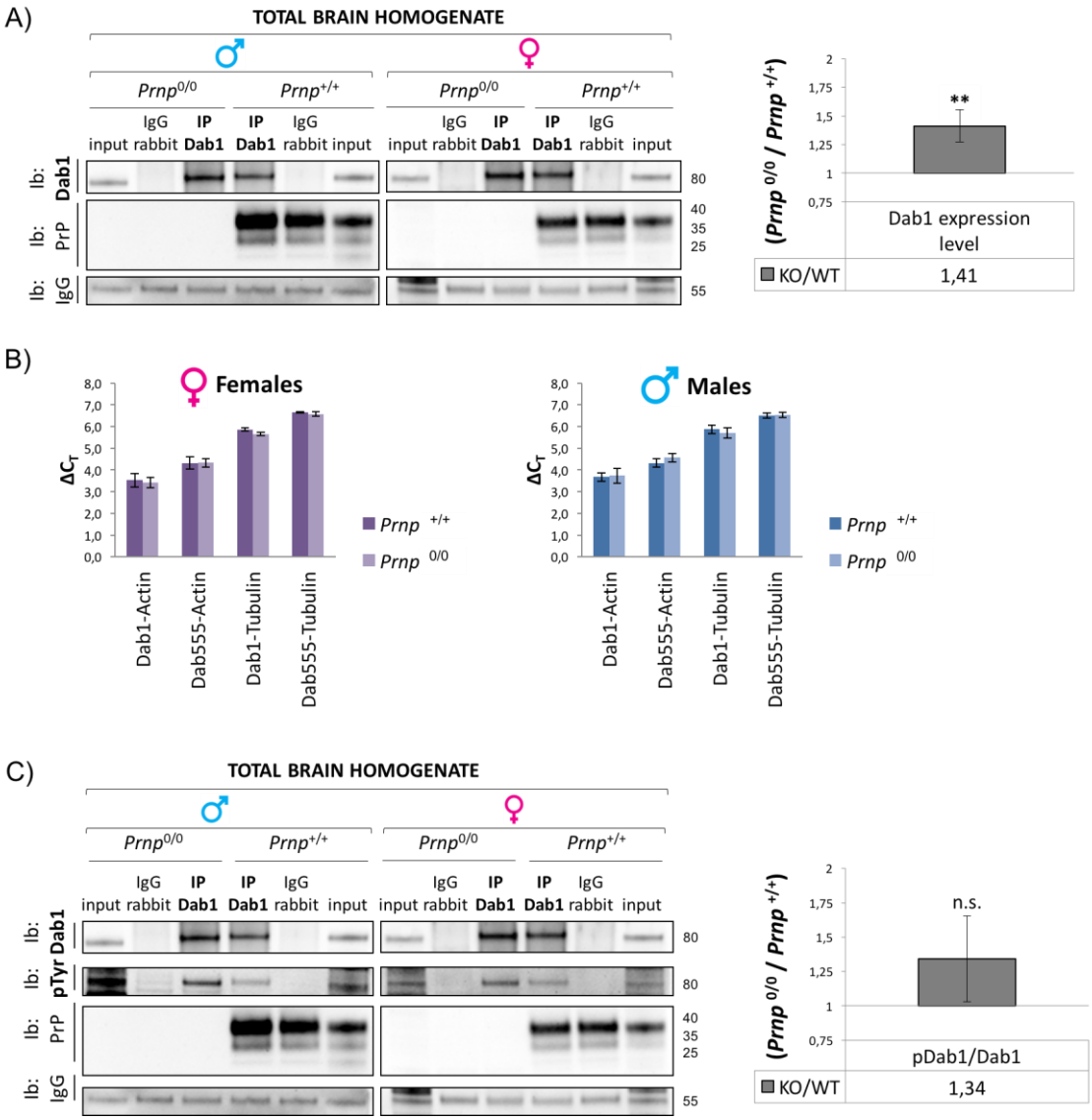

Figure 17. Dab1 expression and activation state in early postnatal mouse brain. A) Dab1 protein levels were measured by immunoprecipitation experiments. Total brain homogenates from P4 *Prnp*$^{0/0}$ and *Prnp*$^{+/+}$ sex-matched pups were used. Immunoprecipitated Dab1 was normalized on the starting amount of protein present in the input material. Sample size in each experiment: n=1; three independent experiments for each group (males and females). Data are shown as ratio between *Prnp*$^{0/0}$ and *Prnp*$^{+/+}$ ± standard error. *p<0.05, **p<0.01, **p<0.001. B) Transcriptional analysis of Dab1 mRNA was performed using two couples of primers: Dab1 recognizes all the three murine Dab1 mRNA isoforms, Dab555 recognizes the longer isoform only. β-Actin and βIII-Tubulin were used as reference genes. Relative expression of Dab1 gene versus the housekeeping gene chosen as reference was calculated using the $\Delta\Delta C_T$ method. Statistical significance: p<0.05. Sample size: n=4 each group. C) Dab1 phosphorylation levels were measured by immunoprecipitation experiments. The amount of phosphorylated Dab1 was normalized on total Dab1 signal. Sample size in each experiment: n=1; three independent experiments for each group (males and females). Data are shown as ratio between *Prnp*$^{0/0}$ and *Prnp*$^{+/+}$ ± standard error. Statistical significance: p<0.05, n.s. = no statistical significance.

REELIN-SIGNALLING PATHWAY EXPRESSION ANALYSIS

Keeping in mind that Dab1 accumulation is observed in conditions of Reelin pathway disruption, we hypothesized that alterations in the expression and activation state of signalling components may be responsible for the increase in Dab1 protein in *Prnp*$^{0/0}$ mice. Therefore, we performed a protein expression analysis of different components of the Reelin-signalling cascade in our PrP^{C}-null mouse model. Each protein signal was normalized on β-Actin as reference. Data are shown as ratio between *Prnp*$^{0/0}$ and *Prnp*$^{+/+}$. Surprisingly, Reelin, VLDLR and ApoER2 expression levels are not modified in *Prnp*$^{0/0}$ brains in comparison to WT samples (Figure 18a). Conversely, preliminary data showed that phosphorylation of Fyn kinase at tyrosine 416, and thus its activation [200], is impaired in *Prnp*$^{0/0}$ brains in comparison to WT controls (Figure 18b).

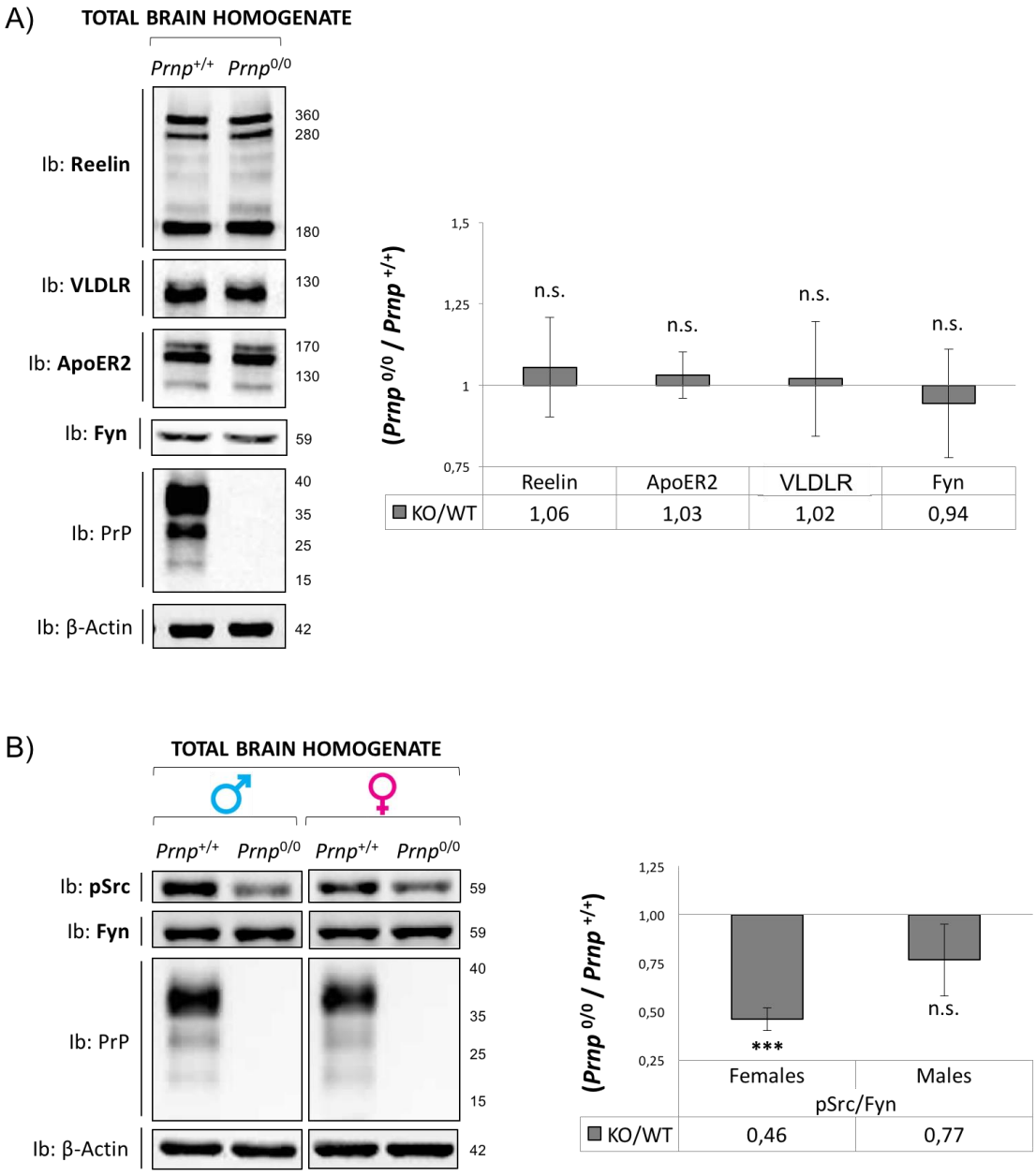

Figure 18. Expression and activation state of different component of the Reelin/Dab1 signalling pathway in early postnatal mouse brain. A) Reelin, ApoER2, VLDLR and Fyn protein levels were measured by WB experiments. Total brain homogenates from P4 *Prnp*$^{0/0}$ and *Prnp*$^{+/+}$ sex-matched pups were used. β-Actin was used as loading control. Sample size in each experiment: n=4; three independent experiments. Data are shown as ratio between *Prnp*$^{0/0}$ and *Prnp*$^{+/+}$ ± standard error. *p<0.05, **p<0.01, **p<0.001, n.s. = no statistical significance. B) Fyn phosphorylation levels in total brain homogenates from P4 *Prnp*$^{0/0}$ and *Prnp*$^{+/+}$ sex-matched pups were measured by WB experiments. The amount of phosphorylated Fyn was normalized on the total protein signal. Sample size in each experiment: n=4; one experiment. Data are shown as ratio between *Prnp*$^{0/0}$ and *Prnp*$^{+/+}$ ± standard error. *p<0.05, **p<0.01, **p<0.001, n.s. = no statistical significance.

We next hypothesized that PrP^C on the cell membrane could play a role as receptor or co-receptor for Reelin, thus modulating its pathway. Interestingly, both PrP^C and ApoER2 are preferentially located in lipid raft microdomains of the plasma membrane [38, 201]. Indeed, co-immunoprecipitation experiments were performed in *Prnp*$^{+/+}$ brain samples in order to investigate the existence of a direct interaction between PrP^C and Reelin or its receptor ApoER2. Despite the application of many different experimental protocols, described in the Materials and Methods paragraph, we were not able to co-immunoprecipitate PrP^C neither with Reelin nor with ApoER2 (Figure 19).

In order to exclude the possibility that PrP^C and ApoER2 may interact at the cell surface through a very weak interaction, we decided to perform protein crosslinking of the analysed brain samples before proceding with the immunoprecipitation procedure. Despite the application of the crosslinking reagent, we were not able to co-immunoprecipitate PrP^C with ApoER2, definitely ruling out the hypothesis of a direct interaction between these two proteins in our experimental setup (Figure 20).

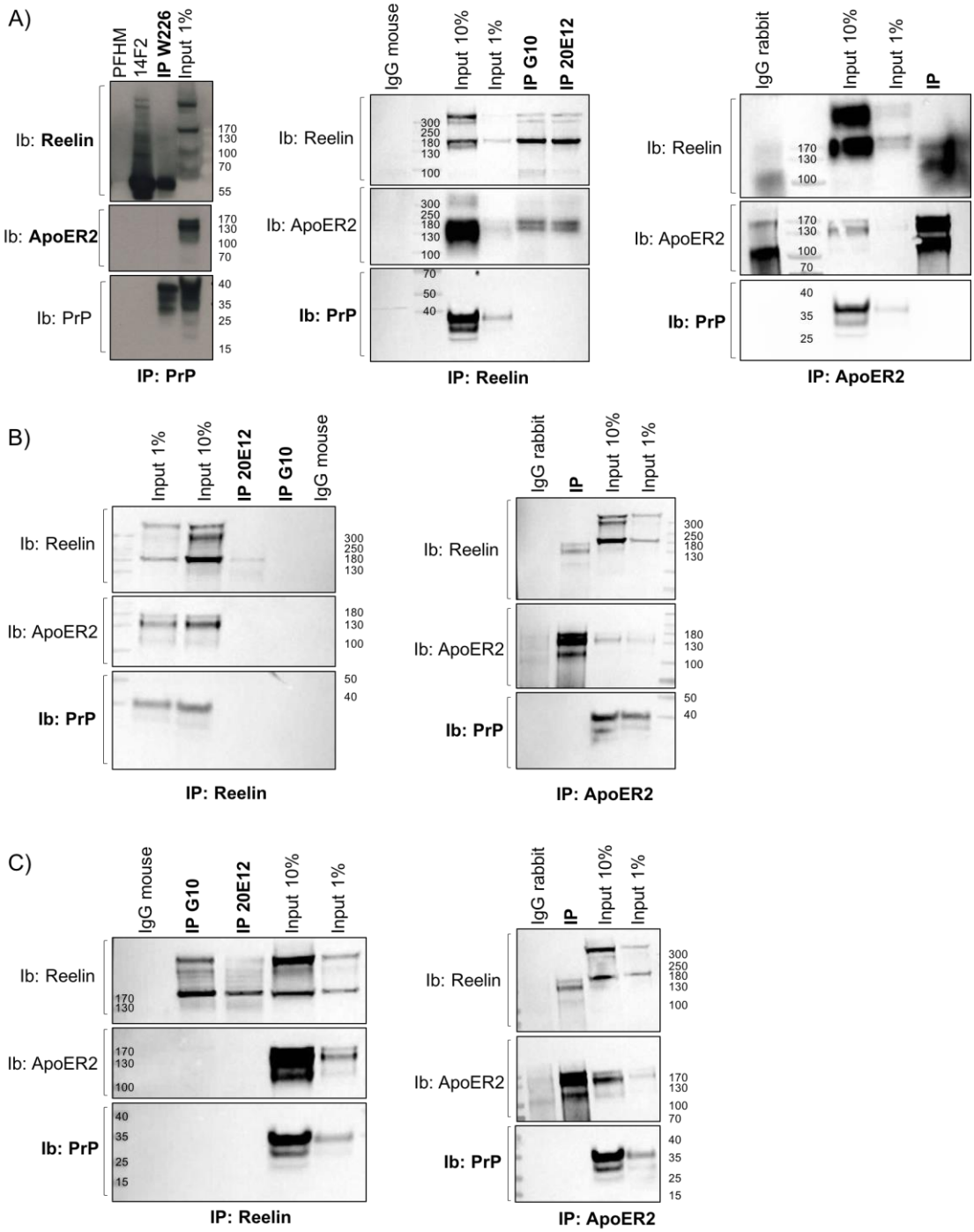

Figure 19. Co-immunoprecipitation experiments between PrP^C and Reelin, and between PrP^C and ApoER2. PrP^C, Reelin or ApoER2 were immunoprecipitated from total brain homogenates from P4 *Prnp*$^{+/+}$ mice. Immunoprecipitated samples were then immunoblotted with anti-PrP, anti-ApoER2 and anti-Reelin antibodies. Reelin signal in ApoER2-immunoprecipitated samples is considered a positive control, and viceversa. 14F2 anti-DISC1 antibody, protein-free hybridoma medium (PFHM) and normal mouse/rabbit IgG served as negative control. Starting material (input) was also loaded on the same membrane. Sample size in each experiment: n=1; three independent experiments. Three different protocols were applied as described (refer to Materials and Methods paragraph for details): A) first approach; B) second approach; C) third approach.

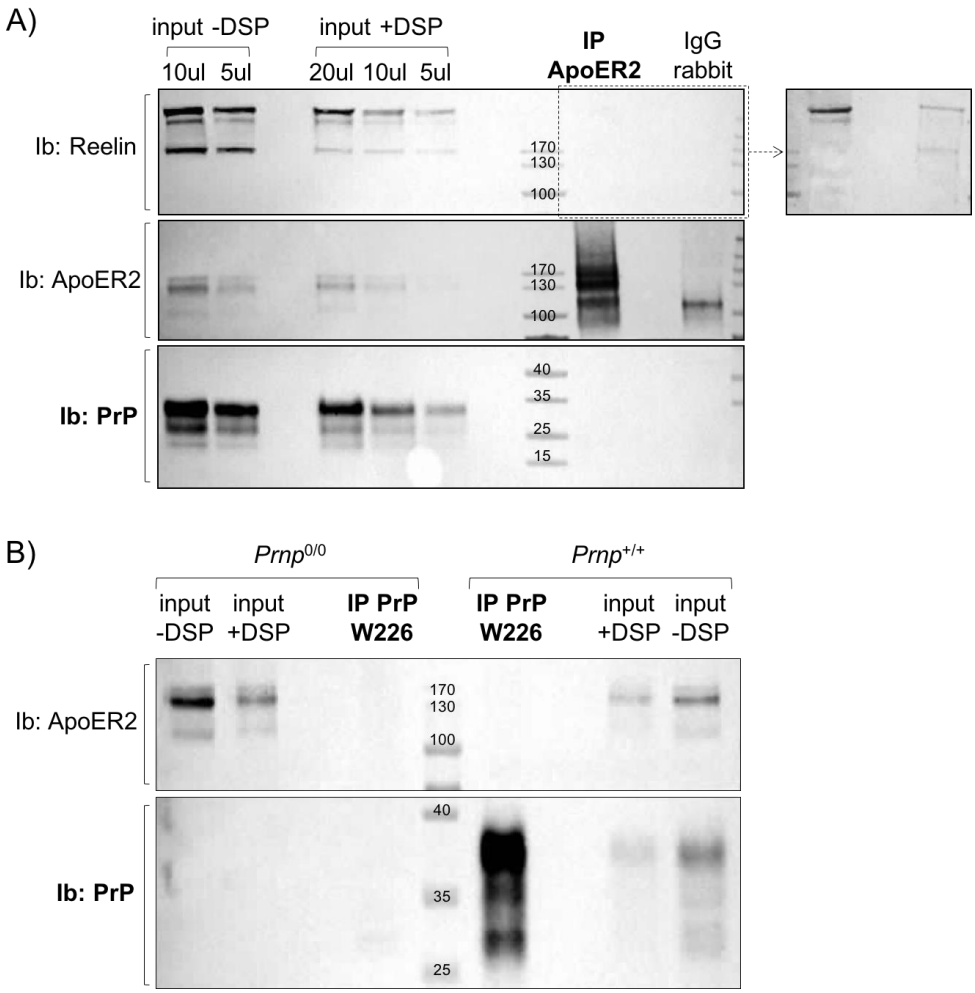

Figure 20. Co-immunoprecipitation experiments between PrP^C and ApoER2 after protein crosslinking. Total brain homogenates from P4 mice were treated with DSP crosslinking reagent prior to immunoprecipitation. A) ApoER2 was immunoprecipitated from *Prnp*$^{+/+}$ brain samples as described. Immunoprecipitated samples were then immunoblotted with anti-PrP, anti-ApoER2 and anti-Reelin antibodies. Reelin signal in ApoER2-immunoprecipitated samples served as positive control. Rabbit IgG served as negative control. Starting material (input), not treated and treated with the crosslinker, was also loaded on the same membrane. Sample size in each experiment: n=1; two independent experiments. B) PrP^C was immunoprecipitated from from *Prnp*$^{+/+}$ and *Prnp*$^{0/0}$ brain samples as described. Immunoprecipitated samples were then immunoblotted with anti-PrP and anti-ApoER2 antibodies. *Prnp*$^{0/0}$ samples served as negative control. Starting material (input), not treated and treated with the crosslinker, was also loaded on the same membrane. Sample size in each experiment: n=1; two independent experiments.

ANALYSIS OF REELIN/DAB1 SIGNALLING PATHWAY ACTIVATION STATE IN *Prnp*$^{+/+}$ AND *Prnp*$^{0/0}$ PRIMARY NEURONAL CULTURES

As already mentioned, due to increased expression of Dab1 in PrP^{C}-null mice and high variability among independent experiments, we were not able to obtain convincing results regarding Dab1 phosphorylation status in brain samples. Therefore, we decided to take advantage of an *ex vivo* model based on primary neuronal cultures. Cortical primary neurons are commonly used in literature to study Reelin-signalling pathway due to the possibility of easy manipulations. Indeed, it has been shown that treatment of cultured neurons with Reelin-conditioned supernatant leads to the activation of downstream cascade and phosphorylation of Dab1 [133]. We stimulated primary cortical neurons from *Prnp*$^{0/0}$ and *Prnp*$^{+/+}$ embryos with Reelin-conditioned supernatant, in order to assess whether the absence of PrP^{C} leads to impairments in the response to Reelin. Besides, we also treated these primary cortical neurons with recombinant full-length mouse PrP and with the fusion protein moPrP-hFc in order to investigate whether PrP^{C} is able to activate Reelin downstream signalling by itself.

STIMULATION WITH REELIN-CONDITIONED MEDIUM

Primary cortical neurons from *Prnp*$^{0/0}$ and *Prnp*$^{+/+}$ embryos were stimulated after 5 DIV with mock- and Reelin-conditioned supernatant, as already described. Reelin content in the conditioned medium was evaluated by WB using an anti-Reelin specific antibody (Figure 21).

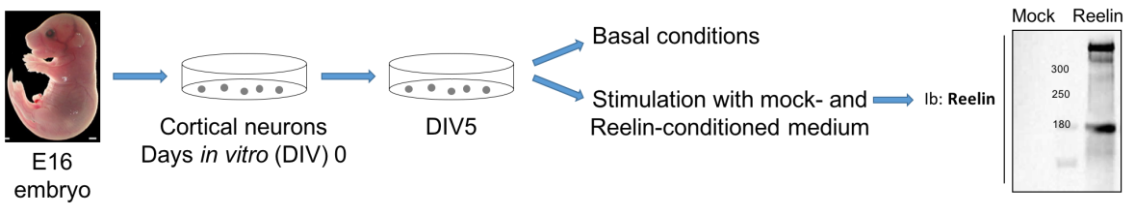

Figure 21. Experimental design used for Reelin-stimulation of primary neurons. Primary cortical neurons were obtained from E16 *Prnp*$^{0/0}$ and *Prnp*$^{+/+}$ embryos and were plated on 6-well plates in neurobasal medium (DIV0). After 5 DIV, either neurons were collected under basal conditions or were stimulated with mock- or Reelin-conditioned medium. Reelin content in the conditioned medium was analysed by WB using anti-Reelin G10 monoclonal antibody (representative image). The same experimental design was used for recMoPrP and PrP-hFc treatment.

Dab1 phosphorylation was measured as ratio between phospho-tyrosine signal and Dab1 total protein signal. Then, the ratio between Reelin-treated samples and mock-treated controls was performed. Data are shown as ratio between *Prnp*$^{0/0}$ and *Prnp*$^{+/+}$. In agreement with previous works reported in literature [133], Reelin treatment is able to trigger a massive Dab1 phosphorylation in wild-type neurons. Dab1 phosphorylation is not modified by PrP^{C} absence under basal conditions. Conversely, Dab1 activation is impaired in *Prnp*$^{0/0}$ neurons compared to *Prnp*$^{+/+}$ controls. Indeed, phosphorylation of Dab1 upon Reelin stimulus is reduced by 30% in absence of PrP^{C} (Figure 22).

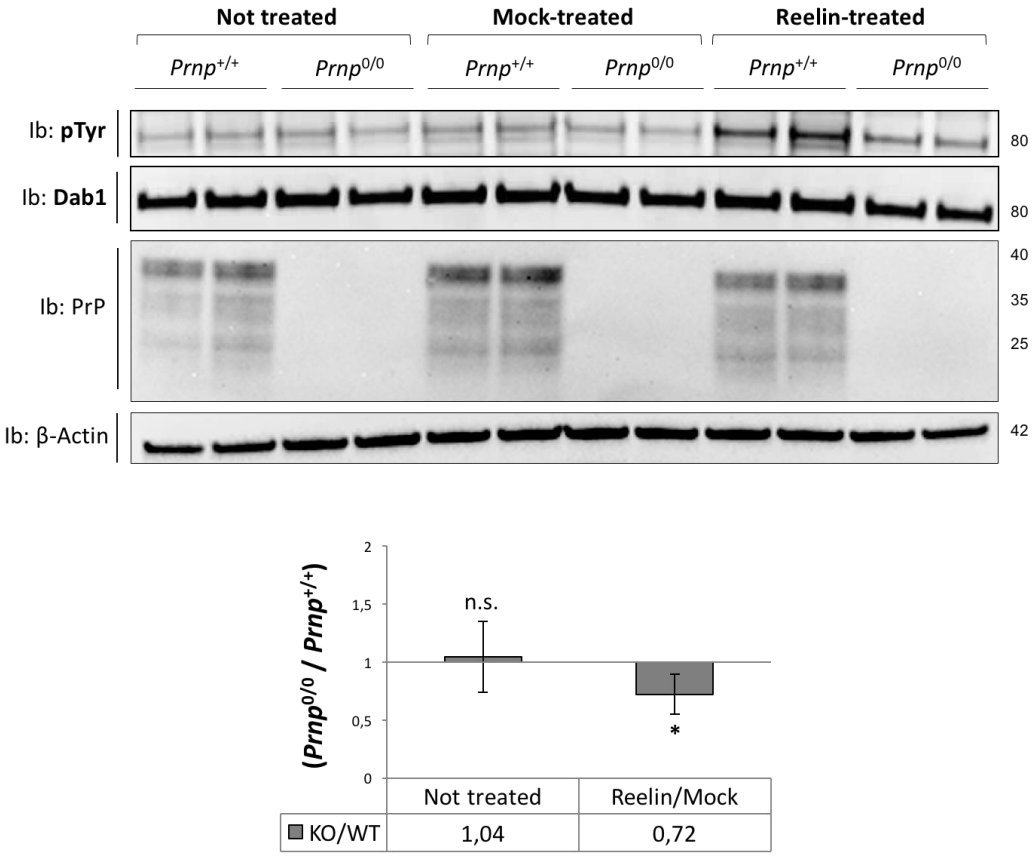

Figure 22. Dab1 phosphorylation in primary cortical neurons upon Reelin stimulus. Dab1 phosphorylation levels were measured by WB analysis. The amount of phosphorylated Dab1 (pTyr) was normalized on the total Dab1 signal, and the ratio between Reelin- and mock-treated samples was performed. Sample size in each experiment: n=2 (technical replicates); six independent experiments. Data are shown as ratio between *Prnp*$^{0/0}$ and *Prnp*$^{+/+}$ ± standard error. *p<0.05, **p<0.01, **p<0.001, n.s. = no statistical significance.

In order to assess whether this impairment in Dab1 response is due to alterations in the Reelin-signalling pathway, we checked the expression and the activation state of different components of the cascade in *Prnp*$^{0/0}$ and *Prnp*$^{+/+}$ cortical neurons after 5 DIV under basal conditions. Western blot analysis revealed that Reelin content in both neuron growth media (secreted protein) and neuronal lysate is unchanged in PrP^{C}-null neurons compared to WT samples (Figure 23a). Moreover, ApoER2 expression levels are not modified by *Prnp* ablation. Finally, Fyn kinase expression levels are not modified in PrP^{C} absence, while its phosphorylation, even without statistical significance, showed a decreasing trend in *Prnp*$^{0/0}$ neurons compared to WT controls (Figure 23b). As Fyn kinase activity could be modulated by NCAM, a known PrP^{C} interactor, we decided to measure its expression in the same samples. Interestingly,

NCAM expression is reduced by 15% in *Prnp*$^{0/0}$ neurons in comparison to WT controls (Figure 23c).

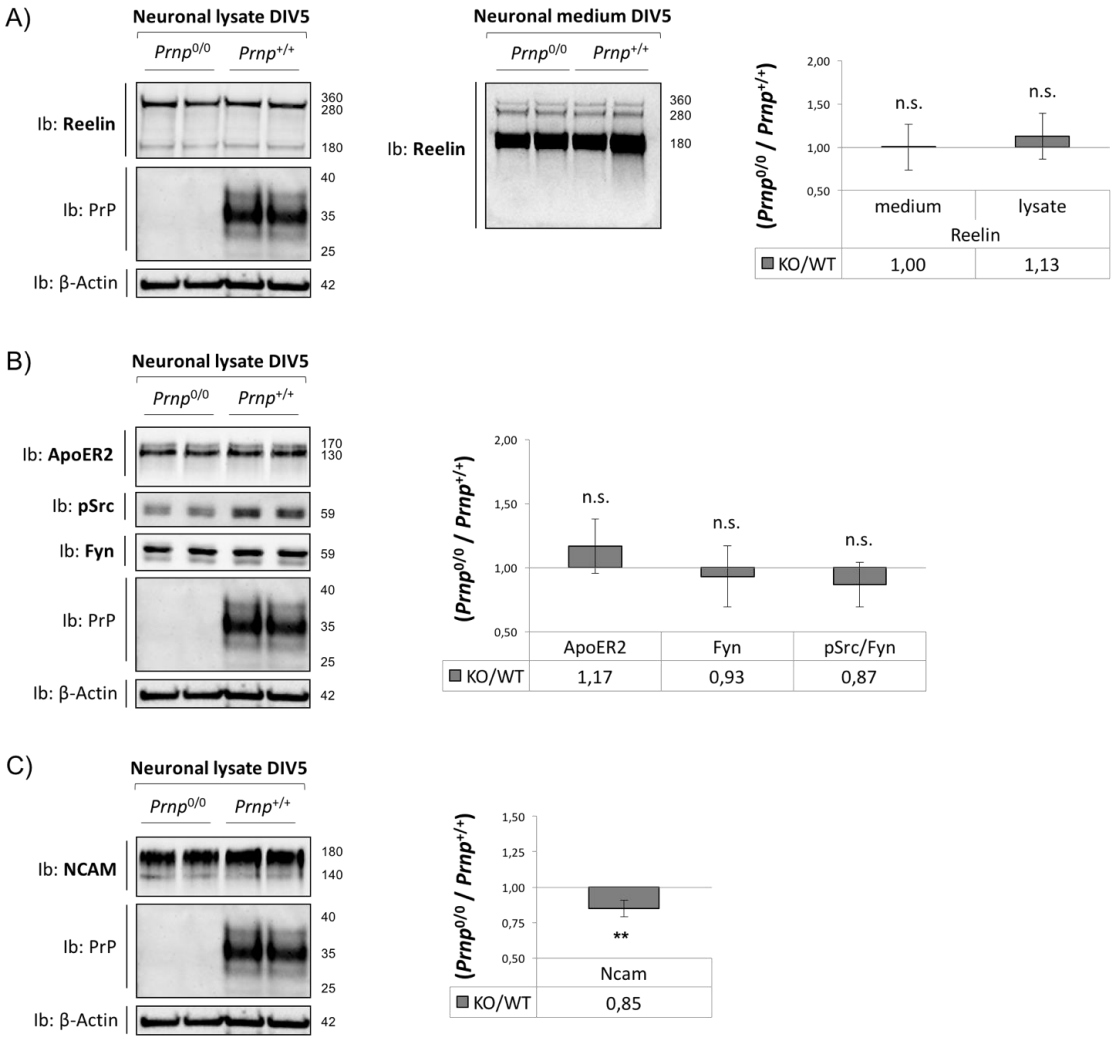

Figure 23. Expression and activation state of different component of the Reelin/Dab1 signalling pathway in E16 primary cortical neurons under basal conditions. A) Reelin expression was measured by WB experiments in primary cortical neurons from E16 *Prnp*$^{0/0}$ and *Prnp*$^{+/+}$ embryos. Protein expression was quantified in both neuronal lysates and neuronal medium after 5 DIV. β-Actin was used as loading control for lysates. B) ApoER2 protein expression and Fyn kinase expression and phosphorylation levels were evaluated by WB experiments in primary cortical neurons from E16 *Prnp*$^{0/0}$ and *Prnp*$^{+/+}$ embryos. Neuronal lysates after 5 days *in vitro* were used. β-Actin was used as loading control for protein expression. The amount of phosphorylated Fyn was normalized on the total protein signal. C) NCAM expression was measured by WB experiments in DIV5 primary cortical neurons from E16 *Prnp*$^{0/0}$ and *Prnp*$^{+/+}$ embryos. β-Actin was used as loading control.

Sample size in each experiment: n=4; two independent experiments. Data are shown as ratio between *Prnp*$^{0/0}$ and *Prnp*$^{+/+}$ ± standard error. *p<0.05, **p<0.01, **p<0.001, n.s. = no statistical significance.

STIMULATION WITH recMoPrP (23-231) AND moPrP-hFc

Taken together, findings obtained from primary neurons stimulated with Reelin suggest that PrP^C plays a role in modulating Reelin-signalling pathway. Indeed, PrP^C absence leads to impaired response. Next, we sought to investigate whether PrP^C is able to activate Reelin downstream signalling cascade, and therefore to promote Dab1 phosphorylation, by itself. To this aim, we stimulated primary cortical neurons with recombinant full-length mouse PrP (recMoPrP 23-231) or with the fusion protein moPrP-hFc, a mouse full-length PrP fused with the Fc region of IgG_1 human immunoglobulin. As described in the Materials and Methods section, recombinant PrP is a monomeric protein produced in bacteria, and therefore does not present its normal glycosylation pattern but is fully unglycosylated. After purification, a refolding protocol allows the recombinant protein to acquire its correct folding. Conversely, fusion moPrP-hFc protein is dimeric (two molecules of PrP bound to each arm of the antibody Fc region) and oriented, and is produced in eukaryotic cells, therefore it is normally present with its typical glycosylation pattern and its physiological folding (Figure 24).

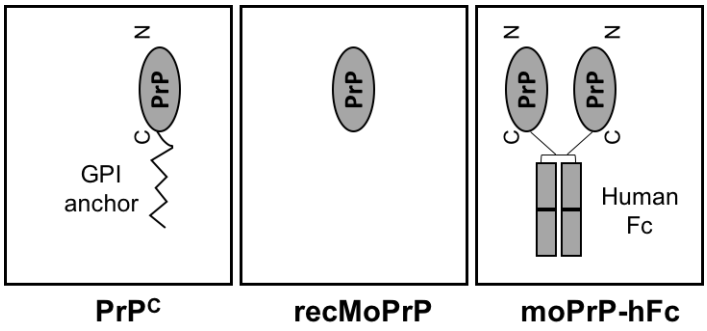

Figure 24. Schematic representation of PrP^C, recombinant mouse full-length PrP and moPrP-hFc fusion protein. PrP^C is a GPI-anchored N-glycosylated protein. The GPI moiety is linked to the C-terminal portion of PrP^C, meaning that PrP^C has a fixed orientation on the cell membrane. The recombinant mouse full-length PrP is a monomeric and unglycosylated protein. Moreover, it lacks a fixed orientation. Fusion moPrP-hFc protein is dimeric and oriented, and it is normally present with its typical glycosylation.

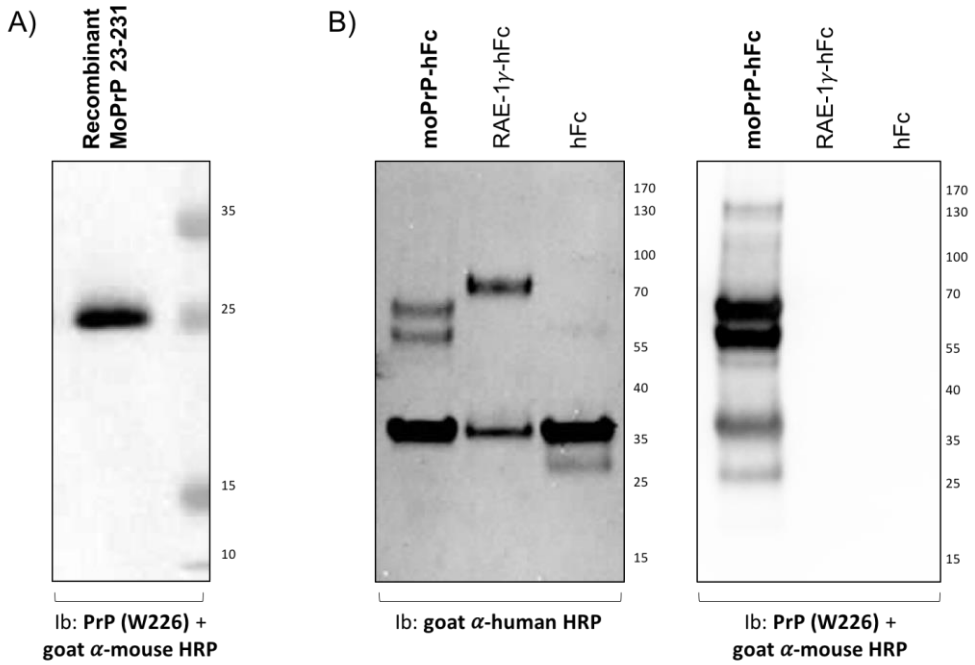

Figure 25. Recombinant mouse full-length PrP (23-231) and moPrP-hFc fusion protein. A) Western blot analysis of 0.1 μg of mouse recPrP (23-231) detected with anti-PrP W226 monoclonal antibody. B) Western blot analysis of 2 μg of moPrP-hFc fusion protein, RAE-1γ-hFc and hFc. The membrane on the left was probed with anti-human HRP-conjugated secondary antibody that recognizes the Fc portion of human immunoglobulins. The membrane on the right was probed with anti-PrP W226 monoclonal antibody. The molecular weight of hFc alone is about 35 kDa. The two molecular weight bands between 55 and 70 kDa correspond to the moPrP-hFc fusion protein.

Primary cortical neurons from *Prnp*$^{0/0}$ and *Prnp*$^{+/+}$ embryos were stimulated after 5 DIV with purified recombinant full-length mouse PrP (23-231), adapting a previously published protocol to our experimental setup [91]. The integrity of purified recombinant MoPrP was assessed by Western blotting using anti-PrP W226 antibody (Figure 25a). Two concentration of recMoPrP were tested, as indicated. PBS-treatment (vehicle-only) was used as negative control. Dab1 and Fyn kinase phosphorylation was measured as ratio between phosphorylated protein and total protein signals. Ratio between recMoPrP-treated samples and PBS-treated controls was then performed. Data are shown as ratio between *Prnp*$^{0/0}$ and *Prnp*$^{+/+}$. As shown in Figure 26, recombinant MoPrP is not able to induce Fyn kinase and Dab1 phosphorylation, neither at 1 μM (Figure 26a) nor at 2 μM (Figure 26b) concentration. In Figure 26c, quantitative analysis of these data is reported.

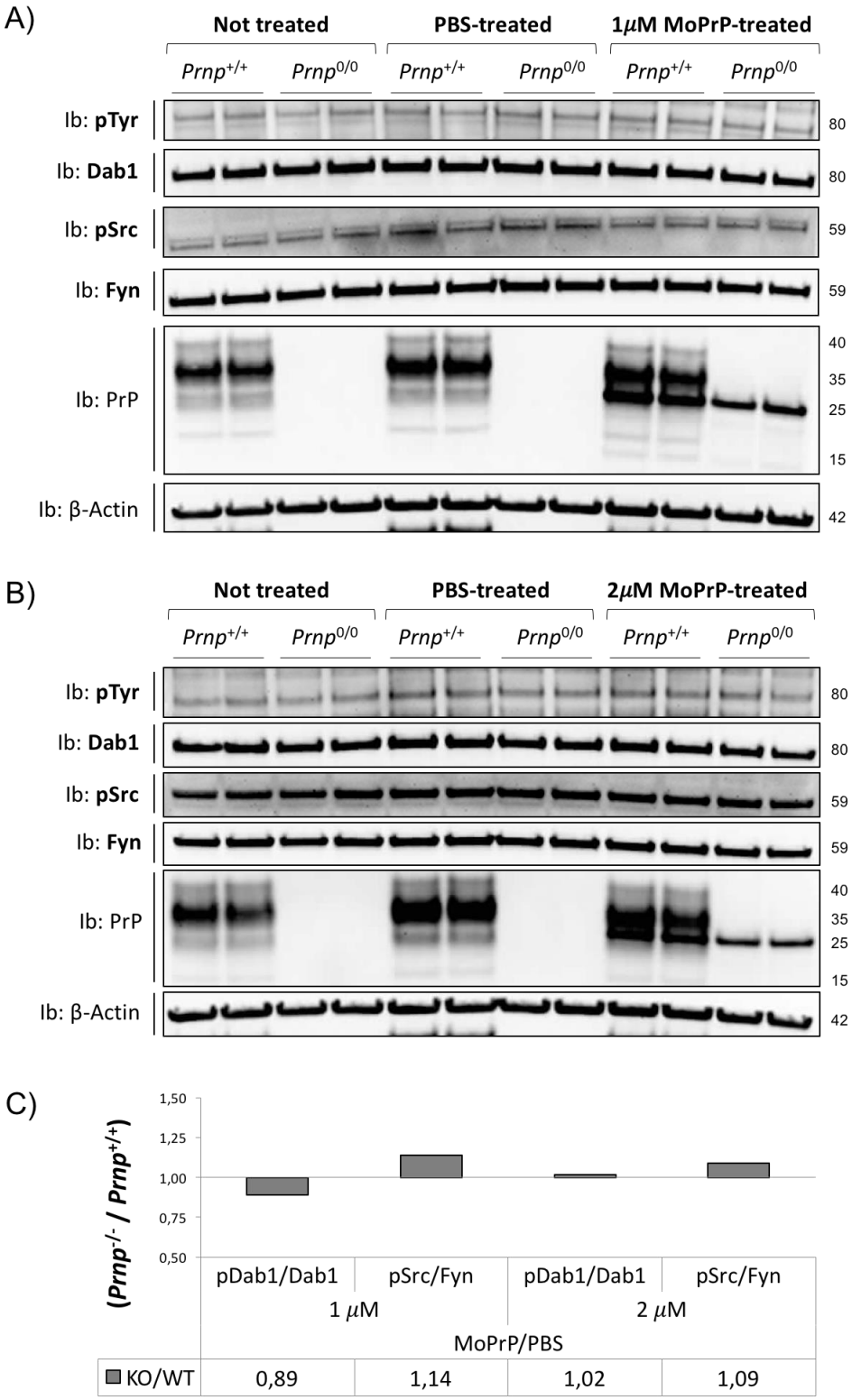

Figure 26. Dab1 and Fyn phosphorylation in primary cortical neurons upon recombinant mouse PrP treatment. Dab1 and Fyn phosphorylation levels were measured by WB analysis. The amount of phosphorylated protein was normalized on the total protein signal, and the ratio between recMoPrP- and PBS-treated samples was performed. Sample size in each experiment: n=2 (technical replicates); one experiment. A) Neurons treated with 1 μM of recMoPrP. B) Neurons treated with 2 μM of recMoPrP. C) Quantitative analysis of data. Data are shown as ratio between *Prnp*$^{0/0}$ and *Prnp*$^{+/+}$.

As monomeric recombinant MoPrP failed to activate Reelin downstream cascade by itself, we next sought to investigate whether dimeric moPrP-hFc is able to induce Fyn kinase activation and, subsequently, Dab1 phosphorylation in dissociated cortical neurons. Indeed, moPrP-hFc treatment of primary hippocampal *Prnp*$^{0/0}$ and *Prnp*$^{+/+}$ neurons results in Fyn kinase activation [74]. Thus, we applied the same stimulation protocol to our experimental setup, administering moPrP-hFc to primary cortical neurons from *Prnp*$^{0/0}$ and *Prnp*$^{+/+}$ embryos after 5 DIV. Western Blot analysis of purified moPrP-hFc allows us to confirm the integrity of the protein used for stimulation (Figure 25b). Control neurons (mock-treated) were treated with purified human Fc (hFc) or with a purified unrelated fusion protein (RAE-1γ-hFc). Dab1 and Fyn kinase phosphorylation was measured as ratio between moPrP-hFc-treated samples and mock-treated controls. Data are shown as ratio between *Prnp*$^{0/0}$ and *Prnp*$^{+/+}$. As shown in Figure 27, neither 2 μg (Figure 26a) nor 4 μg (Figure 26b) of fusion PrP-hFc protein are able to induce Fyn kinase and Dab1 phosphorylation. In Figure 27c, quantitative analysis of these data is reported.

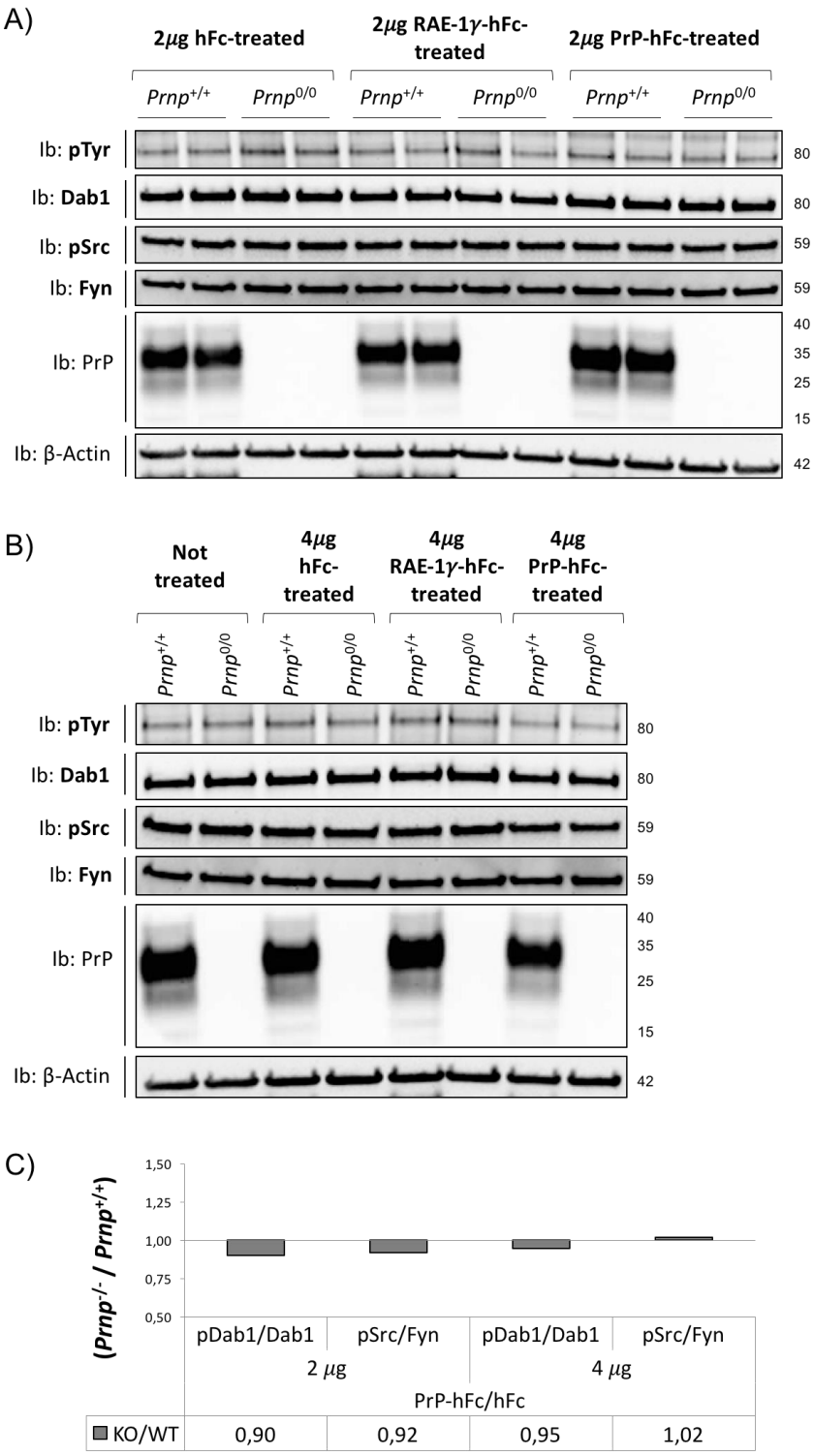

Figure 27. Dab1 and Fyn phosphorylation in primary cortical neurons upon mouse PrP-hFc fusion protein treatment. Dab1 and Fyn phosphorylation levels were measured by WB analysis. The amount of phosphorylated protein was normalized on the total protein signal, and the ratio between moPrP-hFc- and hFc-treated samples was performed. Sample size in each experiment: n=2 (technical replicates); one experiment. A) Neurons treated with 2 μg of moPrP-hFc and 2 μg of hFc as control. B) Neurons treated with 4 μg of moPrP-hFc and 4 μg of hFc as control. C) Quantitative analysis of data. Data are shown as ratio between *Prnp*$^{0/0}$ and *Prnp*$^{+/+}$.

ANALYSIS OF PrP^C EXPRESSION IN DIFFERENT MOUSE MODELS OF REELIN-SIGNALLING DISRUPTION

Taken together, the data presented above suggest that PrP^C is involved in the modulation of the Reelin-signalling pathway, boosting the activation of the downstream cascade in physiological conditions. Indeed, PrP^C absence correlates with impaired Dab1 activation upon Reelin stimulation and Dab1 protein accumulation in brain samples. Next, we sought to address the opposite question, in order to investigate whether Reelin signalling pathway disruption somehow affects PrP^C expression levels in mouse brain. To this aim, we took advantage of different animal models. We measured PrP^C expression levels in *reeler* mutant, $ApoER2^{-/-}$, $VLDLR^{-/-}$, $ApoER2^{-/-}$;$VLDLR^{-/-}$ double knockout and $Dab1^{-/-}$ mouse brain during early postnatal days. Littermates WT animals were used as controls. For $ApoER2^{-/-}$;$VLDLR^{-/-}$ double knockout mice, $VLDLR^{-/-}$ littermates were used as controls. PrP^C expression was normalized on β-Actin. Data are shown as ratio between mutants and respective controls. Due to fertility problems and reduced natality of homozygous mutant mice, we were able to collect very few samples for each genotype. PrP^C expression was measured in three brain regions for each mutant: cortex, cerebellum and hippocampus. For what concern *reeler* mice, PrP^C expression was also evaluated in total brain homogenate.

As shown in Figure 28, we were not able to observe statistically significative differences in the expression of PrP^C in *reeler* mice, in which Reelin is not expressed. We also analysed PrP^C expression in mice in which Reelin-signalling pathway is disrupted because its receptors have been knocked out. However, PrP^C expression seems not affected by the lack of ApoER2 (Figure 29) or VLDLR (Figure 30) alone, or by the ablation of both of them (Figure 31), in any evaluated brain region. Finally, as we observed that PrP^C absence determines a significative alteration in Dab1 expression, we measured the expression of PrP^C in Dab1 knockout mice, to evaluate whether a reverse regulatory mechanism between these two proteins also exists in the mouse brain. However, as shown in Figure 32, PrP^C expression in early postnatal mouse brains

is not affected by Dab1 ablation. These findings suggest that PrP^C is able to modulate Reelin-signalling cascade, but it is not affected by its disruption.

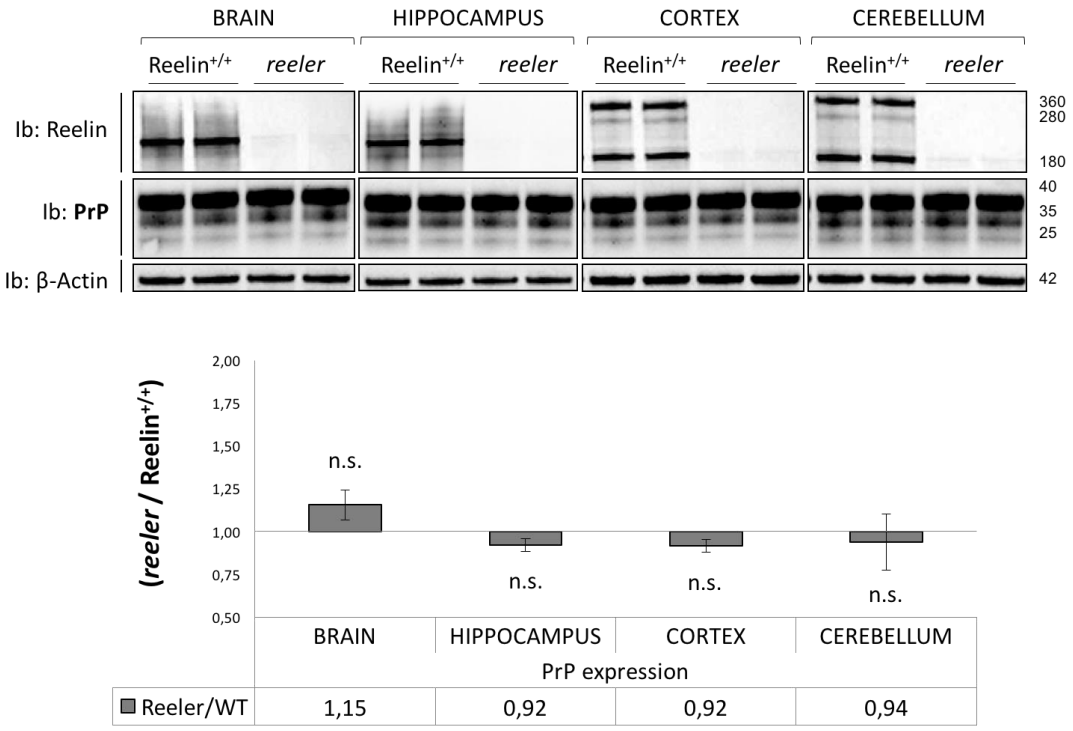

Figure 28. PrP^C expression in *reeler* mice. PrP^C expression was measured by WB experiments in total brain, hippocampus, cortex and cerebellum of P4 *reeler* mice and littermate WT controls. β-Actin was used as loading control. Sample size: n=3; one experiment. Data are shown as ratio between *reeler* and WT ± standard error. Statistical significance: $p<0.05$, n.s. = no statistical significance.

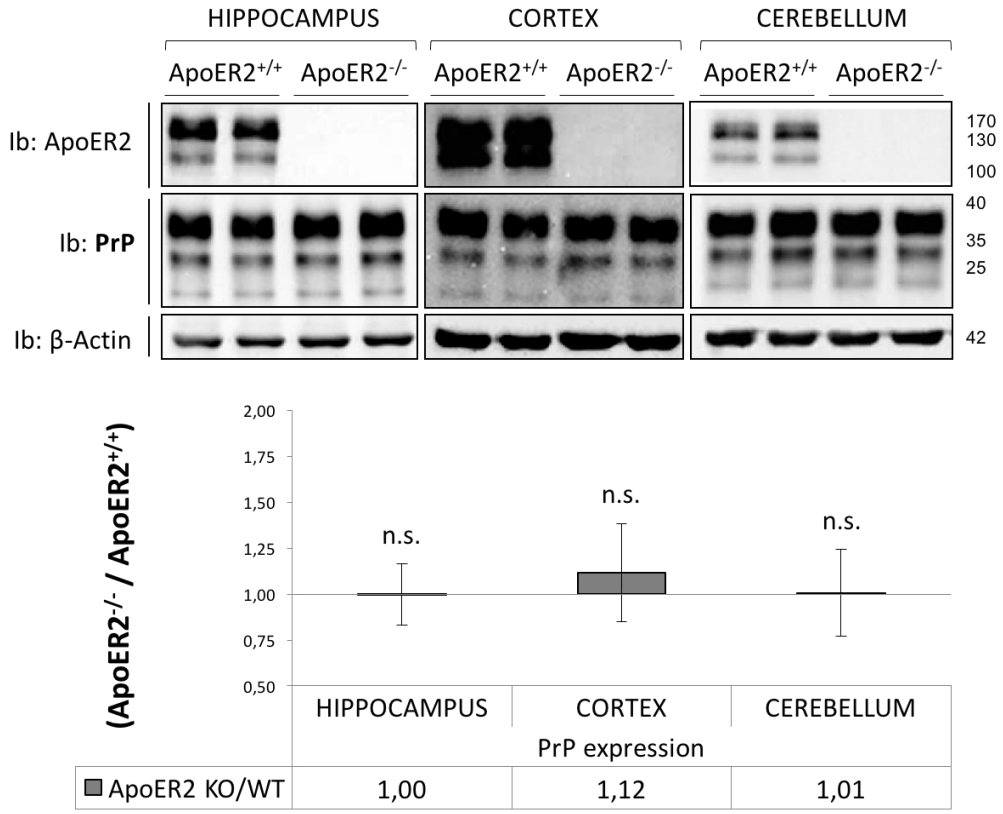

Figure 29. PrP^{C} expression in ApoER2$^{-/-}$ mice. PrP^{C} expression was measured by WB experiments in hippocampus, cortex and cerebellum of P4 ApoER2$^{-/-}$ mice and littermate WT controls. β-Actin was used as loading control. Sample size: n=4; one experiment. Data are shown as ratio between ApoER2$^{-/-}$ and ApoER2$^{+/+}$ ± standard error. Statistical significance: $p<0.05$, n.s. = no statistical significance.

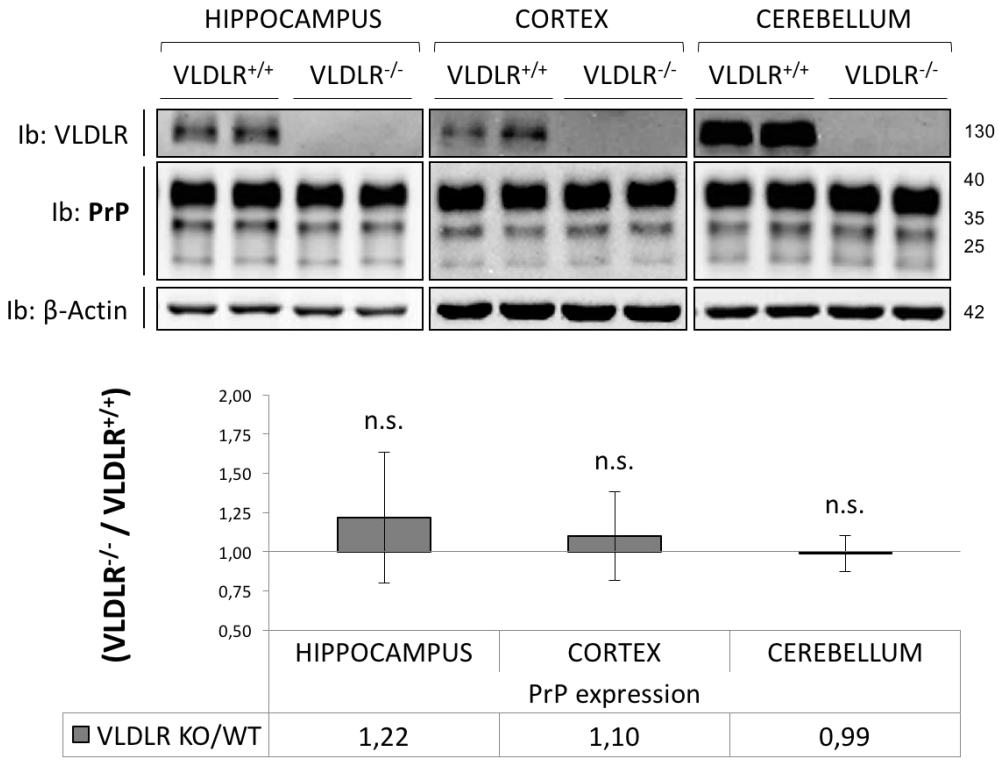

Figure 30. PrP^{C} expression in VLDLR$^{-/-}$ mice. PrP^{C} expression was measured by WB experiments in hippocampus, cortex and cerebellum of P4 VLDLR$^{-/-}$ mice and littermate WT controls. β-Actin was used as loading control. Sample size: n=4; one experiment. Data are shown as ratio between VLDLR$^{-/-}$ and VLDLR$^{+/+}$ ± standard error. Statistical significance: $p<0.05$, n.s. = no statistical significance.

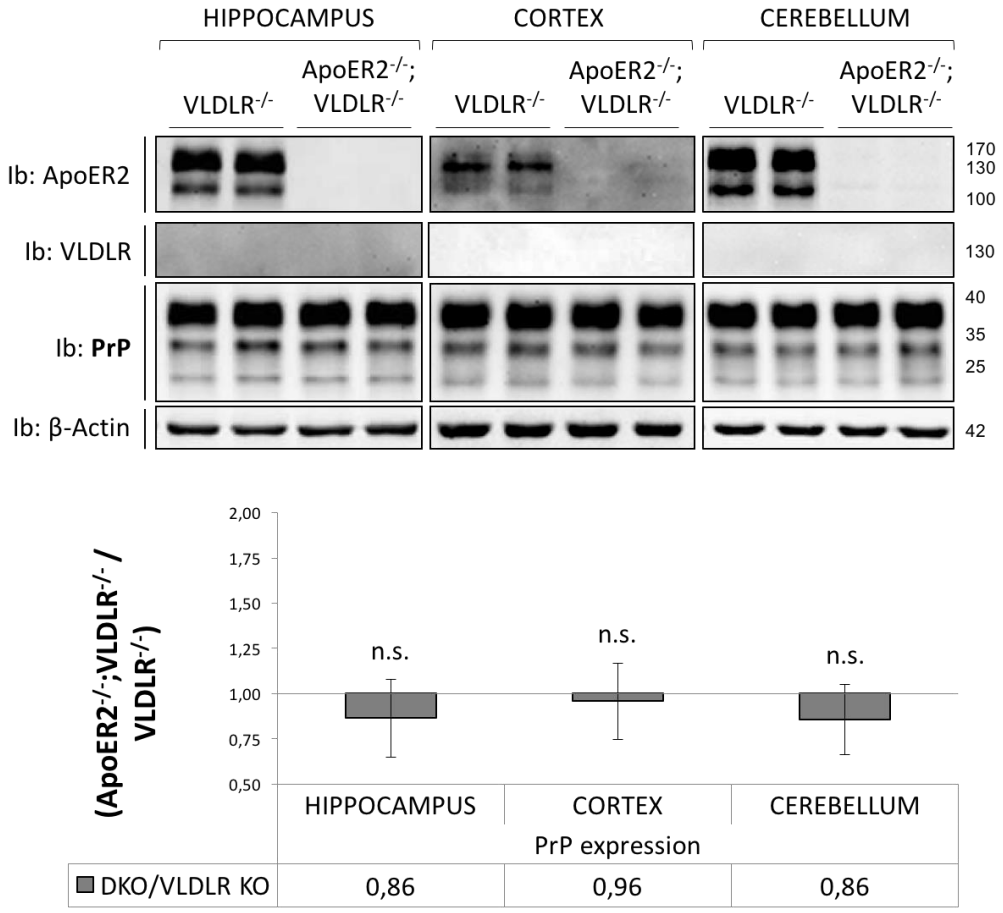

Figure 31. PrP^{C} expression in ApoER2$^{-/-}$;VLDLR$^{-/-}$ mice. PrP^{C} expression was measured by WB experiments in hippocampus, cortex and cerebellum of P4 ApoER2$^{-/-}$;VLDLR$^{-/-}$ mice and littermate VLDLR$^{-/-}$ controls. β-Actin was used as loading control. Sample size: n=4; one experiment. Data are shown as ratio between ApoER2$^{-/-}$;VLDLR$^{-/-}$ and VLDLR$^{-/-}$ ± standard error. Statistical significance: $p<0.05$, n.s. = no statistical significance.

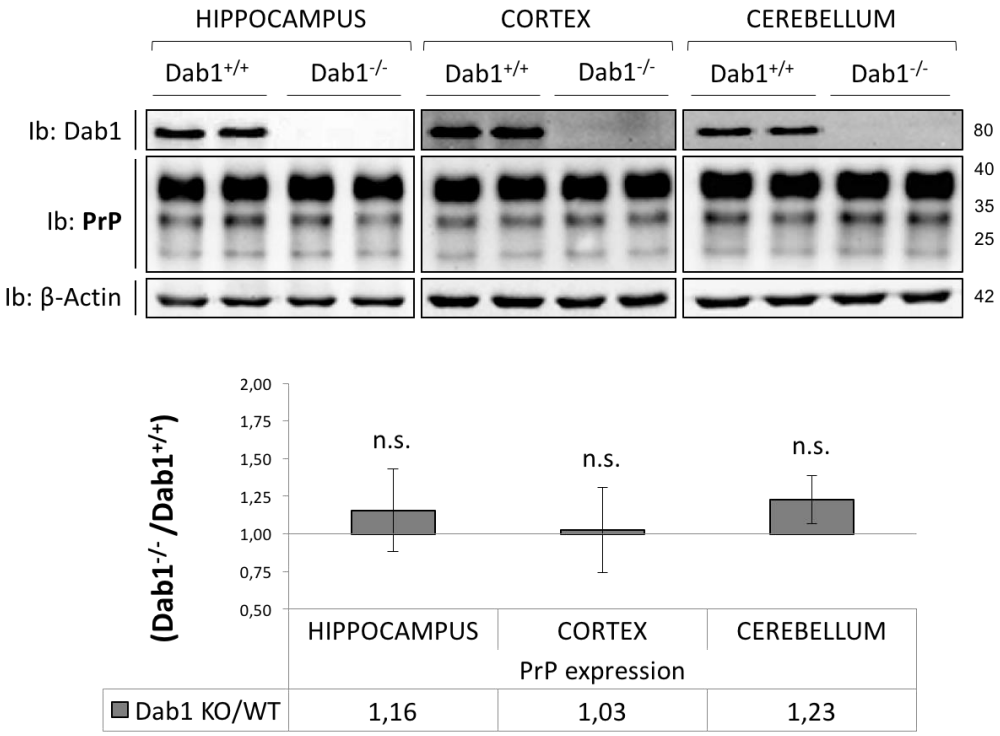

Figure 32. PrP^{C} expression in Dab1$^{-/-}$ mice. PrP^{C} expression was measured by WB experiments in hippocampus, cortex and cerebellum of P4 Dab1$^{-/-}$ mice and littermate WT controls. β-Actin was used as loading control. Sample size: n=4; one experiment. Data are shown as ratio between Dab1$^{-/-}$ and Dab1$^{+/+}$ ± standard error. Statistical significance: $p<0.05$, n.s. = no statistical significance.

ANALYSIS OF REELIN/DAB1 SIGNALLING PATHWAY IN PRION-INFECTED MICE

Interestingly, it has been reported that APP processing and β-amyloid deposition in sporadic Creutzfeldt-Jakob patients are dependent on Dab1 [185]. In light of this, we sought to investigate the effect of prion infection on the Reelin-signalling cascade, taking advantage of a mouse model of prion disease. We performed a first experiment using five CD1 mice intracerebrally inoculated with RML prion strain at the terminal stage of the disease, and five not inoculated age- and sex-matched controls. As already mentioned in the Materials and Methods section, these mice were inoculated with 20 μl of RML infected 10% brain homogenate in the striatum. In Table 7, incubation and survival times for each animal are reported (see also Figure 33).

LINEAGE	ANIMAL NUMBER	SEX	INOCULUM	INJECTION SITE	INCUBATION TIME (d.p.i.)	SURVIVAL TIME (d.p.i.)
Crl:CD1	C1	Male	RML	Striatum	118	132
Crl:CD1	C2	Male	RML	Striatum	118	139
Crl:CD1	C3	Male	RML	Striatum	121	140
Crl:CD1	C7	Male	RML	Striatum	125	153
Crl:CD1	C16	Female	RML	Striatum	135	160

Table 7. Incubation time and survival time of striatum-injected animals. 8-weeks-old CD1 mice were inoculated with RML prion strain in the striatum. Incubation time and survival time for each animal is reported (d.p.i. = days post infection).

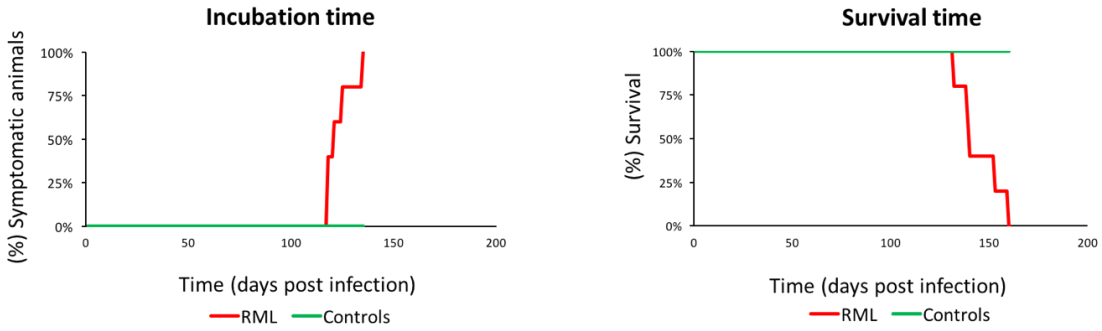

Figure 33. Incubation time and survival time of striatum-injected animals. The graphs report the incubation time (percentage of symptomatic animals in function of time, expressed as days post infection) and the survival time (percentage of alive animals in function of time, expressed as days post infection) of 8-weeks-old CD1 mice inoculated with RML prion strain in the striatum, and not-inoculated controls.

Taking advantage of Western Blot technique, we measured the expression levels of different proteins involved in the Reelin-signalling pathway in brain homogenates obtained from these samples. Each protein signal was normalized on β-Actin as reference. Data are shown as ratio between RML-infected samples and not-inoculated controls. As shown in Figure 34a, in terminal stages of prion infection, Dab1 protein signal is no longer detectable. This result was also confirmed through immunoprecipitation of Dab1 protein from prion infected samples and healthy controls (Figure 34b). Given the strong effect caused by prion infection on Dab1 protein, we evaluated the expression levels of upstream and downstream partners of Dab1 on the same samples. As already explained in details, Reelin-signalling pathway is triggered by binding of Reelin on its receptors ApoER2 and VLDLR, leading to recruitment and activation of Dab1 [117]. Indeed, in order to deeper investigate the status of the signalling cascade, we measured the expression of ApoER2 and VLDLR as upstream partners of Dab1. As observed for Dab1, ApoER2 and VLDLR proteins are no longer detectable in terminally RML infected samples (Figure 34a). Next, we analysed the expression levels of NCAM protein, which is also located at the neuronal surface, in the same samples. Total expression levels of NCAM are not affected by prion infection, but remained unchanged between the two groups of animals. Interestingly, while in the control samples both the 180 kDa and 140 kDa NCAM isoforms could be detected, enrichment in the 140 kDa, with no detectable 180 kDa isoform, could be observed in

RML-infected samples (Figure 34a). As Dab1 activation is mediated by Fyn kinase [133], which in turn is modulated by NCAM [74], we next measured Fyn expression levels in the same samples. Interestingly, Fyn kinase levels are reduced by more than 30% in RML-infected samples compared to controls (Figure 34a). Unfortunately, due to the processing without phosphatase inhibitors, it was not possible to analyse Fyn kinase activation in these samples. Upon tyrosine phosphorylation, Dab1 can transduce many downstream signals. Among them, activated Dab1 could activate PI3K, thus leading to the activation of AKT [131, 135-137]. Therefore, as a downstream partner of Dab1, we analysed AKT expression levels upon prion infection and we observed a 50% decrease in AKT expression in RML-infected samples compared to controls (Figure 34a).

As the downstream signalling cascade is triggered by Reelin, we next analysed its expression in RML-infected samples and matched controls using anti-Reelin mouse monoclonal G10 antibody, that recognizes an epitope (amino acids 164-496) located at the N-terminal region of the protein. This antibody allows the detection of the full-length Reelin and two N-terminal fragments obtained by proteolytic cleavage, N-R6 (about 300 kDa) and N-R2 (about 180 kDa) [129]. We measured the expression of Reelin considering the three molecular weight bands altogether or quantifying each band separately, performing normalization on β-Actin as reference in both cases. Notably, the overall amount of Reelin seems not modified by prion infection in comparison to control samples. However, measuring separately each detectable band of Reelin, it is possible to appreciate pronounced changes in Reelin processing between the two groups of animals. Indeed, while full-length 360 kDa protein is reduced by almost 50% in RML-infected samples compared to controls, a concomitant 2-fold increase of both cleavage products is observed (Figure 34c).

In Figure 34d, statistical analysis of these data is reported.

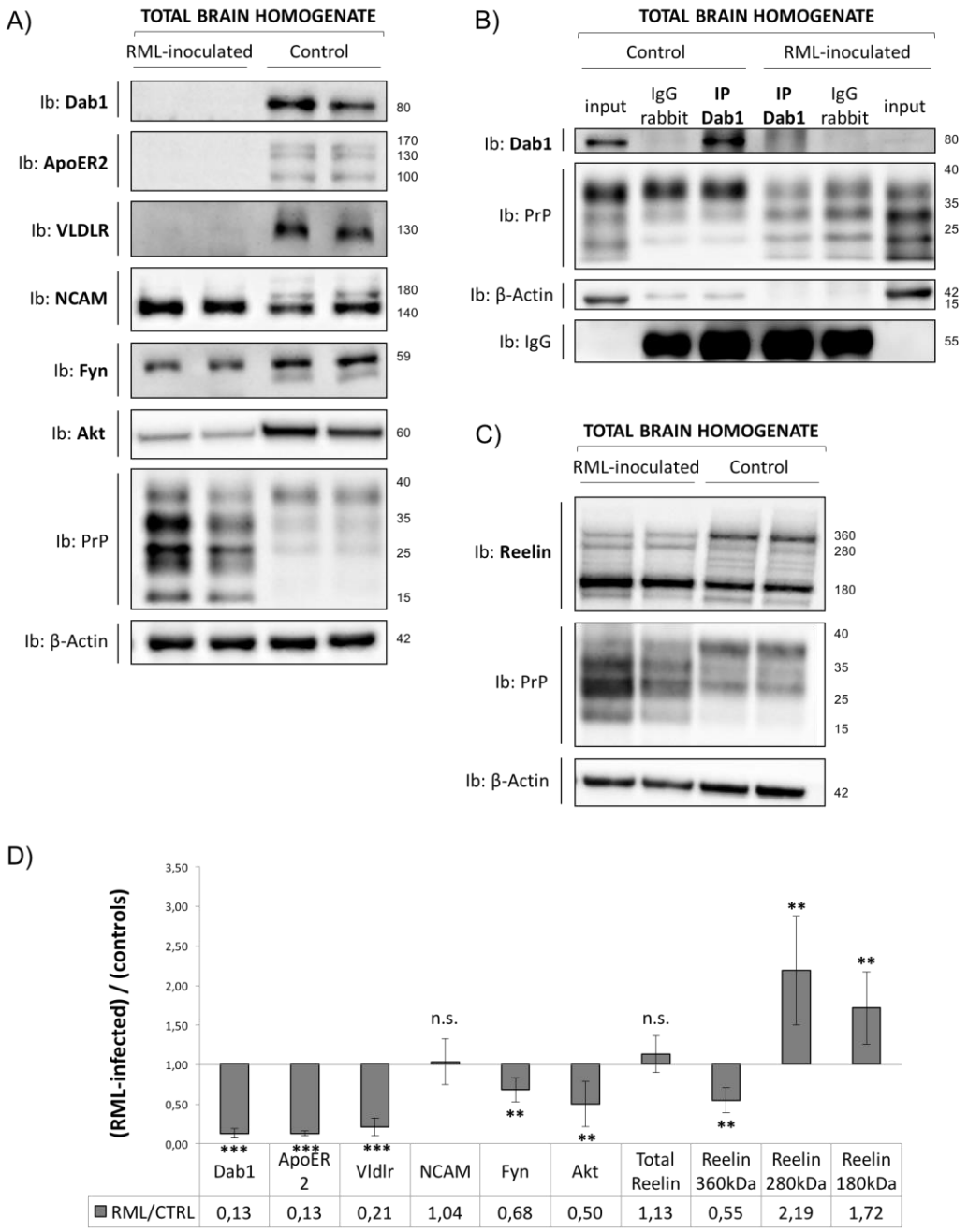

Figure 34. Expression of different component of the Reelin/Dab1 signalling pathway in terminally prion diseased striatum-injected mice. A) Total brain homogenates from terminally sick mice and age-matched controls were analysed by Western Blot for Dab1, ApoER2, VLDLR, NCAM, Fyn and AKT expression. β-Actin was used as loading control. Sample size: n=5; one experiment. B) Immunoprecipitation experiments were performed on total brain homogenates from RML-infected mice and age-matched controls to detect Dab1 protein. Sample size in each experiment: n=1; two independent experiments. C) Reelin expression was measured in total brain homogenates from terminally sick mice and age-matched controls by WB experiments. β-Actin was used as loading control. Sample size: n=5; one experiment. D) The graph reports the quantification anaysis of the experiments shown in A and C. Data are shown as ratio between RML-infected samples and controls ± standard error. *p<0.05, **p<0.01, ***p<0.001, n.s. = no statistical significance.

All these findings were obtained from mice injected with prions in the striatum. In order to assess the role of the injection site on the disruption of the Reelin signalling, we performed the same analysis on mice inoculated with RML prion strain in the hippocampus. We used four CD1 mice intracerebrally inoculated with RML prion strain at a pre-symptomatic stage of the disease, four CD1 mice intracerebrally inoculated with RML prion strain at the terminal stage of the disease, and four not inoculated age- and sex-matched controls, respectively. As already mentioned in the Materials and Methods section, these mice were inoculated with 2.5 μl of RML infected 10% brain homogenate in the hippocampus. In Table 8, survival times for each animal are reported (see also Figure 35).

LINEAGE	ANIMAL NUMBER	SEX	INOCULUM	INJECTION SITE	DISEASE STAGE	SURVIVAL TIME (d.p.i.)
Crl:CD1	1	Female	RML	Hippocampus	Presymptomatic	97
Crl:CD1	2	Female	RML	Hippocampus	Presymptomatic	97
Crl:CD1	3	Female	RML	Hippocampus	Presymptomatic	97
Crl:CD1	4	Female	RML	Hippocampus	Presymptomatic	97
Crl:CD1	5	Female	RML	Hippocampus	Presymptomatic	97
Crl:CD1	6	Female	RML	Hippocampus	Presymptomatic	97
Crl:CD1	7	Female	RML	Hippocampus	Presymptomatic	97
Crl:CD1	8	Female	RML	Hippocampus	Presymptomatic	97
Crl:CD1	9	Female	RML	Hippocampus	Terminal	134
Crl:CD1	10	Female	RML	Hippocampus	Terminal	134
Crl:CD1	11	Female	RML	Hippocampus	Terminal	134
Crl:CD1	12	Female	RML	Hippocampus	Terminal	139
Crl:CD1	13	Female	RML	Hippocampus	Terminal	145
Crl:CD1	14	Female	RML	Hippocampus	Terminal	151
Crl:CD1	15	Female	RML	Hippocampus	Terminal	147
Crl:CD1	16	Female	RML	Hippocampus	Terminal	147

Table 8. Incubation time and survival time of hippocampus-injected animals. 8-weeks-old CD1 mice were inoculated with RML prion strain in the hippocampus. Disease stage and survival time for each animal is reported (d.p.i. = days post infection). Half of the animals were sacrificed 97 d.p.i. (pre-symptomatic stage of the disease).

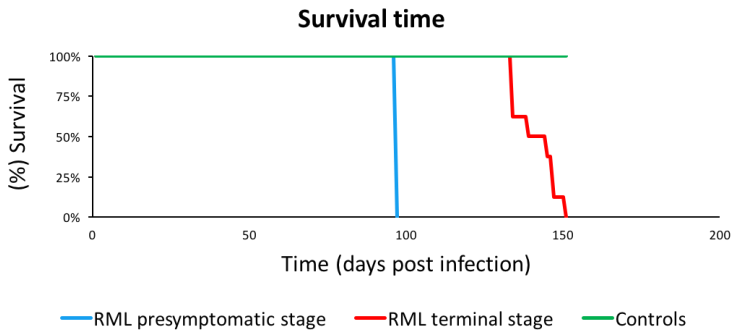

Figure 35. Survival time of hippocampus-injected animals. The graph shows the survival time (percentage of alive animals in function of time, expressed as days post infection) of 8-weeks-old CD1 mice inoculated with RML prion strain in the hippocampus, and not-inoculated controls. Half of the inoculated animals were sacrificed 97 d.p.i. (pre-symptomatic stage of the disease), and respective controls were chosen age-matched.

Given the strong effect caused by prion infection on Dab1 protein observed in striatum-injected mice, we evaluated Dab1 expression levels in brain homogenates obtained from hippocampus-injected samples, both at pre-symptomatic and terminal stage of the disease. Dab1 signal was normalized on β-Actin as reference. Data are shown as ratio between RML-infected samples and age-matched controls. As shown in Figure 36a, we were still able to observe a decrease in Dab1 protein expression in prion infected animals, both at pre-symptomatic and terminal stage of the disease. Indeed, Dab1 protein levels are reduced by 20% in RML-infected samples compared to controls, both at pre-symptomatic and terminal stage of the disease. However, Dab1 downregulation is less pronounced in hippocampus-inoculated animals than that observed in the striatum-infected ones, thus suggesting that the site of prion inoculation influences the degree of Reelin/Dab1 pathway disruption.

Next, we analysed mdab1 gene expression by Real Time PCR experiments. However, transcriptional analysis of mdab1 gene in the same samples reveals that Dab1 mRNA expression is not modified by prion infection (Figure 36b), suggesting that the alteration in Dab1 protein expression is due to post-transcriptional mechanisms, similarly to what observed in *Prnp* knockout mice.

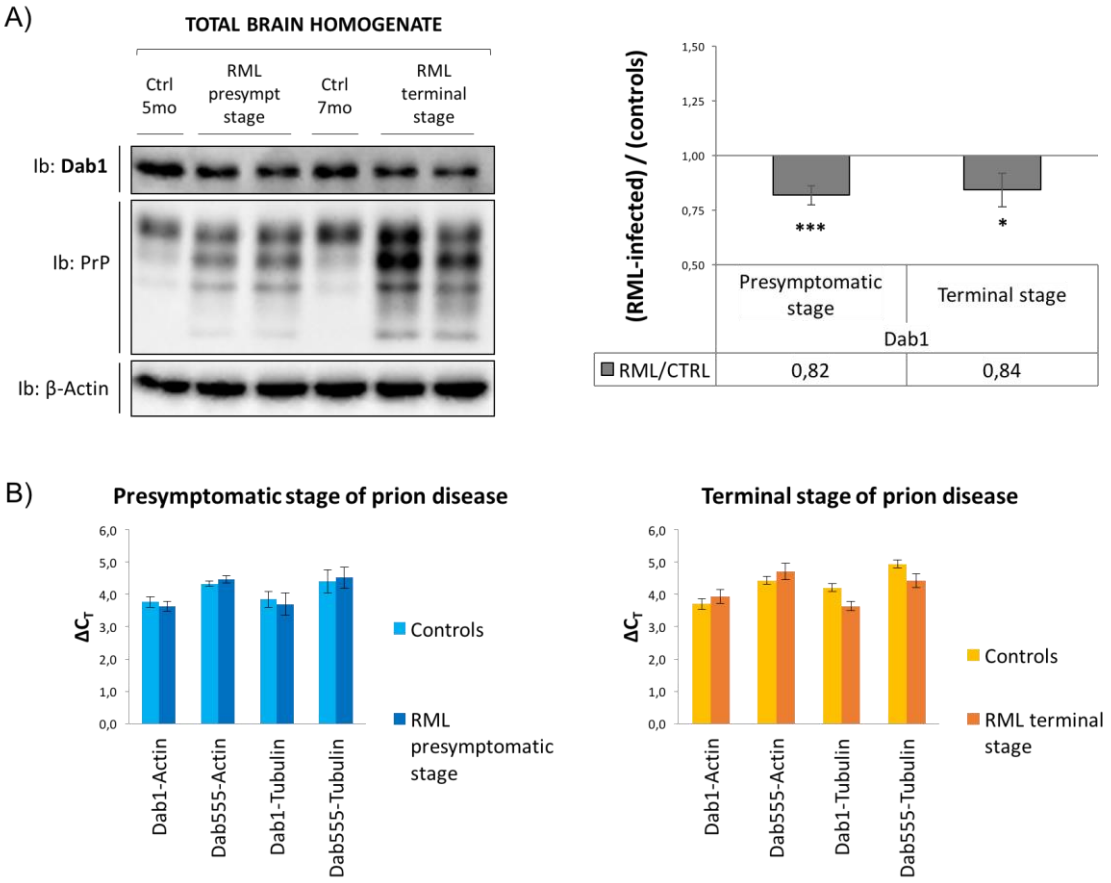

Figure 36. Dab1 expression in pre-symptomatic and terminally prion diseased hippocampus-injected mice. A) Dab1 protein expression was measured by WB experiments in total brain homogenates from RML-inoculated mice, at pre-symptomatic and terminal stage of disease, and age-matched controls. β-Actin was used as loading control. Sample size: n=4; one experiment. Data are shown as ratio between RML-infected samples and controls ± standard error. *p<0.05, **p<0.01, ***p<0.001, n.s. = no statistical significance. B) Transcriptional analysis of Dab1 mRNA was performed using two couples of primers: Dab1 recognizes all the three murine Dab1 mRNA isoforms, Dab555 recognizes the longer isoform only. β-Actin and βIII-Tubulin were used as reference genes. Relative expression of Dab1 gene versus the housekeeping gene chosen as reference was calculated using the $\Delta\Delta C_T$ method. Sample size: n=4; one experiment. Statistical significance: p<0.05.

DAB1 GENE EXPRESSION ANALYSIS IN CREUTZFELDT-JAKOB DISEASE PATIENTS

Sporadic CJD is described as a prion disease with no known cause, characterized by rapid cognitive decline, dementia and ataxia [21]. The type of PrP^{Sc} (types 1 and 2) and the genotype at codon 129 of the *PRNP* gene, the site of a methionine/valine polymorphism, are crucial determinants of the clinicopathological phenotypes of sCJD [23]. As already mentioned, despite the role of Reelin/Dab1 signalling pathway in prion diseases has not been deeply investigated, it has been reported that APP processing and β-amyloid deposition in sporadic Creutzfeldt-Jakob patients are dependent on Dab1. Interestingly, a different effect of Dab1 on Aβ deposition depending PrP^{Sc} type in human sCJD has been shown [185].

Having observed a strong impairment of the Reelin/Dab1 signalling pathway in mouse models of prion infection, and knowing that Dab1 phosphorylation plays a role in sporadic Creutzfeldt-Jakob disease, we next sought to evaluate whether Dab1 expression is affected in human sCJD patients. Indeed, we collected *postmortem* frontal cortices derived from four sCJD type 1 patients, four sCJD type 2 patients and four healthy controls. Moreover, we analysed Dab1 gene transcription in whole blood from two symptomatic sCJD patients and two healthy controls, in an attempt to identify Dab1 as a potential biomarker for prion diseases. Unfortunately, transcriptional analysis of Dab1 gene revealed that Dab1 mRNA expression is not modified by prion infection neither in brain samples (Figure 37) nor in blood (Figure 38) from sCJD affected patients. In line with these results, we alrealdy observed in both *Prnp* knockout and prion infected mouse samples that the alterations in Dab1 expression are present at the protein level, while Dab1 gene expression is unchanged, thus suggesting that PrP^{C} absence or misfolding affect Dab1 homeostasis at post-transcriptional level. Indeed, to unravel the involvement of Dab1 in human prion diseases, it would be interesting to analyse Dab1 protein expression in human samples.

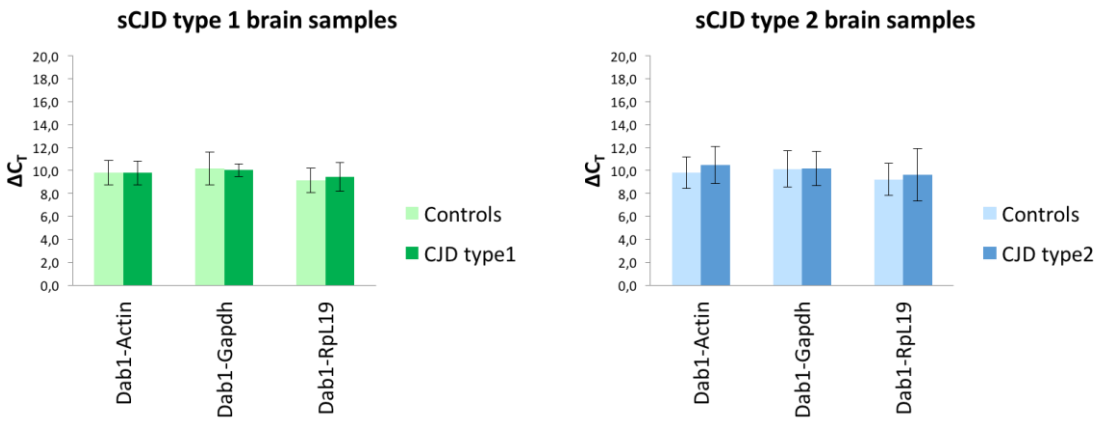

Figure 37. Dab1 gene expression in *postmortem* human sCJD brain samples. Transcriptional analysis of Dab1 mRNA was performed using human Dab1 specific primer couple. β-Actin, GAPDH and RpL19 were used as reference genes. Relative expression of Dab1 gene versus the housekeeping gene chosen as reference was calculated using the $\Delta\Delta C_T$ method. Statistical significance: $p<0.05$. Sample size: n=4 each group.

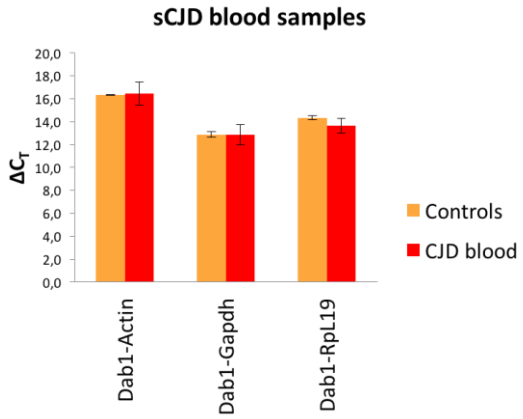

Figure 38. Dab1 gene expression in human sCJD blood samples. Transcriptional analysis of Dab1 mRNA was performed using human Dab1 specific primer couple. β-Actin, GAPDH and RpL19 were used as reference genes. Relative expression of Dab1 gene versus the housekeeping gene chosen as reference was calculated using the $\Delta\Delta C_T$ method. Statistical significance: $p<0.05$. Sample size: n=2 each group.

DISCUSSION

The cellular form of the prion protein (PrP^C), which is encoded by the endogenous gene *Prnp*, has been deeply investigated since its misfolded isoform, PrP^{Sc}, enriched in β-sheets and with the tendency to form aggregates, is the causative agent of prion diseases [2, 37]. Prion diseases, also known as transmissible spongiform encephalophaties, are a group of rare and fatal neurodegenerative disorders, characterized by sporadic, genetic or infectious etiology, that may affect both animals and humans [2, 3, 21]. The pathogenesis of prion diseases is still under debate, as they could be gain of toxic function consequences of the formation of PrP^{Sc}, or could be due to the loss of the normal physiological function of PrP^C [4]. According to the gain of toxic function hypothesis, the prion pathology is attributable to novel toxic properties acquired by PrP^{Sc} [14, 15, 38]. Arguing against a direct neurotoxic effect of the misfolded protein, PrP^{Sc} alone is not sufficient to induce prion disease [16-18]. Therefore, it has been proposed that PrP^C protective activity may be lost upon conversion to PrP^{Sc} [38]. However, genetic ablation of *Prnp* expression results in only subtle phenotypic effects and does not induce neurodegeneration by itself [19, 20]. Indeed, multiple mechanisms may contribute to the pathology of prion diseases, leading to progressive neurodegeneration. In light of this, a better definition of the exact physiological function of PrP^C represents a critical challenge of the prion field, that may help to better understand pathogenetic mechanisms underlying neurodegeneration, as well as to propose new therapeutic strategies.

PrP^C is an endogenous glycoprotein, mainly exposed to the outer layer of the cell surface as N-glycosylated GPI-anchored protein [31, 32]. Although PrP^C is abundantly expressed in the developing and mature nervous system [38, 45], it is also expressed in many non-neuronal tissues, such as blood lymphocytes, gastro-epithelial cells, heart, kidney and muscles, suggesting the involvement of this protein in various physiological processes [39, 40]. The high conservation of PrP^C among mammalian species suggests that it may retain critical physiological roles [22]. Despite many efforts have been done in the past years and several PrP^C-deficient mouse models have been generated, PrP^C

physiological function has not been completely characterized. Indeed, *Prnp* knockout models lack striking phenotypes, thus hindering a conclusive definition of the physiological functions of PrP^C [19, 52]. However, it has been suggested that, in the nervous system, PrP^C plays a role in modulating sleep-wake cycles, hippocampal-dependent spatial learning and memory formation. At the cellular level, PrP^C modulates neurite outgrowth, neuronal excitability and survival, synaptic activity and myelin maintenance [21].

Of great interest for the present work, PrP^C also plays a fundamental role in modulating cell signalling, acting as a dynamic scaffold for the assembly of many different signalling molecules at the neuronal surface [38, 68, 69]. Indeed, it has been shown that PrP^C directly interacts with NCAM at the neuronal surface, promoting NCAM recruiment to lipid rafts and regulating Fyn kinase activity and neurite outgrowth [72, 74]. Moreover, PrP^C could also affect PI3K and Akt/PKB activity [100, 103]. Indeed, it was shown that the recruitment of PI3K by PrP^C promotes cell survival and, interestingly, PI3K activity was found to be reduced in PrP-null mouse brain compared to wild-type animals [100]. These findings, together with reduced phosphorylation of AKT in Prnp knockout mice, suggest that PrP^C may exert a neuroprotective function, and its absence may increase susceptibility to neuronal injuries [103]. Finally, more recently, it has also been shown that PrP^C promotes GSK3β inactivation in a caveolin/Lyn-dependent fashion [95]. All these intracellular kinases could be also regulated by an extracellular matrix glycoprotein, named Reelin, that activates a linear downstream signalling pathway. As previously described, Reelin-signalling pathway is triggered by binding of Reelin on two transmembrane lipoprotein receptors, ApoER2 and VLDLR, that promotes the clustering of receptors on the plasma membrane and the recruitment of the intracellular adaptor protein Dab1. Upon Fyn-mediated tyrosine phosphorylation, Dab1 is activated and can transduce various downstream signals [117].

Interestingly, it has been reported that Reelin-signalling pathway is involved in both Alzheimer's and prion diseases. Indeed, the intracellular adaptor protein Dab1 is able to affect APP processing and intracellular trafficking, increasing its α-cleavage and decreasing Aβ production [182]. Moreover, Dab1 has been shown to influence amyloid beta deposition in sporadic Creutzfeldt–Jakob disease [185].

In light of these considerations, this project was aimed to deeper investigate the functional interaction between the prion protein and the Reelin/Dab1 signalling cascade from a physiological and a pathological point of view.

In the first part of this work, we investigated the role of PrP^C in regulating Reelin/Dab1 signalling taking advantage of *Prnp*$^{0/0}$ mice and *Prnp*$^{+/+}$ littermate controls. Knowing that the expression of both PrP^C and Reelin throughout the nervous system is developmentally regulated, we decided to carry out the experiments concerning brain samples on early postnatal days animals. Indeed, PrP^C and Reelin share a similar distribution in mammalian brain, being expressed since early stages of brain development in cortical and hippocampal structures [45, 158]. PrP^C expression increases markedly during brain development, starting from the embryogenesis and reaching a peak at the end of the synaptogenesis [44]. Reelin is highly expressed by Cajal-Retzius neurons during embryogenesis, but its expression is maintained also postnatally [117, 158]. Indeed, Reelin is still highly expressed in many cells of the cortex and the hippocampus during early postnatal stages [158].

Considering that the intracellular adaptor Dab1 represents the key point of Reelin downstream signal transduction [117], we initially focused our attention on this protein. Indeed, we measured Dab1 expression levels in *Prnp* knockout mouse brains. Our data revealed that Dab1 is strongly upregulated in PrP^C-null mice, with an increase of about 40% in comparison to wild-type littermates controls. Conversely, transcriptional analysis of mdab1 showed that Dab1 gene expression is not influenced by the absence of *Prnp*, suggesting that PrP^C absence may affect Dab1 homeostasis at post-transcriptional level, influencing its syntesis or stability. It is interesting to note that Reelin pathway, as the majority of signalling cascade, displays a negative feedback mechanism by which the signal is switched off. For what concern Reelin cascade, this desensitization mechanism is based on Dab1 downregulation, which in turn is mediated by its poly-ubiquitination and targeting to the proteasome [148]. Indeed, it has been shown that disruption of the Reelin-signalling cascade (by genetic ablation of Reelin, VLDLR, ApoER2, or Fyn and Src) leads to the accumulation of Dab1 protein *in vivo*, while Dab1 mRNA expression remains unchanged [132, 133, 142-145]. Of note, in

our *Prnp* knockout mice we observed the same situation, characterized by Dab1 protein accumulation with no changes in its gene transcription. As *Prnp* ablation induces the same effect of Reelin signalling disruption, we can thus hypothesize that PrP^C may influence Dab1 protein expression by modulating the upstream signalling pathway. Therefore, we decided to evaluate the possible alterations in the expression and activation status of Reelin pathway signalling components that may be responsible for Dab1 upregulation in $Prnp^{0/0}$ mice. Differently from our expectations, our data clearly showed that the expression of Reelin, Reelin receptors ApoER2 and VLDLR, as well as Fyn kinase, is not altered by the absence of PrP^C. However, the activation of Fyn kinase is impaired in $Prnp^{0/0}$ mice, in agreement with previously reported evidences [74]. Fyn kinase recruitment is induced upon Reelin binding to its receptors, leading to Dab1 phosphorylation on tyrosine residues [133]. It is known from the literature that Dab1 poly-ubiquitination and subsequent degradation is dependent on its phosphorylation, thus the protein tends to accumulate when its phosphorylation is impaired [146, 147]. The observation that Fyn kinase activation is impaired in *Prnp* knockout mice, together with Dab1 accumulation, is in line with literature and suggests that PrP^C plays a role in modulating Reelin-signalling pathway. In order to figure out whether PrP^C may directly influence the signalling cascade by interacting with Reelin or its receptors, we performed some co-immunoprecipitation experiments. Interestingly, both PrP^C and ApoER2 are preferentially located in lipid raft microdomains of the plasma membrane [38, 201]. However, we were not able to co-immunoprecipitate PrP^C with neither Reelin nor ApoER2, ruling out the hypothesis of a direct interaction between these proteins.

Knowing that the activation of Fyn kinase is impaired in $Prnp^{0/0}$ mice and that Dab1 protein is upregulated when its phosphorylation is impaired [146, 147], we next sought to investigate Dab1 phosphorylation state in $Prnp^{0/0}$ mice in comparison to $Prnp^{+/+}$ controls. However, due to upregulation of Dab1 in PrP^C-null mice and high variability among samples, we were not able to obtain convincing results regarding Dab1 phosphorylation in brain samples. Therefore, we decided to take advantage of an *ex vivo* model based on cultured primary cortical neurons, that are commonly used in literature to study Reelin-signalling pathway, as treatment with Reelin-conditioned supernatant leads to the activation of the downstream signalling cascade [133]. In

agreement with previous works reported in literature [133], Reelin treatment is able to trigger a massive Dab1 phosphorylation in *Prnp*$^{+/+}$ neurons. Conversely, Dab1 phosphorylation resulted strongly impaired in *Prnp*$^{0/0}$ neurons, that appeared less responsive to Reelin stimulation than the wild-type. As already observed in brain samples, the impairment in Dab1 response is not due to alterations in the expression of Reelin or Reelin receptors, that is not modified by *Prnp* ablation in neurons under basal conditions. However, in line with our previous results on brains, Fyn kinase phosphorylation, even without statistical significance, showed a decreasing trend in *Prnp*$^{0/0}$ neurons compared to WT controls. Indeed, we hypothesized that PrP^{C} may indirectly influence Reelin-signalling pathway, and therefore Dab1 expression and phosphorylation, by modulating Fyn kinase activity, possibly through interaction with NCAM. Indeed, it is well known that PrP^{C} directly interacts with NCAM, modulating Fyn kinase activity [72, 74]. In agreement with this hypothesis, we observed a 15% reduction in NCAM expression in *Prnp*$^{0/0}$ neurons in comparison to WT controls.

Data obtained from cortical neurons stimulated with Reelin suggest that PrP^{C} plays a role in modulating Reelin-signalling pathway, as PrP^{C} absence leads to impaired Dab1 response. As recombinant PrP added to the culture medium is able to regulate neurite outgrowth and to regulate Fyn activation by *in trans* interaction with NCAM [74, 91], we next sought to investigate whether PrP^{C} is able to activate Reelin downstream signalling cascade, and therefore to promote Fyn activation and Dab1 phosphorylation, by itself. However, in our experimental system, neither recombinant full-length mouse PrP nor mouse PrP-hFc fusion protein was able to induce Fyn and Dab1 activation. We adjusted the published protocol to our experimental setup that however differs from those used in the literature. Indeed, PrP-hFc-mediated Fyn activation was previously shown on CHO cells [74], while the modulation of neurite outgrowth induced by recombinant PrP was proven on rat embryonic hippocampal neurons [91]. Likely, we still need to better adapt these protocols to our murine embryonic cortical neurons in order to induce the activation of Fyn and to understand whether PrP^{C} may subsequently induce Dab1 phosphorylation by itself.

Taken together, all these findings suggest that PrP^{C} may influence Reelin cascade, promoting the downstream signal transduction, likely modulating Dab1 function through NCAM/Fyn pathway. Indeed, *Prnp* ablation leads to reduced NCAM

expression, impaired Fyn activation and, ultimately, impaired Dab1 activation and downregulation. Dab1 should be downregulated in neurons to properly terminate their migration and to allow the formation of organized layered structures. Indeed, a precise regulation of Dab1 levels is required to control the precise location of the migration arrest. Impairment of Dab1 downregulation is thus predicted to cause strong cortical developmental defects [202]. Indeed, even though neuronal migration defects are not yet reported as a phenotype of *Prnp* knockout mice, it would be interesting to perform immunohystochemical analysis to evaluate the presence of subtle differences in cortical migration pattern.

In the second part of the project we addressed the opposite question to understand whether alteration of the Reelin-signalling pathway could affect the expression of PrP^C. Indeed, we took advantage of different mouse models of Reelin pathway disruption. Among them, the spontaneously arising mutant *reeler* mouse, in which Reelin expression is completely abolished, presents behavioural abnormalities, such as ataxia, tremors and reeling gaits [150], due to cerebellar malformation and disrupted laminar organization of cortical layers [152]. Moreover, ApoER2 and VLDLR knockout mice, together with ApoER2/VLDLR double knockout mice were analysed. As already mentioned, while the loss of ApoER2 or VLDLR alone causes only subtle phenotypes, the ablation of both receptors causes the *reeler* phenotype [144]. Finally, as we observed that PrP^C absence determines a significative alteration in Dab1 expression, we measured the expression of PrP^C in Dab1 knockout mice, characterized by a *reeler* phenotype [157], to evaluate whether a reverse regulatory mechanism between these two proteins also exists in the mouse brain. We decided to carry out this analysis on early postnatal days animals, applying the same conditions used for the experiments concerning *Prnp* knockout brain samples. Considering the physiological distribution of Reelin during the postnatal period [117], we decided to analyse three brain regions: cortex, hippocampus and cerebellum. However, PrP^C expression levels did not resulted significantly different in none of the genotypes analysed in comparison to their respective controls. These findings suggest that, while PrP^C is able to modulate Reelin-signalling cascade and in particular Dab1 activation state, disruption of this pathway seems not able to affect PrP^C expression. However, we need to take into account that,

due to fertility problems and reduced natality of homozygous mutant mice, we were able to collect very few samples for each genotype. Therefore, more samples need to be collected and analysed to confirm these data.

Finally, in the last part of the project we investigated the functional interaction between the prion protein and the Reelin/Dab1 signalling cascade from a pathological point of view. Indeed, as already mentioned, the role of the Reelin/Dab1 signalling cascade in prion diseases has not been deeply investigated. In order to unravel the effect of prion infection on this signalling cascade, RML-inoculated mice were used as prion pathology model. Conversely to the Dab1 upregulation observed in *Prnp* knockout mice, prion-infected animals display a complete abolishment of Dab1 protein expression, together with the loss of both Reelin receptors. Disruption of the Reelin-signalling cascade may leads to impaired synaptic function and cytoskeleton dinamics, likely contributing to neurodegeneration. Interestingly, the site of prion inoculation seems to influence the degree of Reelin/Dab1 pathway disruption. Indeed, less pronounced Dab1 downregulation could be observed in hippocampus-inoculated animals compared to the striatum-infected ones. However, comparable survival time of the two groups of animals suggests that the different effect on Dab1 expression is not due to lower levels of infectivity, thus we may hypothesize that it could be due to a differential spread of prions throughout brain regions. Interestingly, reduced Dab1 expression is already pronounced in the pre-symptomatic stage of the infection, thus suggesting that Reelin pathway disruption is an early event of prion diseases. Similarly to what already observed in *Prnp* knockout mice, the impairment in Dab1 protein expression during prion infection does not correlate with an alteration in its gene transcription, suggesting that PrP^{C} misfolding, as PrP^{C} absence, affects Dab1 homeostasis at post-transcriptional level.

Interestingly for the present work, it is known from the literature that Dab1 is involved in APP processing and β-amyloid deposition in sporadic Creutzfeldt-Jakob patients [185]. Having observed a strong impairment of the Reelin/Dab1 signalling pathway in mouse models of prion infection, we next evaluated whether Dab1 expression is affected in human sCJD patients. As the effect of Dab1 on β-amyloid deposition in sCJD is dependent on PrP^{Sc} type [185], *postmortem* frontal cortices from sCJD type 1

patients and sCJD type 2 patients, together with whole blood samples from symptomatic sCJD patients, were analysed. As shown, transcriptional analysis of Dab1 gene revealed that its expression is not modified by prion infection neither in brain samples nor in blood from sCJD affected patients, thus confirming the results obtained in prion infected mouse models. Indeed, to better understand the involvement of Dab1 in human prion diseases, it would be interesting to analyse Dab1 protein expression in human samples.

As downstream signalling cascade is triggered by Reelin, we sought to evaluate whether its expression is also impaired by prion infection. As already mentioned, upon secretion, Reelin is processed by cleavage in two sites located, respectively, between repeats 2 and 3 and between repeats 6 and 7. As a result, Reelin is cleaved into five fragments that could be discriminated on molecular weight basis [126, 129]. Commonly used N-terminal antibodies allow detecting the full-length Reelin and two smaller fragments, named N-R6 (about 300 kDa) and N-R2 (about 180 kDa). Indeed, we decided to measure the expression of Reelin in prion-infected mice considering the three molecular weight bands altogether or quantifying each band separately. Notably, the overall amount of Reelin is not modified by prion infection in comparison to control samples, while pronounced changes in Reelin processing could be observed. Indeed, while full-length 360 kDa protein is reduced by almost 50% in prion-inoculated animals compared to controls, a concomitant 2-fold increase of both cleavage products is observed. Interestingly, despite the physiological function of the cleavage is not fully understood, Reelin processing is thought to play an important role in Alzheimer's disease, as dysfunction of Reelin proteolysis in post-mortem AD tissues has been reported [179]. Indeed, increased levels of N-R2 fragment have been observed in AD and frontotemporal dementia patients [180, 181]. Our findings suggest that Reelin processing may also play a role in prion diseases, thus supporting the hypothesis that Reelin-signalling pathway is involved in the pathogenesis of several of neurodegenerative diseases. Recently, three enzymes involved in Reelin processing have been identified: the serine protease tissue plasminogen activator (tPA), the extracellular matrix metalloproteinase ADAMTS-4 and the disintegrin and metalloproteinase ADAMTS-5 [127]. Interestingly, PrP^{Sc} is specifically recognized by the serine protease zymogen plasminogen [203], and recombinant PrP is able to stimulate

the activity of tPA in a copper-dependent manner, thus suggesting that tPA-catalyzed plasminogen activation may play a role in the pathogenesis of the disease [204]. Moreover, both tPA activity and tPA gene expression were found elevated in TSE-infected brains as compared to healthy controls. Together with the observation that the survival time of plasminogen-deficient and tPA-deficient prion-infected mice is reduced compared to wild-type animals, these findings suggest that enhanced tPA activity observed in prion infected brains may reflect a neuroprotective response [205]. Indeed, we may speculate that increased activity of tPA promotes increased Reelin processing, that in turn may play a role in the pathogenesis of the disease. However, more experiments are needed in order to understand whether increased Reelin cleavage has a neuroprotective role during prion diseases or is a secondary effect of prion infection. Alternatively, it could be the result of a compensatory mechanism due to downstream signalling disruption.

Interestingly, total expression levels of NCAM are not affected by prion infection, but, while in the control samples both the 180 kDa and 140 kDa NCAM isoforms could be detected, enrichment in the 140 kDa, with no detectable 180 kDa isoform, could be observed in prion-infected mice. NCAM is a cell adhesion macromolecule that exists in three major alternatively spliced isoforms ($NCAM^{180kDa}$, $NCAM^{140kDa}$, and $NCAM^{120kDa}$), that have different molecular weight, distribution, and function [206, 207]. Indeed, distinct roles in synaptic maturation for different NCAM isoforms have been proposed [208]. Differential expression of NCAM isoforms has been associated to several pathological states, such as tumors [209, 210]. Moreover, overexpression of $NCAM^{140kDa}$ isoform, with no changes in $NCAM^{120kDa}$ and $NCAM^{180kDa}$ isoforms has been observed in renal fibrosis [211]. Finally, upregulation of $NCAM^{140kDa}$ isoform correlates with increased apoptosis of cardiomyocites in ischemic cardiomiopathy, thus having a role in the pathogenesis of the disease [212]. Interestingly, we observed an increase in the $NCAM^{140kDa}$ isoform in prion-infected animals compared to controls. Even though *in vivo* experiments on $NCAM^{-/-}$ knockout animals failed to show differences in incubation time and PrP^{Sc} deposition compared to wild-type animals [72], it would be interesting to deeper investigate whether differential expression of NCAM isoforms plays a role in the pathogenesis of the disease.

As Dab1 activation is mediated by Fyn kinase [133], which in turn could be modulated by PrP^{C} through NCAM [74], we decided to evaluate the effect of prion infection on Fyn expression. Interestingly, we observed a significative reduction in Fyn expression levels in prion-inoculated animals. However, Fyn deficiency does not affect PrP^{Sc} accumulation or the clinical symptoms in mouse models of prion disease, but only moderately shortens the survival time, thus suggesting an involvement of Fyn kinase in mediating neuroprotective functions [92]. Indeed, the impairment in Fyn kinase expression observed in our prion mouse model may result in impaired neuroprotection and may contribute to neuronal loss. Unfortunately, it was not possible to analyse Fyn kinase activation in these samples, while increased levels of phosphorylated Fyn were previously reported both in chronically prion-infected cell lines and in animal models of prion disease [93, 94]. In Alzheimer's disease, it has been shown that increased Fyn kinase activity correlates with altered tyrosine phosphorylation of the NR2B subunit of NMDAR, that in turn modulates its gating properties, leading to abnormal synaptic function and neuronal loss [213]. As increased Fyn kinase activity may contribute to synaptic and neuronal loss also in prion diseases [94], experiments aimed to evaluate Fyn activation in our mouse models of prion infection are ongoing.

CONCLUSIONS AND PERSPECTIVES

In this project, the role of PrP^{C} in Reelin-signalling pathway modulation was investigated, taking advantage of *Prnp*$^{+/+}$ and *Prnp*$^{0/0}$ mice. Expression of different components of the cascade was evaluated in early postnatal stages of brain development, focusing our attention especially on Dab1 protein and gene expression. Furthermore, the activation status of the signalling pathway was investigated in primary cortical neurons upon Reelin stimulus. Moreover, different mouse models of Reelin-signalling disruption were analyzed for PrP^{C} expression. In the last part of the project, the role of Reelin-signalling cascade in mouse models of prion disease and human sCJD patients was investigated.

As already discussed, in PrP^{C} loss-of-function mouse models we observed Dab1 protein upregulation together with impairment of Fyn kinase activation. Moreover, in *Prnp* null cortical neurons, reduced NCAM expression, reduced Fyn activation and impairment in Dab1 activation were detected. Thus, we may propose a model in which, physiologically, PrP^{C} modulates the Reelin-signalling pathway indirectly, not physically interacting with Reelin or Reelin receptors, but, more likely, through the interaction with NCAM and the regulation of Fyn kinase activity, finally influencing Dab1 phosphorylation and downstream signal transduction.

On the other side, pathological misfolding of PrP^{C} to PrP^{Sc} was also shown to play a strong effect on the Reelin/Dab1 signalling cascade. Complete disruption of the pathway, with ApoER2, VLDLR and Dab1 ablation, together with altered Reelin processing, was observed in mouse models of prion disease. Indeed, PrP^{C} misfolding seems to play a different role on the Reelin-signalling cascade in comparison to PrP^{C} ablation. Therefore, we may speculate that the effects observed in prion infected mouse models are not due to the loss-of-physiological-function of PrP^{C} but, more likely, PrP^{Sc} acquires a different pathological function.

Taken together, these findings suggest that, physiologically, PrP^{C} influences Reelin cascade, promoting the downstream signal transduction and modulating Dab1 function through NCAM/Fyn pathway. Pathologically, PrP^{Sc} leads to complete Dab1 signalling disruption, likely contributing to neurodegeneration. Therefore, we shown functional interaction between the prion protein and the Reelin/Dab1 signalling cascade under physiological and pathological conditions.

ACKNOWLEDGEMENTS

Coming to the end of these four years, I would like to thank Professor Giuseppe Legname for giving me the possibility to work in his laboratory and to carry out a very challenging and stimulating research project. During these years I had the possibility to attend conferences and workshops, and I really appreciated this chance.

I would like to thank Professor Carsten Korth and Professor Hans Bock for hosting me in their laboratories to carry out a part of this project. I'm really grateful for the time they dedicated to me and for the very useful discussions that we had when I was in Düsseldorf. I also was to thank all their lab members, and especially Dr. Nicholas Bradshaw and Dr. Friederike Kipkeew for their precious help.

I would also like to thank our collaborators from Milan, Professor Fabrizio Tagliavini and Dr. Fabio Moda, for providing us prion-infected mouse samples.

I would like to thank all the past and present members of the Prion Biology Lab, and in particular my first mentors Gabriele and Lisa. I also want to thank Silvia for the human CJD samples, Hoa for the recombinant PrP and Tihana for the PrP-Fc protein. A special thank is for Elisa, who shared with me not only the lab bench but was always present to discuss my doubts and my data. I would also like to thank my friend Lara, who shared with me these four years, I'm really happy we went through this adventure together.

I'm really grateful to all the SISSA Staff, and especially to Beatrice, who helped me with the primary cultures. Thank you so much not only for your technical help, but also for the nice time we spend together while preparing the cultures.

I also want to say a great thank you to all the members of the Common Molecular Laboratory and especially to Roberta, for her great help and for the useful discussions we had.

I would like to thank all my friends outside SISSA, the ones you could always count to, even though you are completely absorbed by your work and you don't have much time to spend with. Thank you Alessandro, Riccardo, Cristiano, Chiara and Arianna for the great moments we had during these years.

A great thank you is for my parents Marcella and Ivan and my sister Anna, thank you for supporting me during these four years every time I needed, thank you for being always present.

The biggest thank you is for my husband Antonio, thank you for loving me as much as you can. I know you are always here for me and you greatly supported me during these years, thank you for sharing every moment with me.

BIBLIOGRAPHY

1. Jellinger, K.A., *Basic mechanisms of neurodegeneration: a critical update.* J Cell Mol Med, 2010. **14**(3): p. 457-87.
2. Prusiner, S.B., *Shattuck lecture--neurodegenerative diseases and prions.* N Engl J Med, 2001. **344**(20): p. 1516-26.
3. Aguzzi, A., M. Heikenwalder, and G. Miele, *Progress and problems in the biology, diagnostics, and therapeutics of prion diseases.* J Clin Invest, 2004. **114**(2): p. 153-60.
4. Soto, C. and N. Satani, *The intricate mechanisms of neurodegeneration in prion diseases.* Trends Mol Med, 2011. **17**(1): p. 14-24.
5. Prusiner, S.B., *Novel proteinaceous infectious particles cause scrapie.* Science, 1982. **216**(4542): p. 136-44.
6. Alper, T., et al., *Does the agent of scrapie replicate without nucleic acid?* Nature, 1967. **214**(5090): p. 764-6.
7. Prusiner, S.B., et al., *Purification and structural studies of a major scrapie prion protein.* Cell, 1984. **38**(1): p. 127-34.
8. Oesch, B., et al., *A cellular gene encodes scrapie PrP 27-30 protein.* Cell, 1985. **40**(4): p. 735-46.
9. Basler, K., et al., *Scrapie and cellular PrP isoforms are encoded by the same chromosomal gene.* Cell, 1986. **46**(3): p. 417-28.
10. Prusiner, S.B., *Molecular structure, biology, and genetics of prions.* Adv Virus Res, 1988. **35**: p. 83-136.
11. Pan, K.M., et al., *Conversion of alpha-helices into beta-sheets features in the formation of the scrapie prion proteins.* Proc Natl Acad Sci U S A, 1993. **90**(23): p. 10962-6.
12. Cohen, F.E., et al., *Structural clues to prion replication.* Science, 1994. **264**(5158): p. 530-1.
13. Aguzzi, A., F. Montrasio, and P.S. Kaeser, *Prions: health scare and biological challenge.* Nat Rev Mol Cell Biol, 2001. **2**(2): p. 118-26.

14. Hetz, C., et al., *Caspase-12 and endoplasmic reticulum stress mediate neurotoxicity of pathological prion protein.* EMBO J, 2003. **22**(20): p. 5435-45.
15. Simoneau, S., et al., *In vitro and in vivo neurotoxicity of prion protein oligomers.* PLoS Pathog, 2007. **3**(8): p. e125.
16. Bueler, H., et al., *Mice devoid of PrP are resistant to scrapie.* Cell, 1993. **73**(7): p. 1339-47.
17. Brandner, S., et al., *Normal host prion protein necessary for scrapie-induced neurotoxicity.* Nature, 1996. **379**(6563): p. 339-43.
18. Mallucci, G., et al., *Depleting neuronal PrP in prion infection prevents disease and reverses spongiosis.* Science, 2003. **302**(5646): p. 871-4.
19. Bueler, H., et al., *Normal development and behaviour of mice lacking the neuronal cell-surface PrP protein.* Nature, 1992. **356**(6370): p. 577-82.
20. Mallucci, G.R., et al., *Post-natal knockout of prion protein alters hippocampal CA1 properties, but does not result in neurodegeneration.* EMBO J, 2002. **21**(3): p. 202-10.
21. Aguzzi, A., F. Baumann, and J. Bremer, *The prion's elusive reason for being.* Annu Rev Neurosci, 2008. **31**: p. 439-77.
22. Colby, D.W. and S.B. Prusiner, *Prions.* Cold Spring Harb Perspect Biol, 2011. **3**(1): p. a006833.
23. Parchi, P., et al., *Molecular basis of phenotypic variability in sporadic Creutzfeldt-Jakob disease.* Ann Neurol, 1996. **39**(6): p. 767-78.
24. Kobayashi, A., et al., *Type 1 and type 2 human PrPSc have different aggregation sizes in methionine homozygotes with sporadic, iatrogenic and variant Creutzfeldt-Jakob disease.* J Gen Virol, 2005. **86**(Pt 1): p. 237-40.
25. Hsiao, K., et al., *Linkage of a prion protein missense variant to Gerstmann-Straussler syndrome.* Nature, 1989. **338**(6213): p. 342-5.
26. Westaway, D., et al., *Structure and polymorphism of the mouse prion protein gene.* Proc Natl Acad Sci U S A, 1994. **91**(14): p. 6418-22.
27. Saeki, K., et al., *Three-exon structure of the gene encoding the rat prion protein and its expression in tissues.* Virus Genes, 1996. **12**(1): p. 15-20.
28. Horiuchi, M., et al., *Genomic structure of the bovine PrP gene and complete nucleotide sequence of bovine PrP cDNA.* Anim Genet, 1998. **29**(1): p. 37-40.

29. Puckett, C., et al., *Genomic structure of the human prion protein gene.* Am J Hum Genet, 1991. **49**(2): p. 320-9.

30. Manson, J.C. and N.L. Tuzi, *Transgenic models of the transmissible spongiform encephalopathies.* Expert Rev Mol Med, 2001. **2001**: p. 1-15.

31. Stahl, N., et al., *Scrapie prion protein contains a phosphatidylinositol glycolipid.* Cell, 1987. **51**(2): p. 229-40.

32. Stahl, N., D.R. Borchelt, and S.B. Prusiner, *Differential release of cellular and scrapie prion proteins from cellular membranes by phosphatidylinositol-specific phospholipase C.* Biochemistry, 1990. **29**(22): p. 5405-12.

33. Caughey, B. and G.S. Baron, *Prions and their partners in crime.* Nature, 2006. **443**(7113): p. 803-10.

34. Zahn, R., et al., *NMR solution structure of the human prion protein.* Proc Natl Acad Sci U S A, 2000. **97**(1): p. 145-50.

35. Viles, J.H., et al., *Copper binding to the prion protein: structural implications of four identical cooperative binding sites.* Proc Natl Acad Sci U S A, 1999. **96**(5): p. 2042-7.

36. Haraguchi, T., et al., *Asparagine-linked glycosylation of the scrapie and cellular prion proteins.* Arch Biochem Biophys, 1989. **274**(1): p. 1-13.

37. Aguzzi, A. and A.M. Calella, *Prions: protein aggregation and infectious diseases.* Physiol Rev, 2009. **89**(4): p. 1105-52.

38. Linden, R., et al., *Physiology of the prion protein.* Physiol Rev, 2008. **88**(2): p. 673-728.

39. Horiuchi, M., et al., *A cellular form of prion protein (PrPC) exists in many non-neuronal tissues of sheep.* J Gen Virol, 1995. **76 (Pt 10)**: p. 2583-7.

40. Fournier, J.G., et al., *Distribution and submicroscopic immunogold localization of cellular prion protein (PrPc) in extracerebral tissues.* Cell Tissue Res, 1998. **292**(1): p. 77-84.

41. Mobley, W.C., et al., *Nerve growth factor increases mRNA levels for the prion protein and the beta-amyloid protein precursor in developing hamster brain.* Proc Natl Acad Sci U S A, 1988. **85**(24): p. 9811-5.

42. Lazarini, F., J.P. Deslys, and D. Dormont, *Regulation of the glial fibrillary acidic protein, beta actin and prion protein mRNAs during brain development in mouse.* Brain Res Mol Brain Res, 1991. **10**(4): p. 343-6.

43. Manson, J., et al., *The prion protein gene: a role in mouse embryogenesis?* Development, 1992. **115**(1): p. 117-22.

44. Sales, N., et al., *Developmental expression of the cellular prion protein in elongating axons.* Eur J Neurosci, 2002. **15**(7): p. 1163-77.

45. Benvegnu, S., I. Poggiolini, and G. Legname, *Neurodevelopmental expression and localization of the cellular prion protein in the central nervous system of the mouse.* J Comp Neurol, 2010. **518**(11): p. 1879-91.

46. Sales, N., et al., *Cellular prion protein localization in rodent and primate brain.* Eur J Neurosci, 1998. **10**(7): p. 2464-71.

47. Herms, J., et al., *Evidence of presynaptic location and function of the prion protein.* J Neurosci, 1999. **19**(20): p. 8866-75.

48. Haeberle, A.M., et al., *Synaptic prion protein immuno-reactivity in the rodent cerebellum.* Microsc Res Tech, 2000. **50**(1): p. 66-75.

49. Moya, K.L., et al., *Immunolocalization of the cellular prion protein in normal brain.* Microsc Res Tech, 2000. **50**(1): p. 58-65.

50. Shyng, S.L., M.T. Huber, and D.A. Harris, *A prion protein cycles between the cell surface and an endocytic compartment in cultured neuroblastoma cells.* J Biol Chem, 1993. **268**(21): p. 15922-8.

51. Taylor, D.R. and N.M. Hooper, *The prion protein and lipid rafts.* Mol Membr Biol, 2006. **23**(1): p. 89-99.

52. Steele, A.D., S. Lindquist, and A. Aguzzi, *The prion protein knockout mouse: a phenotype under challenge.* Prion, 2007. **1**(2): p. 83-93.

53. Manson, J.C., et al., *129/Ola mice carrying a null mutation in PrP that abolishes mRNA production are developmentally normal.* Mol Neurobiol, 1994. **8**(2-3): p. 121-7.

54. Bremer, J., et al., *Axonal prion protein is required for peripheral myelin maintenance.* Nat Neurosci, 2010. **13**(3): p. 310-8.

55. Tobler, I., et al., *Altered circadian activity rhythms and sleep in mice devoid of prion protein.* Nature, 1996. **380**(6575): p. 639-42.

56. Coitinho, A.S., et al., *Cellular prion protein ablation impairs behavior as a function of age.* Neuroreport, 2003. **14**(10): p. 1375-9.

57. Klamt, F., et al., *Imbalance of antioxidant defense in mice lacking cellular prion protein.* Free Radic Biol Med, 2001. **30**(10): p. 1137-44.

58. Brown, D.R., R.S. Nicholas, and L. Canevari, *Lack of prion protein expression results in a neuronal phenotype sensitive to stress.* J Neurosci Res, 2002. **67**(2): p. 211-24.

59. Khosravani, H., et al., *Prion protein attenuates excitotoxicity by inhibiting NMDA receptors.* J Cell Biol, 2008. **181**(3): p. 551-65.

60. Sakaguchi, S., et al., *Loss of cerebellar Purkinje cells in aged mice homozygous for a disrupted PrP gene.* Nature, 1996. **380**(6574): p. 528-31.

61. Moore, R.C., et al., *Ataxia in prion protein (PrP)-deficient mice is associated with upregulation of the novel PrP-like protein doppel.* J Mol Biol, 1999. **292**(4): p. 797-817.

62. Silverman, G.L., et al., *Doppel is an N-glycosylated, glycosylphosphatidylinositol-anchored protein. Expression in testis and ectopic production in the brains of Prnp(0/0) mice predisposed to Purkinje cell loss.* J Biol Chem, 2000. **275**(35): p. 26834-41.

63. Rossi, D., et al., *Onset of ataxia and Purkinje cell loss in PrP null mice inversely correlated with Dpl level in brain.* EMBO J, 2001. **20**(4): p. 694-702.

64. Nishida, N., et al., *A mouse prion protein transgene rescues mice deficient for the prion protein gene from purkinje cell degeneration and demyelination.* Lab Invest, 1999. **79**(6): p. 689-97.

65. Weissmann, C. and E. Flechsig, *PrP knock-out and PrP transgenic mice in prion research.* Br Med Bull, 2003. **66**: p. 43-60.

66. Nuvolone, M., et al., *Strictly co-isogenic C57BL/6J-Prnp-/- mice: A rigorous resource for prion science.* J Exp Med, 2016. **213**(3): p. 313-27.

67. Gasperini, L., et al., *Prion protein and copper cooperatively protect neurons by modulating NMDA receptor through S-nitrosylation.* Antioxid Redox Signal, 2015. **22**(9): p. 772-84.

68. Didonna, A., *Prion protein and its role in signal transduction.* Cell Mol Biol Lett, 2013. **18**(2): p. 209-30.

69. Hirsch, T.Z., et al., *PrP(C) signalling in neurons: from basics to clinical challenges.* Biochimie, 2014. **104**: p. 2-11.

70. Simons, K. and D. Toomre, *Lipid rafts and signal transduction.* Nat Rev Mol Cell Biol, 2000. **1**(1): p. 31-9.

71. Pawson, T., *Protein modules and signalling networks.* Nature, 1995. **373**(6515): p. 573-80.

72. Schmitt-Ulms, G., et al., *Binding of neural cell adhesion molecules (N-CAMs) to the cellular prion protein.* J Mol Biol, 2001. **314**(5): p. 1209-25.

73. Slapsak, U., et al., *The N-terminus of the Prion Protein Mediates Functional Interactions with NCAM Fibronectin Domain.* J Biol Chem, 2016.

74. Santuccione, A., et al., *Prion protein recruits its neuronal receptor NCAM to lipid rafts to activate p59fyn and to enhance neurite outgrowth.* J Cell Biol, 2005. **169**(2): p. 341-54.

75. Amin, L., et al., *Characterization of prion protein function by focal neurite stimulation.* J Cell Sci, 2016.

76. Gauczynski, S., et al., *The 37-kDa/67-kDa laminin receptor acts as the cell-surface receptor for the cellular prion protein.* EMBO J, 2001. **20**(21): p. 5863-75.

77. Hundt, C., et al., *Identification of interaction domains of the prion protein with its 37-kDa/67-kDa laminin receptor.* EMBO J, 2001. **20**(21): p. 5876-86.

78. Graner, E., et al., *Cellular prion protein binds laminin and mediates neuritogenesis.* Brain Res Mol Brain Res, 2000. **76**(1): p. 85-92.

79. Zanata, S.M., et al., *Stress-inducible protein 1 is a cell surface ligand for cellular prion that triggers neuroprotection.* EMBO J, 2002. **21**(13): p. 3307-16.

80. Schmitt-Ulms, G., et al., *Time-controlled transcardiac perfusion cross-linking for the study of protein interactions in complex tissues.* Nat Biotechnol, 2004. **22**(6): p. 724-31.

81. Kessels, H.W., et al., *The prion protein as a receptor for amyloid-beta.* Nature, 2010. **466**(7308): p. E3-4; discussion E4-5.

82. Lauren, J., et al., *Cellular prion protein mediates impairment of synaptic plasticity by amyloid-beta oligomers.* Nature, 2009. **457**(7233): p. 1128-32.

83. Balducci, C., et al., *Synthetic amyloid-beta oligomers impair long-term memory independently of cellular prion protein.* Proc Natl Acad Sci U S A, 2010. **107**(5): p. 2295-300.

84. Calella, A.M., et al., *Prion protein and Abeta-related synaptic toxicity impairment.* EMBO Mol Med, 2010. **2**(8): p. 306-14.

85. Rutishauser, D., et al., *The comprehensive native interactome of a fully functional tagged prion protein.* PLoS One, 2009. **4**(2): p. e4446.

86. Thomas, S.M. and J.S. Brugge, *Cellular functions regulated by Src family kinases.* Annu Rev Cell Dev Biol, 1997. **13**: p. 513-609.

87. Parsons, S.J. and J.T. Parsons, *Src family kinases, key regulators of signal transduction.* Oncogene, 2004. **23**(48): p. 7906-9.

88. Mouillet-Richard, S., et al., *Signal transduction through prion protein.* Science, 2000. **289**(5486): p. 1925-8.

89. Schneider, B., et al., *NADPH oxidase and extracellular regulated kinases 1/2 are targets of prion protein signaling in neuronal and nonneuronal cells.* Proc Natl Acad Sci U S A, 2003. **100**(23): p. 13326-31.

90. Beggs, H.E., P. Soriano, and P.F. Maness, *NCAM-dependent neurite outgrowth is inhibited in neurons from Fyn-minus mice.* J Cell Biol, 1994. **127**(3): p. 825-33.

91. Kanaani, J., et al., *Recombinant prion protein induces rapid polarization and development of synapses in embryonic rat hippocampal neurons in vitro.* J Neurochem, 2005. **95**(5): p. 1373-86.

92. Schwarz, A., et al., *Unchanged scrapie pathology in brain tissue of tyrosine kinase Fyn-deficient mice.* Neurodegener Dis, 2004. **1**(6): p. 266-8.

93. Nixon, R.R., *Prion-associated increases in Src-family kinases.* J Biol Chem, 2005. **280**(4): p. 2455-62.

94. Gyllberg, H., et al., *Increased Src kinase level results in increased protein tyrosine phosphorylation in scrapie-infected neuronal cell lines.* FEBS Lett, 2006. **580**(11): p. 2603-8.

95. Hernandez-Rapp, J., et al., *A PrP(C)-caveolin-Lyn complex negatively controls neuronal GSK3beta and serotonin 1B receptor.* Sci Rep, 2014. **4**: p. 4881.

96. Loberto, N., et al., *The membrane environment of endogenous cellular prion protein in primary rat cerebellar neurons.* J Neurochem, 2005. **95**(3): p. 771-83.

97. Brunet, A., S.R. Datta, and M.E. Greenberg, *Transcription-dependent and -independent control of neuronal survival by the PI3K-Akt signaling pathway.* Curr Opin Neurobiol, 2001. **11**(3): p. 297-305.

98. Bartholomeusz, C. and A.M. Gonzalez-Angulo, *Targeting the PI3K signaling pathway in cancer therapy.* Expert Opin Ther Targets, 2012. **16**(1): p. 121-30.

99. Chen, S., et al., *Prion protein as trans-interacting partner for neurons is involved in neurite outgrowth and neuronal survival.* Mol Cell Neurosci, 2003. **22**(2): p. 227-33.

100. Vassallo, N., et al., *Activation of phosphatidylinositol 3-kinase by cellular prion protein and its role in cell survival.* Biochem Biophys Res Commun, 2005. **332**(1): p. 75-82.

101. Bedogni, B., et al., *Redox regulation of cAMP-responsive element-binding protein and induction of manganous superoxide dismutase in nerve growth factor-dependent cell survival.* J Biol Chem, 2003. **278**(19): p. 16510-9.

102. Ostrakhovitch, E.A., et al., *Copper ions strongly activate the phosphoinositide-3-kinase/Akt pathway independent of the generation of reactive oxygen species.* Arch Biochem Biophys, 2002. **397**(2): p. 232-9.

103. Weise, J., et al., *Deletion of cellular prion protein results in reduced Akt activation, enhanced postischemic caspase-3 activation, and exacerbation of ischemic brain injury.* Stroke, 2006. **37**(5): p. 1296-300.

104. Weise, J., et al., *Overexpression of cellular prion protein alters postischemic Erk1/2 phosphorylation but not Akt phosphorylation and protects against focal cerebral ischemia.* Restor Neurol Neurosci, 2008. **26**(1): p. 57-64.

105. Roffe, M., et al., *Prion protein interaction with stress-inducible protein 1 enhances neuronal protein synthesis via mTOR.* Proc Natl Acad Sci U S A, 2010. **107**(29): p. 13147-52.

106. Lopes, M.H., et al., *Interaction of cellular prion and stress-inducible protein 1 promotes neuritogenesis and neuroprotection by distinct signaling pathways.* J Neurosci, 2005. **25**(49): p. 11330-9.

107. Chiarini, L.B., et al., *Cellular prion protein transduces neuroprotective signals.* EMBO J, 2002. **21**(13): p. 3317-26.

108. Caiati, M.D., et al., *PrPC controls via protein kinase A the direction of synaptic plasticity in the immature hippocampus.* J Neurosci, 2013. **33**(7): p. 2973-83.

109. Mazzoni, I.E., et al., *Lymphoid signal transduction mechanisms linked to cellular prion protein.* Biochem Cell Biol, 2005. **83**(5): p. 644-53.

110. Caetano, F.A., et al., *Endocytosis of prion protein is required for ERK1/2 signaling induced by stress-inducible protein 1.* J Neurosci, 2008. **28**(26): p. 6691-702.

111. Pradines, E., et al., *Cellular prion protein coupling to TACE-dependent TNF-alpha shedding controls neurotransmitter catabolism in neuronal cells.* J Neurochem, 2009. **110**(3): p. 912-23.

112. Pradines, E., et al., *CREB-dependent gene regulation by prion protein: impact on MMP-9 and beta-dystroglycan.* Cell Signal, 2008. **20**(11): p. 2050-8.

113. Fuhrmann, M., et al., *Loss of the cellular prion protein affects the Ca2+ homeostasis in hippocampal CA1 neurons.* J Neurochem, 2006. **98**(6): p. 1876-85.

114. Beraldo, F.H., et al., *Role of alpha7 nicotinic acetylcholine receptor in calcium signaling induced by prion protein interaction with stress-inducible protein 1.* J Biol Chem, 2010. **285**(47): p. 36542-50.

115. Beraldo, F.H., et al., *Metabotropic glutamate receptors transduce signals for neurite outgrowth after binding of the prion protein to laminin gamma1 chain.* FASEB J, 2011. **25**(1): p. 265-79.

116. Santos, T.G., et al., *Laminin-gamma1 chain and stress inducible protein 1 synergistically mediate PrPC-dependent axonal growth via Ca2+ mobilization in dorsal root ganglia neurons.* J Neurochem, 2013. **124**(2): p. 210-23.

117. Herz, J. and Y. Chen, *Reelin, lipoprotein receptors and synaptic plasticity.* Nat Rev Neurosci, 2006. **7**(11): p. 850-9.

118. Quattrocchi, C.C., et al., *Reelin is a serine protease of the extracellular matrix.* J Biol Chem, 2002. **277**(1): p. 303-9.

119. Devanathan, V., et al., *Cellular form of prion protein inhibits Reelin-mediated shedding of Caspr from the neuronal cell surface to potentiate Caspr-mediated inhibition of neurite outgrowth.* J Neurosci, 2010. **30**(27): p. 9292-305.

120. DeSilva, U., et al., *The human reelin gene: isolation, sequencing, and mapping on chromosome 7.* Genome Res, 1997. **7**(2): p. 157-64.

121. Dityatev, A. and M. Schachner, *Extracellular matrix molecules and synaptic plasticity.* Nat Rev Neurosci, 2003. **4**(6): p. 456-68.

122. D'Arcangelo, G., et al., *Reelin is a secreted glycoprotein recognized by the CR-50 monoclonal antibody.* J Neurosci, 1997. **17**(1): p. 23-31.

123. Utsunomiya-Tate, N., et al., *Reelin molecules assemble together to form a large protein complex, which is inhibited by the function-blocking CR-50 antibody.* Proc Natl Acad Sci U S A, 2000. **97**(17): p. 9729-34.

124. de Bergeyck, V., et al., *A panel of monoclonal antibodies against reelin, the extracellular matrix protein defective in reeler mutant mice.* J Neurosci Methods, 1998. **82**(1): p. 17-24.

125. Nakano, Y., et al., *The extremely conserved C-terminal region of Reelin is not necessary for secretion but is required for efficient activation of downstream signaling.* J Biol Chem, 2007. **282**(28): p. 20544-52.

126. Lambert de Rouvroit, C., et al., *Reelin, the extracellular matrix protein deficient in reeler mutant mice, is processed by a metalloproteinase.* Exp Neurol, 1999. **156**(1): p. 214-7.

127. Krstic, D., M. Rodriguez, and I. Knuesel, *Regulated proteolytic processing of Reelin through interplay of tissue plasminogen activator (tPA), ADAMTS-4, ADAMTS-5, and their modulators.* PLoS One, 2012. **7**(10): p. e47793.

128. Jossin, Y., et al., *The central fragment of Reelin, generated by proteolytic processing in vivo, is critical to its function during cortical plate development.* J Neurosci, 2004. **24**(2): p. 514-21.

129. Kohno, S., et al., *Mechanism and significance of specific proteolytic cleavage of Reelin.* Biochem Biophys Res Commun, 2009. **380**(1): p. 93-7.

130. D'Arcangelo, G., et al., *Reelin is a ligand for lipoprotein receptors.* Neuron, 1999. **24**(2): p. 471-9.

131. Hiesberger, T., et al., *Direct binding of Reelin to VLDL receptor and ApoE receptor 2 induces tyrosine phosphorylation of disabled-1 and modulates tau phosphorylation.* Neuron, 1999. **24**(2): p. 481-9.

132. Bock, H.H. and J. Herz, *Reelin activates SRC family tyrosine kinases in neurons.* Curr Biol, 2003. **13**(1): p. 18-26.

133. Arnaud, L., et al., *Fyn tyrosine kinase is a critical regulator of disabled-1 during brain development.* Curr Biol, 2003. **13**(1): p. 9-17.

134. Keshvara, L., et al., *Identification of reelin-induced sites of tyrosyl phosphorylation on disabled 1.* J Biol Chem, 2001. **276**(19): p. 16008-14.

135. Bock, H.H., et al., *Phosphatidylinositol 3-kinase interacts with the adaptor protein Dab1 in response to Reelin signaling and is required for normal cortical lamination.* J Biol Chem, 2003. **278**(40): p. 38772-9.

136. Jossin, Y. and A.M. Goffinet, *Reelin signals through phosphatidylinositol 3-kinase and Akt to control cortical development and through mTor to regulate dendritic growth.* Mol Cell Biol, 2007. **27**(20): p. 7113-24.

137. Beffert, U., et al., *Reelin-mediated signaling locally regulates protein kinase B/Akt and glycogen synthase kinase 3beta.* J Biol Chem, 2002. **277**(51): p. 49958-64.

138. Ballif, B.A., et al., *Activation of a Dab1/CrkL/C3G/Rap1 pathway in Reelin-stimulated neurons.* Curr Biol, 2004. **14**(7): p. 606-10.

139. Assadi, A.H., et al., *Interaction of reelin signaling and Lis1 in brain development.* Nat Genet, 2003. **35**(3): p. 270-6.

140. Chen, Y., et al., *Reelin modulates NMDA receptor activity in cortical neurons.* J Neurosci, 2005. **25**(36): p. 8209-16.

141. Beffert, U., et al., *Modulation of synaptic plasticity and memory by Reelin involves differential splicing of the lipoprotein receptor Apoer2.* Neuron, 2005. **47**(4): p. 567-79.

142. Sheldon, M., et al., *Scrambler and yotari disrupt the disabled gene and produce a reeler-like phenotype in mice.* Nature, 1997. **389**(6652): p. 730-3.

143. Rice, D.S., et al., *Disabled-1 acts downstream of Reelin in a signaling pathway that controls laminar organization in the mammalian brain.* Development, 1998. **125**(18): p. 3719-29.

144. Trommsdorff, M., et al., *Reeler/Disabled-like disruption of neuronal migration in knockout mice lacking the VLDL receptor and ApoE receptor 2.* Cell, 1999. **97**(6): p. 689-701.

145. Kuo, G., et al., *Absence of Fyn and Src causes a reeler-like phenotype.* J Neurosci, 2005. **25**(37): p. 8578-86.

146. Arnaud, L., B.A. Ballif, and J.A. Cooper, *Regulation of protein tyrosine kinase signaling by substrate degradation during brain development.* Mol Cell Biol, 2003. **23**(24): p. 9293-302.

147. Bock, H.H., et al., *Apolipoprotein E receptors are required for reelin-induced proteasomal degradation of the neuronal adaptor protein Disabled-1.* J Biol Chem, 2004. **279**(32): p. 33471-9.

148. Feng, L., et al., *Cullin 5 regulates Dab1 protein levels and neuron positioning during cortical development.* Genes Dev, 2007. **21**(21): p. 2717-30.

149. D'Arcangelo, G., *Reelin mouse mutants as models of cortical development disorders.* Epilepsy Behav, 2006. **8**(1): p. 81-90.

150. Falconer, D.S., *Two new mutants, 'trembler' and 'reeler', with neurological actions in the house mouse (Mus musculus L.).* J Genet, 1951. **50**(2): p. 192-201.

151. D'Arcangelo, G., et al., *A protein related to extracellular matrix proteins deleted in the mouse mutant reeler.* Nature, 1995. **374**(6524): p. 719-23.

152. Katsuyama, Y. and T. Terashima, *Developmental anatomy of reeler mutant mouse.* Dev Growth Differ, 2009. **51**(3): p. 271-86.

153. Sweet, H.O., et al., *Scrambler, a new neurological mutation of the mouse with abnormalities of neuronal migration.* Mamm Genome, 1996. **7**(11): p. 798-802.

154. Gonzalez, J.L., et al., *Birthdate and cell marker analysis of scrambler: a novel mutation affecting cortical development with a reeler-like phenotype.* J Neurosci, 1997. **17**(23): p. 9204-11.

155. Goldowitz, D., et al., *Cerebellar disorganization characteristic of reeler in scrambler mutant mice despite presence of reelin.* J Neurosci, 1997. **17**(22): p. 8767-77.

156. Yoneshima, H., et al., *A novel neurological mutant mouse, yotari, which exhibits reeler-like phenotype but expresses CR-50 antigen/reelin.* Neurosci Res, 1997. **29**(3): p. 217-23.

157. Howell, B.W., et al., *Neuronal position in the developing brain is regulated by mouse disabled-1.* Nature, 1997. **389**(6652): p. 733-7.

158. Alcantara, S., et al., *Regional and cellular patterns of reelin mRNA expression in the forebrain of the developing and adult mouse.* J Neurosci, 1998. **18**(19): p. 7779-99.

159. Marin-Padilla, M., *Cajal-Retzius cells and the development of the neocortex.* Trends Neurosci, 1998. **21**(2): p. 64-71.

160. Frotscher, M., *Dual role of Cajal-Retzius cells and reelin in cortical development.* Cell Tissue Res, 1997. **290**(2): p. 315-22.

161. Frotscher, M., *Cajal-Retzius cells, Reelin, and the formation of layers.* Curr Opin Neurobiol, 1998. **8**(5): p. 570-5.

162. Hong, S.E., et al., *Autosomal recessive lissencephaly with cerebellar hypoplasia is associated with human RELN mutations.* Nat Genet, 2000. **26**(1): p. 93-6.

163. Brich, J., et al., *Genetic modulation of tau phosphorylation in the mouse.* J Neurosci, 2003. **23**(1): p. 187-92.

164. Kocherhans, S., et al., *Reduced Reelin expression accelerates amyloid-beta plaque formation and tau pathology in transgenic Alzheimer's disease mice.* J Neurosci, 2010. **30**(27): p. 9228-40.

165. Cuchillo-Ibanez, I., et al., *Beta-amyloid impairs reelin signaling.* PLoS One, 2013. **8**(8): p. e72297.

166. Hoe, H.S., et al., *Interaction of reelin with amyloid precursor protein promotes neurite outgrowth.* J Neurosci, 2009. **29**(23): p. 7459-73.

167. Rice, H.C., T.L. Young-Pearse, and D.J. Selkoe, *Systematic evaluation of candidate ligands regulating ectodomain shedding of amyloid precursor protein.* Biochemistry, 2013. **52**(19): p. 3264-77.

168. Pujadas, L., et al., *Reelin delays amyloid-beta fibril formation and rescues cognitive deficits in a model of Alzheimer's disease.* Nat Commun, 2014. **5**: p. 3443.

169. Trommsdorff, M., et al., *Interaction of cytosolic adaptor proteins with neuronal apolipoprotein E receptors and the amyloid precursor protein.* J Biol Chem, 1998. **273**(50): p. 33556-60.

170. Howell, B.W., et al., *The disabled 1 phosphotyrosine-binding domain binds to the internalization signals of transmembrane glycoproteins and to phospholipids.* Mol Cell Biol, 1999. **19**(7): p. 5179-88.

171. Parisiadou, L. and S. Efthimiopoulos, *Expression of mDab1 promotes the stability and processing of amyloid precursor protein and this effect is counteracted by X11alpha.* Neurobiol Aging, 2007. **28**(3): p. 377-88.

172. Cuchillo-Ibanez, I., et al., *Reelin in Alzheimer's Disease, Increased Levels but Impaired Signaling: When More is Less.* J Alzheimers Dis, 2016. **52**(2): p. 403-16.

173. Hoareau, C., et al., *Amyloid precursor protein cytoplasmic domain antagonizes reelin neurite outgrowth inhibition of hippocampal neurons.* Neurobiol Aging, 2008. **29**(4): p. 542-53.

174. Leeb, C., C. Eresheim, and J. Nimpf, *Clusterin is a ligand for apolipoprotein E receptor 2 (ApoER2) and very low density lipoprotein receptor (VLDLR) and signals via the Reelin-signaling pathway.* J Biol Chem, 2014. **289**(7): p. 4161-72.

175. Wu, Z.C., et al., *Clusterin in Alzheimer's disease.* Adv Clin Chem, 2012. **56**: p. 155-73.

176. Sasaki, K., et al., *Increased clusterin (apolipoprotein J) expression in human and mouse brains infected with transmissible spongiform encephalopathies.* Acta Neuropathol, 2002. **103**(3): p. 199-208.

177. Freixes, M., et al., *Clusterin solubility and aggregation in Creutzfeldt-Jakob disease.* Acta Neuropathol, 2004. **108**(4): p. 295-301.

178. Xu, F., E. Karnaukhova, and J.G. Vostal, *Human cellular prion protein interacts directly with clusterin protein.* Biochim Biophys Acta, 2008. **1782**(11): p. 615-20.

179. Lussier, A.L., E.J. Weeber, and G.W. Rebeck, *Reelin Proteolysis Affects Signaling Related to Normal Synapse Function and Neurodegeneration.* Front Cell Neurosci, 2016. **10**: p. 75.

180. Saez-Valero, J., et al., *Altered levels of cerebrospinal fluid reelin in frontotemporal dementia and Alzheimer's disease.* J Neurosci Res, 2003. **72**(1): p. 132-6.

181. Botella-Lopez, A., et al., *Reelin expression and glycosylation patterns are altered in Alzheimer's disease.* Proc Natl Acad Sci U S A, 2006. **103**(14): p. 5573-8.

182. Hoe, H.S., et al., *DAB1 and Reelin effects on amyloid precursor protein and ApoE receptor 2 trafficking and processing.* J Biol Chem, 2006. **281**(46): p. 35176-85.

183. Hoe, H.S., et al., *Fyn modulation of Dab1 effects on amyloid precursor protein and ApoE receptor 2 processing.* J Biol Chem, 2008. **283**(10): p. 6288-99.

184. Minami, S.S., H.S. Hoe, and G.W. Rebeck, *Fyn kinase regulates the association between amyloid precursor protein and Dab1 by promoting their localization to detergent-resistant membranes.* J Neurochem, 2011. **118**(5): p. 879-90.

185. Gavin, R., I. Ferrer, and J.A. del Rio, *Involvement of Dab1 in APP processing and beta-amyloid deposition in sporadic Creutzfeldt-Jakob patients.* Neurobiol Dis, 2010. **37**(2): p. 324-9.

186. Lledo, P.M., et al., *Mice deficient for prion protein exhibit normal neuronal excitability and synaptic transmission in the hippocampus.* Proc Natl Acad Sci U S A, 1996. **93**(6): p. 2403-7.

187. Prusiner, S.B., et al., *Ablation of the prion protein (PrP) gene in mice prevents scrapie and facilitates production of anti-PrP antibodies.* Proc Natl Acad Sci U S A, 1993. **90**(22): p. 10608-12.

188. Herrick, T.M. and J.A. Cooper, *A hypomorphic allele of dab1 reveals regional differences in reelin-Dab1 signaling during brain development.* Development, 2002. **129**(3): p. 787-96.

189. Leemhuis, J., et al., *Reelin signals through apolipoprotein E receptor 2 and Cdc42 to increase growth cone motility and filopodia formation.* J Neurosci, 2010. **30**(44): p. 14759-72.

190. Giachin, G., et al., *Prion protein interaction with soil humic substances: environmental implications.* PLoS One, 2014. **9**(6): p. e100016.

191. Ilc, G., et al., *NMR structure of the human prion protein with the pathological Q212P mutation reveals unique structural features.* PLoS One, 2010. **5**(7): p. e11715.

192. Peretz, D., et al., *Antibodies inhibit prion propagation and clear cell cultures of prion infectivity.* Nature, 2001. **412**(6848): p. 739-43.

193. Petsch, B., et al., *Biological effects and use of PrPSc- and PrP-specific antibodies generated by immunization with purified full-length native mouse prions.* J Virol, 2011. **85**(9): p. 4538-46.

194. Livak, K.J. and T.D. Schmittgen, *Analysis of relative gene expression data using real-time quantitative PCR and the 2(-Delta Delta C(T)) Method.* Methods, 2001. **25**(4): p. 402-8.

195. Grison, A., et al., *Mesencephalic dopaminergic neurons express a repertoire of olfactory receptors and respond to odorant-like molecules.* BMC Genomics, 2014. **15**: p. 729.

196. Simonetti, M., R. Giniatullin, and E. Fabbretti, *Mechanisms mediating the enhanced gene transcription of P2X3 receptor by calcitonin gene-related peptide in trigeminal sensory neurons.* J Biol Chem, 2008. **283**(27): p. 18743-52.

197. Zhou, Y., et al., *High-throughput screening of a CRISPR/Cas9 library for functional genomics in human cells.* Nature, 2014. **509**(7501): p. 487-91.

198. Barbisin, M., et al., *Gene expression profiling of brains from bovine spongiform encephalopathy (BSE)-infected cynomolgus macaques.* BMC Genomics, 2014. **15**: p. 434.

199. Ono, T., et al., *Positive transcriptional regulation of the human micro opioid receptor gene by poly(ADP-ribose) polymerase-1 and increase of its DNA binding affinity based on polymorphism of G-172 -> T.* J Biol Chem, 2009. **284**(30): p. 20175-83.

200. Roskoski, R., Jr., *Src kinase regulation by phosphorylation and dephosphorylation.* Biochem Biophys Res Commun, 2005. **331**(1): p. 1-14.

201. Reddy, S.S., et al., *Similarities and differences in structure, expression, and functions of VLDLR and ApoER2.* Mol Neurodegener, 2011. **6**: p. 30.

202. Kerjan, G. and J.G. Gleeson, *A missed exit: Reelin sets in motion Dab1 polyubiquitination to put the break on neuronal migration.* Genes Dev, 2007. **21**(22): p. 2850-4.

203. Fischer, M.B., et al., *Binding of disease-associated prion protein to plasminogen.* Nature, 2000. **408**(6811): p. 479-83.

204. Ellis, V., et al., *Plasminogen activation is stimulated by prion protein and regulated in a copper-dependent manner.* Biochemistry, 2002. **41**(22): p. 6891-6.

205. Xanthopoulos, K., et al., *Tissue plasminogen activator in brain tissues infected with transmissible spongiform encephalopathies.* Neurobiol Dis, 2005. **20**(2): p. 519-27.

206. Schuster, T., et al., *Immunoelectron microscopic localization of the neural recognition molecules L1, NCAM, and its isoform NCAM180, the NCAM-*

associated polysialic acid, beta1 integrin and the extracellular matrix molecule tenascin-R in synapses of the adult rat hippocampus. J Neurobiol, 2001. **49**(2): p. 142-58.

207. Kolkova, K., *Biosynthesis of NCAM.* Adv Exp Med Biol, 2010. **663**: p. 213-25.
208. Polo-Parada, L., et al., *Distinct roles of different neural cell adhesion molecule (NCAM) isoforms in synaptic maturation revealed by analysis of NCAM 180 kDa isoform-deficient mice.* J Neurosci, 2004. **24**(8): p. 1852-64.
209. Todaro, L., et al., *Alteration of serum and tumoral neural cell adhesion molecule (NCAM) isoforms in patients with brain tumors.* J Neurooncol, 2007. **83**(2): p. 135-44.
210. Volker, H.U., et al., *Expression of CD56 isoforms in primary and relapsed adult granulosa cell tumors of the ovary.* Diagn Pathol, 2008. **3**: p. 29.
211. Markovic-Lipkovski, J., et al., *Variable Expression of Neural Cell Adhesion Molecule Isoforms in Renal Tissue: Possible Role in Incipient Renal Fibrosis.* PLoS One, 2015. **10**(9): p. e0137028.
212. Tur, M.K., et al., *The 140-kD isoform of CD56 (NCAM1) directs the molecular pathogenesis of ischemic cardiomyopathy.* Am J Pathol, 2013. **182**(4): p. 1205-18.
213. Um, J.W., et al., *Alzheimer amyloid-beta oligomer bound to postsynaptic prion protein activates Fyn to impair neurons.* Nat Neurosci, 2012. **15**(9): p. 1227-35.